Engineering of Microbioreactors and Microbiomes for the Biodegradation of Volatile Organic Compounds

by

Kelsey E. Deaton

Department of Civil & Environmental Engineering
Duke University

Date:_____

Approved:

_____
Marc Deshusses, Supervisor

_____
Claudia Gunsch

_____
Michael Bergin

_____
Joshua Granek

Dissertation submitted in partial fulfillment of the requirements
for the degree of Doctor of Philosophy
in the Department of Civil & Environmental Engineering
in the Graduate School of Duke University

2022

ABSTRACT

Engineering of Microbioreactors and Microbiomes for the Biodegradation of Volatile Organic Compounds

by

Kelsey Deaton

Department of Civil & Environmental Engineering
Duke University

Date:_____

Approved:

_____
Marc Deshusses, Supervisor

_____
Claudia Gunsch

_____
Michael Bergin

_____
Joshua Granek

An abstract of a dissertation
submitted in partial fulfillment of the requirements
for the degree of Doctor of Philosophy
in the Department of Civil & Environmental Engineering
in the Graduate School of Duke University

2022

Abstract

Some of the worst air quality is found in enclosed indoor spaces that do not have the capability for sufficient ventilation. Despite the major health risk of indoor air pollutants, such as volatile organic compounds (VOCs), current technologies to treat indoor VOC pollution could be improved. There is a critical need for a new technology that can effectively control VOCs in enclosed indoor environments. Biofiltration can potentially be adapted for indoor air treatment by intensifying the process with miniaturization. Microbioreactors have maximized surface-to-volume ratios, which allows for increased mass transfer of pollutants and oxygen to bacteria in the aqueous phase, resulting in superior biodegradation of VOCs.

Accurate measurements of mass transfer coefficients are critical for reliable characterization of bioreactors. While standardized methods to measure mass transfer coefficients (MTCs) have been established for simple stirred tank reactors, existing methods to characterize MTCs have not yet been standardized for alternative reactor types such as miniaturized and biofiltration reactors, leading to inconsistencies in implementation and confusion about the validity of comparisons across different methodologies, volume scales, or reactor types. The accuracy of two commonly used lab-scale methods was critically evaluated for the measurement of mass transfer coefficients in a miniature plug-flow reactor. A detailed mathematical model was developed and applied to each experimental method, which, unlike conventional methods, enabled accurate calculation of the mass transfer coefficients.

Building upon promising preliminary microbioreactor prototypes, a systematic study of major reactor design parameters was carried out with the aim of improving reactor

performance. A design-build-test-learn platform was developed that enabled new reactor design prototypes to be rapidly designed using CAD software, manufactured with 3D printing, and inserted interchangeably in an experimental testing system. Several microbioreactors were manufactured with varying microchannels sizes and configurations. The mass transfer coefficients were characterized and a selection of microbioreactor prototypes was evaluated in a study of toluene biodegradation in continuously operated microbioreactors. The results illustrated that microbioreactors with smaller channel dimensions had higher MTCs, which also translated to higher rates of toluene removal.

The results of the microbioreactor evaluation studies indicate good performance for biological treatment of toluene and methanol as single model VOC substrates. Realistic treatment environments will have mixtures of pollutants, with several to potentially hundreds of separate volatile pollutants. The treatment of pollutant mixtures has been shown to be more difficult for many microorganisms to treat effectively. Recently, several tools have emerged to enable a rational approach to design of microbial communities. Community metabolic network modeling was evaluated for use in engineering a microbial consortium to effectively and resiliently biodegrade VOCs. Model-predicted microbial communities were experimentally assessed alongside pure strains and conventionally enriched cultures for biodegradation of toluene and styrene as a model VOC mixture. Experimental results demonstrated mixed success for model predictions, which indicated that automated metabolic network modeling of microbial communities can serve as a powerful screening tool, and future research should focus on combining these methods with curated and quantitative metabolic models.

Altogether, the aim of this dissertation was to engineer a high-performing microbioreactor-microbiome system for biological VOC removal. The methods developed in this collection of work will facilitate future research on microbioreactors, including accurate characterization of MTCs and a platform for microbioreactor prototyping and design assessment. The investigations here addressed knowledge gaps between the impact of microbioreactor design on MTCs and continuous cultivation of VOC-degrading microorganisms. Additionally, one of the first attempts to rationally design a pollutant-degrading microbial community using metabolic network modeling was presented, illustrating the exciting opportunities for the future of microbiome engineering for environmental benefits.

Contents

Abstract iv

Contents vii

List of Tables x

List of Figures xi

Acknowledgements xiii

1 Introduction 1

1.1 Indoor Air Quality 1

1.2 Current VOC Treatment for Indoor Spaces 2

1.3 The Promise of Microbioreactors 3

1.4 Preliminary Work and Proof-of-Concept 4

1.5 Overall Objective and Research Aims 5

2 Critical Assessment of Gassing-In Methods to Determine Mass Transfer Coefficient in Miniature and Microbioreactors with Gas-Liquid Flow 6

2.1 Introduction 6

2.2 Experimental Methods 13

2.2.1 Reactors and Experimental Set Up 13

2.2.2 Dynamic Method Experimental Set Up 13

2.2.3 Steady State Experimental Set Up 16

2.2.4 Dynamic Method Conventional Data Analysis 16

2.2.5 Steady State Method Conventional Data Analysis 17

2.2.6 Measurement of DO Probe Response Time 18

2.3 Model Development 18

2.3.1 Theory and Approach 18

2.3.2 Mass Balances on DO in the Reactor System 20
2.3.3 Mass Balances on DO in the Ancillary System 21
2.3.4 Including DO Probe Response Time in Each Model 21
2.3.5 Model Evaluation 22
2.4 Results and Discussion 22
2.4.1 Evaluation of Experimental and Data Analysis Methods 22
2.4.2 Importance of the Ancillary System 26
2.5 Conclusions and Recommendations for Best Practices 31
3 Evaluation of Microbioreactor Design on Performance: Mass Transfer and Continuous Biological Operation 32
3.1 Introduction 32
3.2 Methods 34
3.2.1 Microbioreactor Design and 3D Printing 34
3.2.2 Mass Transfer Coefficient Determination 37
3.2.3 Biological Performance 38
3.2.4 Data Analysis 42
3.3 Results 43
3.3.1 Evaluation of Microbioreactor Design and 3D-Printing 43
3.3.2 Mass Transfer Coefficients 43
3.3.3 Biodegradation Performance 46
3.4 Conclusions 54
4 Comparison of Microbial Community Design Approaches for Biodegradation of Multiple VOCs 56
4.1 Introduction 56
4.2 Methods 60

4.2.1 Metabolic Network Modeling and Species Selection....60
4.2.2 Microbial Cultivation....63
4.2.3 Biodegradation Experiments....65
4.2.4 DNA Extraction, qPCR, and Amplicon Sequencing....66
4.3 Results and Discussion....68
4.3.1 M2M Modeling and Identification of Minimal Communities....68
4.3.2 Evaluation of the Enrichment Culture Composition....74
4.3.3 VOC Biodegradation....76
4.3.4 Minimal Community Stability....81
4.4 Conclusion....83
5 Conclusions....85
6 Appendix A. Supplementary Material for Chapter 3. 87
7 Appendix B. Supplementary Material for Chapter 4. 89
7.1 Inputs to M2M Model....89
7.2 Supplementary Model Results....92
7.3 Solutions graphs for model runs with styrene and toluene degradation pathways II – V as targets 93
7.4 Producers of each target metabolite in example minimal communities.....97
7.5 Quality profile of activated sludge forward and reverse reads for 16s rRNA gene amplicon sequencing. 99
7.6 Alternative Presentations of Relative Abundance....100
7.7 Accumulation of Yellow Compound in Enrichment Culture....102
References....105
Biography....116

List of Tables

Table 2.1: Parameter Definitions 6

Table 2.2: Acronyms..... 7

Table 3.1: Specifications of the various microbioreactor beds. 36

Table 4.1 Curation of annotated genome assemblies as inputs for metabolic network modeling.....61

Table 4.2 Primer and probe sequences for qPCR assays.....68

Table 4.3 Taxonomic summary of the key species identified through metabolic network modeling, grouped by genus. 72

Table 4.4 Strains chosen for minimal consortia experiments. 74

Table 7.1 M2M model “seeds” or metabolite inputs to the model. 89

Table 7.2 Target metabolites of toluene and styrene degradation pathways.....90

Table 7.3 Taxonomic classification of key species for toluene and styrene degradation targets. 92

Table 7.4 Producers of metabolic targets for Target Set I 97

Table 7.5 Producers of metabolic targets for Target Set III 98

List of Figures

Figure 2.1: CAD design (Left) and picture of the microchannel reactor bed within the case (Right). 13

Figure 2.2: Diagrams of the experimental setups. 15

Figure 2.3: Generalized conceptual schematic of the mathematical model. 20

Figure 2.4: Typical fits of models and data analysis to experimental data. 23

Figure 2.5: Comparison of the reactor K_La values determined by each data analysis method. 24

Figure 2.6: Comparison of K_La values between the two experimental methods 25

Figure 2.7: Comparison of the K_La_{Anc} values for the ancillary system determined by conventional data analysis or model-fitting for both experimental methods. 27

Figure 2.8: Comparison of the reactor K_La values from different data analysis methods of the same SSM experimental data. 28

Figure 3.1 CAD designs and photos of microbioreactors. 35

Figure 3.2 Diagrams of the abiotic experimental setups for mass transfer testing. 38

Figure 3.3: Diagram of the experimental setup for biological experiments. 40

Figure 3.4: Maximum K_La for all reactor beds of varying microchannel cross-sectional area (A). 44

Figure 3.5 Overall volumetric MTCs of microbioreactors of varying channel size (A) with straight channels (Left) and patterned channels (Right) as a function of liquid flow rate. 45

Figure 3.6: Elimination capacities from days 4-12. 47

Figure 3.7: Comparison of the EC at increasing LR for each microbioreactor. 48

Figure 3.8: Reactor-only EC (R.EC) of the microbioreactors. 49

Figure 3.9 Continuous operation of microbioreactor 0.5-S. 51

Figure 3.10 MicroCT scans of microbioreactor cross sections before (left) and after (right) toluene vapor biodegradation experiments for the straight-channeled reactors. 53

Figure 4.1 MetaCyc styrene degradation pathway. 63

Figure 4.2 MetaCyc superpathway of aerobic toluene degradation. 63

Figure 4.3 Solution graph of the minimal communities and key species for toluene (pathway I) and styrene degradation products. 69

Figure 4.4 Relative abundance of OTUs at the order level determined by 16s rRNA gene sequencing from samples of activated sludge and enrichment cultures. 75

Figure 4.5 Alpha diversity measures of community richness for activated sludge (AS) and enrichment culture (EnA & EnB) samples. 76

Figure 4.6 VOC removal and growth of pure cultures on 50 mg L^{-1} toluene or styrene. .79

Figure 4.7 VOC removal and growth by cultures with 100 mg L^{-1} TVOC. 80

Figure 4.8 Quantification of 16s genes for NA and PF in a minimal consortium over the course of the experiment. 82

Figure 6.1 Images of two microbioreactors at the end of over 300 hours of operation. ..87

Figure 6.2 Experimental set up for biological performance experiments. 88

Figure 7.1 Solution graph of the minimal communities and key species for toluene (degradation pathway II) and styrene degradation products. 93

Figure 7.2 Solution graph of the minimal communities and key species for toluene (degradation pathway III) and styrene degradation products. 94

Figure 7.3 Solution graph of the minimal communities and key species for toluene (degradation pathway IV) and styrene degradation products. 95

Figure 7.4 Solution graph of the minimal communities and key species for toluene (degradation pathway V) and styrene degradation products. 96

Figure 7.5 Forward (top) and reverse (bottom) read quality profiles. 99

Figure 7.6 Relative abundance of OTUs at the genus level. 100

Figure 7.7 Relative abundance of OTUs at the class level. 101

Figure 7.8 Yellow color of the enrichment culture 2 hours after dosing with 100 mg/L (initial liquid concentration) of toluene and styrene each. 102

Figure 7.9 Color of the enrichment culture 19 hours after dosing with 100 mg/L (initial liquid concentration) of toluene and styrene each. 103

Figure 7.10 Relative abundance of OTUs at the class level. 104

Acknowledgements

My first thank you goes to my advisor, Marc Deshusses. Your support and advocacy for me and my work has gone beyond anything I expected when I joined your lab over six years ago. Thank you for taking a chance on me by bringing me into your research group. Thank you for adapting your mentorship as I needed, at times with more space and others more accountability. I appreciate the freedom you gave me to pursue my own ideas, through several rabbit holes, down a few paths to dead ends, but ultimately, to work I am truly proud of.

Thank you to my committee – Claudia Gunsch, Michael Bergin, and Joshua Granek – thank you for feedback on my research and encouragement through the process. Thank you so much for your patience, flexibility, and understanding. When things got complicated, your immediate support and sympathy was the reassurance I needed to see this all through to the end.

Thank you to Dwina Martin, you have been my most valuable resource. Your technical expertise, mentorship, and friendship were critical to me on a daily basis. I came to you for anything and everything and 99.9% of the time you had the answer or could point me towards it.

Thank you to the undergraduate researchers who helped make this work possible – Adrianne Pink, Isabella Rundell, Stephanie Pascual, and Abhi Jain.

Thank you to the Duke campus resources that helped make this work possible – the Co-Lab for 3D-printing of the microbioreactors, the Duke Sequencing & Genomic Technologies Core Resource for 16s amplicon sequencing services, and Justin Gladman of the Shared Materials Instrumentation Facility for MicroCT imaging.

Thank you to those who worked for almost two years to protect me and my right to an education – Sheila Broderick of Duke Women's Center, those at Duke's Office of Institutional Equity, Beth Posner and Sabrina Gamero of the UNC School of Law Clinics, and Captain Greg Stotsenberg of Duke University Police.

Thank you to Luis Rafael López de León. You have been an excellent role model. Your positivity is a gift. Thank you for your feedback, both constructive and positive, on this work. I would publish this dissertation with your comments left in if I could.

Thank you to all of my mentors over the years who inspired me to love science and helped me get to Duke – Janice Jones, Jeffrey Krause, Laura Windecker, and Mark Brzezinski, who mentored me at UCSB; Anne Schauer-Gimenez, Allison Pieja, and Molly Morse, who founded the amazing company Mango Materials and inspired me to also get a PhD in Civil & Environmental Engineering.

Thank you to all the other students in department who have been my friends and allies in this very hard work of trying to do science. Stew, thank you for always having good ideas for how to implement something well and to talk through my conundrum of the moment. Thank you to all of the students of the Gunsch lab, who were my go-to's for all things microbiology. In particular, thank you to Paige Varner, my last chapter would not have been possible in such a short time without your work and generosity. Thank you to Eva Kim, I would not have made it through my last chapter without your technical expertise and encouragement; all of the difficulties were worth it to discover your friendship.

Thank you to Kim Bourne and Joana Sipe. Thank you for the validation, the encouragement, the zoom work sessions, for everything. Thank you for being my

company in misery. It was wonderful to go through the journey of getting our doctorates together, along with all of life's other journeys, and I can't wait to just hang out again.

Thank you to Trisha Dupnock for being my ultimate Apex Woman role model. I am so impressed with everything you do. I adore everything about your unapologetically badass self, which always inspires me to appreciate those aspects of my own. I am so grateful for your advocacy. You are caring, generous, and an absolute joy of a friend.

Thank you to all my friends who bring so much joy to my life. I'm lucky to have so many amazing people who have loved and supported me over the years, some for decades. What an amazing bunch of absolute nerds. I admire and love you all.

Thank you to my dogs, Tucker and Lyra, for being adorable and silly and making sure I get at least 30 minutes of exercise and playtime every day.

Thank you to my husband, Will Shorrock, for being my best friend and biggest supporter. I would never have had the confidence to even apply to graduate school without you. Thank you for helping me with all things code, for the pep talks, and for doing literally all the cooking these last couple months. I can't wait for the next stage of our lives together.

Thank you to my parents, who have worked so hard and done so much to give me every possible opportunity I ever wanted. I'll do my best to make it worth it. This is for you.

1 Introduction

1.1 Indoor Air Quality

Few people realize that indoor air quality is often worse than outdoors. Residential concentrations of organic chemicals are often 2-5 times greater than outdoor concentrations [1]. Volatile organic compounds (VOCs) are a major contributor to indoor air pollution and are ubiquitous in homes, with several common VOCs (benzene, toluene, ethylbenzene, xylene, styrene, naphthalene, α-pinene) being found in 100% of homes sampled in several major U.S. cities [2]. The major sources of VOCs indoors are from paint, cleaning supplies, and outdoor sources such as gas combustion and industrial emissions that find their way indoors [3]. Indoor air quality is mostly maintained by providing an adequate air exchange rate, which involves ventilation with less polluted outdoor air.

Some of the worst air quality is found in enclosed spaces like factories and airplanes that do not have the capability for sufficient ventilation. For example, toluene, a common VOC found in homes at 0.03 to 1.9 $\mu g/m^3$, has been measured on commercial airplanes at over 100 times typical residential levels at 130 $\mu g/m^3$ [4]. In environments where air exchange is impossible, such as the International Space Station, the levels of total VOCs are much higher, with average concentrations of 14 mg m^{-3} [5]. Even higher levels have been found on submarines with total VOC levels as high as 67 mg m^{-3} [6]. Chronic exposure to VOCs can cause respiratory irritation, cognitive dysfunction, cancer, damage to the liver and to the central nervous system [7], [1].

1.2 Current VOC Treatment for Indoor Spaces

Due to the major health risk, current methods to treat indoor VOC pollution could be improved. Solely relying on ventilation is insufficient when outdoor air can contribute VOC emissions from industry and gas combustion that then become concentrated indoors. For some indoor environments, such as submarines, ventilation is not even an option. Therefore, the VOCs must be removed from the air and either contained or destroyed. While various technologies to remove VOCs are available, many are either ineffective, expensive, or unreliable.

Activated carbon sorption filters are the most effective at removing gaseous pollutants or vapors and can be simply integrated into an existing HVAC system [8]. However, activated carbon filters are fairly expensive, need to be replaced multiple times a year, can be damaged by ozone, and are ineffective at filtering compounds with a very high vapor pressure such as formaldehyde [8]. Furthermore, these filters must be properly disposed of in a timely manner or VOCs can desorb from the filter and be released back into the indoor environment.

Photocatalytic oxidation (PCO) is another appealing technology, because the oxidative process can fully degrade VOCs to harmless CO_2, however, they can consume large amounts of energy (1066 kJ/h for 56 m^3 room [9]), rely on high-intensity UV, and can produce harmful byproducts such as ozone or acetic acid if oxidation is incomplete [10]. Furthermore, the effectiveness of commercial PCO systems varies widely, with some products shown to be largely ineffective [8]. In a study of commercially available indoor technologies claiming to treat VOCs, the best performing technology was a combined activated carbon filter and UV-PCO unit which was only able to remove 44% of VOCs [8].

However, this same unit was effectively unable to remove formaldehyde and acetaldehyde, representatives of VOCs with very high vapor pressures.

The treatment of VOCs in indoor spaces presents special difficulties in comparison to treating industrial exhausts at the source: VOCs are present in very low pollutant concentrations, there is risk of bioaerosol release if using a biological filter, and need for low humidity. Indoor environments are also variable in the types and concentrations of VOCs present, depending on the building materials and activities that take place inside.

Biofiltration is a successful technology to treat contaminated air and has been widely implemented at large scales for industrial exhausts [11]. Large volumes of air with dilute concentrations of contaminants are passed through a humidified packed bed on which pollutant-degrading bacteria grow as a biofilm. Biofiltration of air is advantageous because it can be operated at ambient temperatures, can adapt to changing conditions, generally does not produce harmful byproducts, requires little energy, and has low operation and maintenance costs [12]. However, biofiltration as implemented for industrial application is not directly suited for indoor air treatment due to potential moisture and bioaerosol release.

1.3 The Promise of Microbioreactors

Small-scale reactors, including microfluidic systems, could be the key to adapting biofiltration to indoor air treatment. Microfluidic reactors have much higher surface area to volume ratios, which provide opportunities for faster mass transfer rates [13]. Microfluidic reactors can also offer high levels of control of multiphase flows like gas-liquid flow [14]. Successful applications of microreactors have been seen in high-throughput biological screenings [15], chemical reactions [16], and detection for environmental sensors [17].

Microfluidic reactors have higher surface area to volume ratios, leading to faster mass transfer rates [13] and offer high levels of control for gas-liquid flow [14].

One obstacle to biofiltration of indoor air is the low pollutant concentrations. Microbial biodegradation rates are likely to be limited by such low substrate concentrations, which makes for an inefficient system [18]. This realization led to a DARPA-funded project whereby industry collaborators at the Warner Babcock Institute (WBI) aimed to create a pollutant microconcentrator for VOCs which would be coupled with microbioreactors. This microconcentrator could greatly improve overall performance, since mass transfer can often limit microbial kinetic reaction rates as it limits the availability of carbon substrate and oxygen.

1.4 Preliminary Work and Proof-of-Concept

The overarching vision of this work was a microconcentrator-microbioreactor device for indoor VOC treatment. The microconcentrator to be developed will use a patterned adsorbent to capture VOCs from indoor air and release them in a smaller, concentrated stream to the microbioreactor. This two-stage microconcentrator-microbioreactor system would limit the volume of air treated by the microbioreactor, reducing the potential contribution of humidity and bioaerosols.

Recent work from our lab focused on adapting conventional biofiltration technology, which is widely used to treat contaminated air streams in industrial settings, to indoor air treatment using microfluidic reactors. In a proof of concept study, miniaturized packed bed biotrickling filters (mini-BTFs) and a glass capillary microbioreactor were evaluated in studies of biological removal of toluene or methanol [19]. Our preliminary work with capillary microbioreactors showed especially promising results for VOC removal. The capillary microbioreactor achieved high volumetric performance, with

maximum elimination capacity values ranging up to 3,000 g m^{-3} h^{-1} of toluene or 10,000 g m^{-3} h^{-1} of methanol, i.e., 50-200 times that of conventional bioreactors. During a following two-month study on operational optimization, the capillary microbioreactors were capable of continuous operation with efficient treatment and minimal clogging [20].

1.5 Overall Objective and Research Aims

The objective of this research was to investigate various factors critical to the successful design and implementation of microbioreactor system for treatment of VOCs in indoor air. This dissertation addresses this goal through the following aims:

1) **Development and validation of experimental methods and mathematical models for accurate characterization of mass transfer coefficients in miniature and microbioreactors.** I hypothesized that conventional experimental methods could be adapted for application to microbioreactors through detailed accounting of the experimental system and by building mathematical models that account for the various transfer phenomena and dynamics involved to analyze the experimental data.

2) **Development of a platform for rapid prototyping and evaluation of microbioreactor designs, which was applied to the assessment of microbioreactor design parameters on mass transfer and long-term biological removal of toluene as a model VOC.** I proposed to use 3D-printing for rapid prototyping of designs and an interchangeable case to facilitate experimental evaluation. This platform was used to test the hypothesis that microbioreactors with smaller channel dimensions would have higher MTCs, yet the advantage of better mass transfer may have a trade-off with increased issues of biomass clogging.

3) **Evaluation of the potential for community metabolic network modeling as a tool for strategic engineering of VOC-degrading microbial communities**. I hypothesized

that minimal microbial consortia designed using community metabolic network modeling would be able to effectively degrade a target mixture of VOCs. This was tested with the metabolic network modeling on a curated database of annotated genomes followed by experimental testing for a case scenario of toluene and styrene biodegradation.

2 Critical Assessment of Gassing-In Methods to Determine Mass Transfer Coefficient in Miniature and Microbioreactors with Gas-Liquid Flow[1]

2.1 Introduction

Table 2.1: Parameter Definitions

Parameter	Unit	Definition
K_La	h^{-1}	Overall volumetric gas to liquid (G/L) mass transfer coefficient for the reactor
K_La_{Anc}	h^{-1}	Overall volumetric G/L mass transfer coefficient of the ancillary system
a	$m^2\,m^{-3}$	Specific interfacial surface area between the two phases per reactor volume
T_P	min	DO probe lag constant
V_L	mL	Liquid volume
V_{Anc}	mL	Total ancillary system volume
V_R	mL	Empty reactor volume
V_T	mL	Total volume of the experimental system
F_L	mL min^{-1}	Liquid flow rate
DO_t	mg L^{-1}	Dissolved oxygen concentration at time t
DO_{sat}	mg L^{-1}	Dissolved oxygen concentration at saturation
DO_{in}	mg L^{-1}	Dissolved oxygen concentration at the reactor inlet
DO_{out}	mg L^{-1}	Dissolved oxygen concentration at the reactor outlet
DO_{ss}	mg L^{-1}	Dissolved oxygen concentration at the reactor outlet at steady state
DO_{Anc}	mg L^{-1}	Dissolved oxygen concentration in the ancillary system
DO_{probe}	mg L^{-1}	Dissolved oxygen concentration at the surface of the DO probe
DF_{LM}	mg L^{-1}	Log mean of the DO driving force

[1] This chapter has been published as K. E. Deaton, L. R. López de León, S. Pascual, and M. A. Deshusses, "Critical assessment of gassing-in methods to determine mass transfer coefficient in miniature and microbioreactors with gas-liquid flow," *Biochemical Engineering Journal*, vol. 187, p. 108655, Nov. 2022, doi: 10.1016/j.bej.2022.108655.

Table 2.2: Acronyms

Acronym	Definition
DM	Dynamic gassing-in experimental method
SSM	Steady state gassing-in experimental method
G/L	Gas to liquid
MTC	Mass transfer coefficient
NLR	Non-linear regression
CSTR	Continuously stirred tank reactor
PFR	Plug flow reactor

Oxygen is a critical requirement for aerobic biological systems, when oxygen is used as the terminal electron acceptor. For many engineered biological systems, such as bioreactors, where microorganisms are grown in aqueous media or biofilms, providing sufficient oxygen is often the limiting factor for systems with fast-growing microorganisms [21], [22]. An extensive body of research has focused on maximizing the provision of oxygen to aerobic cultures, particularly in suspended growth systems. In aerobic wastewater treatment, aeration is critical to achieving treatment standards, often limiting the sizing of systems or triggering the use of pure oxygen [23]. As aeration typically accounts for 50-70% of total energy costs in wastewater treatment systems, greater efficiency in oxygen delivery can result in large cost savings [23]. Even biofiltration and gas-phase reactors, which are commonly used for treatment of gaseous waste streams, can be limited by the mass transfer of oxygen or hydrophobic pollutants to the biofilm [24]. For example, the removal of hydrogen sulfide from biogas was improved by increasing the mass transfer of oxygen in previously limited biotrickling filters [22].

Due to the importance of oxygen for aerobic microbial growth, the capacity to transfer oxygen is often used to characterize bioreactors. While the mass transfer coefficient (MTC) can be measured for each compound individually [25], oxygen is the common requirement for all aerobic systems, which makes the gas-to-liquid (G/L) oxygen

MTC a convenient metric for standardized comparison of mass transfer performance. Oxygen transfer from gas to liquid is governed by the driving force for mass transfer, defined as the difference between the dissolved oxygen saturation concentration (DO_{sat}) in the bulk liquid phase when in equilibrium with the gas phase and the current DO in the bulk liquid (DO), and the overall volumetric G/L MTC. Gas-to-liquid mass transfer is often represented by two resistances in series [26] , the resistance on the gas side of the interface $1/k_g$, and that on the liquid side of the interface $1/k_L$. For hydrophobic or insoluble compounds such as oxygen, the rate of G/L mass transfer is generally controlled by the liquid-side resistance, so that k_L can be approximated by the overall volumetric MTC, K_L [20].

In well-mixed reactors consisting of a single control volume, such as an ideal stirred tank reactor, the mass balance on DO as it is transferred from the gas to liquid phase is described by Equation 2.1Equation 2.1.

$$\frac{dDO}{dt} = K_L \cdot a \cdot (DO_{sat} - DO) \qquad \text{Equation 2.1}$$

where K_L is the overall volumetric MTC of oxygen for transfer between gas and liquid phases, and *a* is the specific interfacial surface area between the two phases per reactor volume ($m^2\ m^{-3}$). However, as the interfacial surface area is difficult to quantify in most bioreactor systems, the two parameters are often combined into a single parameter (K_La) that is much easier to measure and is widely accepted to characterize gas-to-liquid mass transfer. Thus, K_La is commonly used to characterize the oxygen transfer capacity of bioreactors and engineered microbial growth systems and compare their design and performance [19], [24], [27], [28].

There has been an extensive body of research on various methods to measure MTCs in widely varied bioreactors. Given the huge scale and public importance of

wastewater treatment, standard methods were needed to characterize aerated treatment reactors. Therefore, standard guidelines were established by the American Society of Civil Engineers (ASCE) for measuring oxygen mass transfer coefficients in these suspended growth systems. These guidelines are only applicable to completely mixed reactors (at small or large-scale) that can be modeled as one control volume [29]. Briefly, the DO of pure water is depleted by sparging with nitrogen gas or by reacting with a reducing chemical such as sulfite. Then, air or oxygen is supplied to the system and the DO increase is monitored over time until it reaches the DO_{sat} (or a value close to it). The value of K_La is then determined by fitting the experimental data to a non-linear regression (NLR) of Equation 2.1 with K_La as the fitting parameter. The ASCE guidelines were written primarily for large-scale wastewater treatment systems such as activated sludge tanks, but are also indicated for most standard continuously stirred tank reactors (CSTR) or bubble columns. This basic method has also become the standard for lab-scale reactors or CSTRs that consist of a single well-mixed tank where the working volume of the reactor is equal or close to the liquid volume [30].

In contrast, other bioreactors that deviate from a standard stirred tank reactor, such as flow through or gas-phase reactors, do not have the benefit of a set of standard guidelines for K_La determination. Many individual studies have developed various methods for the measurement of K_La [31]–[35], yet there has been no collective agreement on a standard method for these alternative reactors. In general, the K_La of biofilters, biotrickling filters, and monolith reactors has been determined by adapting the ASCE method to suit operation of plug flow reactors (PFRs) and the nature of the gas-liquid interfacial area in these reactors being a function of the packing material surface area. In a simple stirred tank reactor, the working volume is generally just the liquid volume, or

sometimes with the gas holdup added. A common practice in biofiltration is to normalize calculations to the entire reactor or bed volume, called the empty reactor volume (often neglecting the matrix volume for porous packed beds), which is then considered the working volume [31], [32] or a study may distinguish between the total volume, porous media volume, and liquid volume in a reactor [36]. Alternatively, a bubble column reactor may be normalized to the volume of liquid or dispersed gas bubbles [34]. Therefore, the reactor working volume (V_R) must be appropriately defined based on reactor type, and should be used in the calculations to properly normalize the volumetric G/L MTC, as described above and shown in Equation 2.22.2, which describes the mass balance on DO in a PFR.

$$V_L \frac{dDO}{dt} = F_L \cdot (DO_{in} - DO_{out}) + K_L a \cdot (DF_{LM}) \cdot V_R \qquad Equation\ 2.2$$

where V_L is the liquid volume, V_R is the reactor working volume, F_L is the liquid flow rate, DO_{in} is the DO concentration in the inlet liquid, DO_{out} is the DO concentration measured in the liquid outlet, and DF_{LM} is the logarithmic mean between the driving force at the inlet (DO_{sat} – DO_{in}) and the driving force at the outlet (DO_{sat} – DO_{out}), as shown in Equation 2.32.3. Note that V_R includes both the volume of liquid V_L and the volume of gas (i.e., the gas holdup).

$$DF_{LM} = \frac{DO_{out} - DO_{in}}{ln\{(DO_{sat} - DO_{in})/(DO_{sat} - DO_{out})\}} \qquad Equation\ 2.3$$

The two most widely used experimental methods to determine $K_L a$ in plug flow reactors are a steady-state measurement method [31] and a dynamic measurement method [35] for oxygen absorption. The steady-state method features constant inlet flows

of aeration gas and deoxygenated water, and measuring the outlet DO at steady state. The rate of oxygen transfer is used to calculate K_La. In the dynamic method, the water is recycled from the outlet back to the inlet (making a pseudo-batch system for the liquid phase) under constant aeration conditions, and the increase in DO is measured over time. The dynamic response (time series) of DO increase is used to calculate K_La. However, many studies further adapt these methods with their own variations to suit their unique experimental set-ups, for instance by including the volume of liquid recycle tubing [35] or nutrient media holding tanks [37] in the calculations, though with the assumption that these ancillary volumes do not contribute to G/L mass transfer even if they include some mechanism for G/L exchange of their own, such as mixing [35]. Some studies use other methods entirely, such as an off-gassing measurement [38], sulfite oxidation [39] or by using correlations [31], [32].

For miniature and microbioreactors, there are several mass transfer determination methods based on a wide variety of techniques such as oxygen absorption, chemical reactions, or others, which have been nicely summarized elsewhere [40], [41], though the most common methods are briefly described here. One method is to analyze the DO concentration at the outlet of a microchannel using oxygen electrodes [42] similar to the dynamic method described above. Another method that is very common due to simplicity is to measure the mass transfer rate of carbon dioxide instead of oxygen, using titration or gas phase concentrations to measure the amount of CO_2 absorbed [43]. Colorimetric methods can also be used to measure the amount of oxygen transferred into the liquid phase using an oxygen-sensitive dye [44] or with an oxygen-reactive enzyme that produces a colorful product [45]. Gas transfer in capillary microreactors can also be determined by measuring the length of gas slugs and their decrease as gas transfers to

the liquid phase [46], [47]. For scientists used to working with bench-scale systems, determination of K_La in miniature and microbioreactors require specific equipment and/or specialized techniques. However, gassing-in techniques using conventional oxygen sensors have not been evaluated for miniature and micro-scale reactors.

Given the variations in experimental methods for determination G/L MTCs in the literature, a set of guidelines and best practices are needed to standardize methods for various reactor types. Furthermore, there has recently been increased interest in the study of capillary bioreactors [20], [48], [49], scaled-down systems [50], [51], and microbioreactor cultivation [52], [53] in fields typically concerned with lab and large-scale processes. Therefore, the goal of this study was to analyze conventional lab-scale methods for the determination of K_La, specifically for their use in characterizing miniature and micro(bio)reactors with plug flow or recirculated flow operation. Given the recent expanded interest in small-scale systems, it would be advantageous to have the option to use readily available equipment and familiar methods. However, there must be critical evaluation of the feasibility and accuracy of conventional-scale methods implemented at much smaller scales. This was done by measuring the oxygen transfer in a miniature reactor using two experimental methods common in mass transfer coefficient determination. A detailed mathematical model was developed for G/L transfer in the microreactor system and adapted to analyze the experimental data obtained using both experimental methods. The mass transfer coefficients obtained from model fitting were compared to those obtained by conventional data analysis methods. Based on the results, guidelines for experimental methods and data analysis procedures are proposed to ensure accurate and consistent determination of mass transfer coefficients across reactor type and scale.

2.2 Experimental Methods

2.2.1 Reactors and Experimental Set Up

A microchannel reactor (Figure 2.1) was used for the mass transfer experiments described herein. The reactor consisted of a monolith microchannel bed placed in an outer gas-tight case. The monolith microchannel bed was designed using AutoCAD Inventor and printed using a 3D Systems Multijet MJP3600 3D printer with a polycarbonate-like filament, VisiJet M3 Crystal (3D Systems, Rock Hill, SC). The outer case was printed with poly-lactic acid filament on an Ultimaker3 3D printer (Ultimaker, Utretcht, Netherlands). The working volume (or empty bed volume) of the reactor was 3.84 mL. The reactor system featured two-phase flow of gas and liquid, typically air and water, with large gas to liquid volume ratios ranging from 1:1 to 7:1.

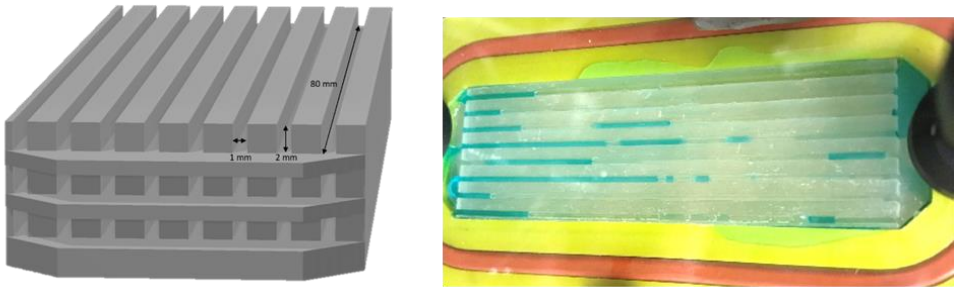

Figure 2.1: CAD design (Left) and picture of the microchannel reactor bed within the case (Right). The reactor includes 24 channels, each 1 x 2 x 80 mm. The picture on the right shows the reactor in its gas-tight case, and with blue food coloring used to show the liquid phase.

2.2.2 Dynamic Method Experimental Set Up

The Dynamic Method (DM) was adapted from the ASCE Standard Method for Measurement of Oxygen Transfer in Clean Water [29]. The standard method is intended for a reactor that can be modeled as a simple, completely mixed batch reactor, whereas the reactor system described here is more appropriately modeled as plug flow with liquid

recycle. The experimental set up is depicted in Figure 2.2. Deionized (DI) water was used as the liquid phase and the total liquid volume of the system was kept constant at 20 mL. All experiments were conducted at room temperature (22 ºC) and temperature of the water was monitored to be consistent with room conditions. Before each test, the DO concentration in the water was reduced to 0.1 – 0.5 mg L^{-1} by sparging with purified nitrogen gas (N_2) through the gas inlet. When a low DO reading was reached, the gas inlet was quickly switched to the aeration gas, either air or pure oxygen, which was fed to the inlet tee and kept at a constant flow rate of 100 mL min^{-1} by a mass flow controller (Alicat Scientific, Tucson, AZ). The water was fed to the inlet tee of the reactor by a peristaltic pump (Masterflex, Vernon Hills, IL) at flow rates ranging from 14 to 88 mL min^{-1}. From the inlet tee, the gas and liquid phases flowed through the reactor and into a 10 mL reservoir, or DO probe sampling container, where an optical DO probe and data logger (Vernier, Beaverton, OR) continuously recorded the DO of the water coming out of the reactor at a sampling rate of one point per second. The channels within the reactor were too small for any off-the-shelf oxygen sensors, so the DO had to be measured once the water left the reactor. The DO probe was inserted through the bottom of the DO probe sampling container and arranged facing upwards to prevent the attachment of gas bubbles from interfering with the measurement. The gas phase was allowed to exit the system through the top of the DO probe sampling container. The water was recycled back to the inlet using 3 mm ID PVC tubing, creating a closed-loop system for the liquid phase. The DO was measured until the DO saturation value (DO_{sat}) was reached, i.e., 8.6 – 9.0 mg L^{-1} when air was used as the aeration gas. The DO_{sat} value is constant throughout the system, but was measured to capture any potential variation due to changes in ambient conditions or probe variability.

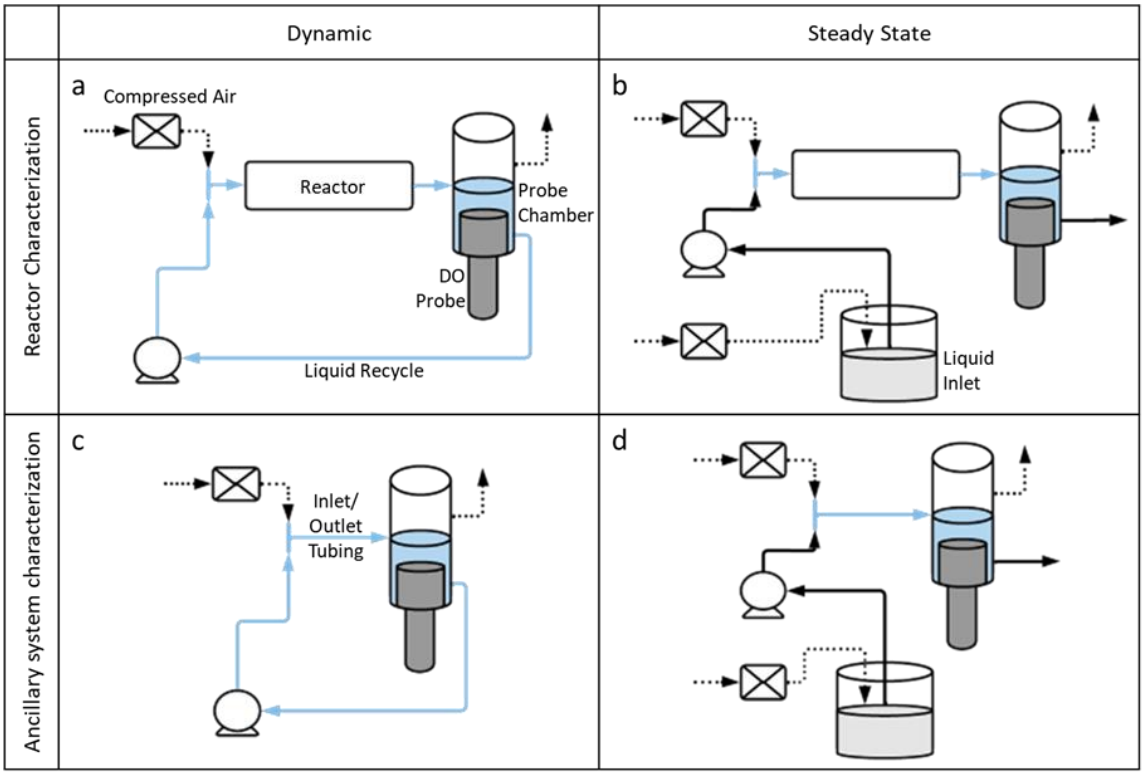

Figure 2.2: Diagrams of the experimental setups. Dotted lines represent gas flow. Solid lines represent liquid flow. Blue coloring denotes the ancillary system, consisting of the liquid volume in the DO probe sampling container, the inlet/outlet tubing, and recycle tubing.

As will be discussed in detail, for miniature reactors, volumes other than the reactor volume can play an important role. We designated these volumes as the *ancillary system*. The ancillary system refers to all liquid-containing volumes excluding the reactor. For the DM, the ancillary system includes the inlet, outlet, and recycle tubing and the DO probe sampling container, as shown in Figure 2.2c and in blue in the reactor experimental set up in Figure 2.2a. The mass transfer contribution from the ancillary system was measured in order to account for differences in experimental set up, for example, liquid volume or length of tubing. Thus, mass transfer investigations were conducted as described above, except for the absence of the reactor, to determine the G/L MTC of the ancillary system alone (K_La_{Anc}). The gas and liquid phases met at the inlet tee, flowed through the inlet and

outlet tubing to the DO probe sampling container, and the water was brought back to the inlet through the recycle tubing.

2.2.3 Steady State Experimental Set Up

The Steady State Method (SSM) was adapted from a study on determining mass transfer coefficients in biofilters [31], which itself adopted methodologies for flow-through reactors in which fast gas-liquid mass transfer occurs and/or for which the dynamic method may not be practical. The SSM was based on the same conceptual mass balance on DO as that of the DM. The complete reactor system is shown in Figure 2.2b while the ancillary system alone is shown in Figure 2.2d. The SSM differs from DM by not recycling the water from the effluent port back to the inlet. Instead, a once through mode is used for both gas and liquid and the steady state DO concentration is measured. Deoxygenated water was pumped to the inlet tee from a flask of DI water that was constantly sparged with N_2 gas to maintain a DO close to 0 mg L^{-1}. The gas and water then flowed out of the reactor via outlet tubing to the DO probe sampling container where the DO of the water was measured. The volume of water in the DO probe sampling container was kept constant at 10 mL, with the total volume of water in the system was 11 mL. The water passed through the DO probe sampling container and was discharged to a collection reservoir. The DO was measured until a steady state value (DO_{SS}) was held for at least one minute. The DO_{sat} value was measured prior to experiments by recording the DO value of air-saturated water. For the SSM, the ancillary system includes the inlet and outlet tubing and the DO probe sampling container.

2.2.4 Dynamic Method Conventional Data Analysis

Simple spreadsheet analysis has been the conventional approach to determine the value of G/L K_La when using the dynamic method. The conventional data analysis for

DM, following the ASCE Standard guidelines for procedure and parameter fitting [29], [30], determines the value of $K_L a$ by fitting a non-linear regression (NLR) to experimental data using Equation 4, which is the general solution to Equation 2. In this work, fitting experimental data was conducted using the Solver function in Microsoft Excel by changing the values of $K_L a$ and DO_{sat} to fit the experimental data by minimizing the square of the difference between the experimental DO value at each time point and the calculated value from Equation 2.4.

$$DO_t = DO_{sat} - \left[\frac{DO_{sat} - DO_{initial}}{e^{\left(K_L a \cdot t \cdot \frac{V_R}{V_L}\right)}}\right] \qquad Equation\ 2.4$$

The use of Equation 2.4 requires the following assumptions: (i) isothermal conditions, (ii) complete mixing throughout the liquid volume, (iii) the main resistance to oxygen mass transfer is in the liquid film, which has been characterized previously in similar reactors, thus volumetric $k_L a$ can be assumed to be the overall volumetric $K_L a$ [19]; (iv) the mass transfer coefficient is constant through the reactor; (v) there is no axial dispersion; (vi) the oxygen concentration in the gas phase is not depleted significantly, thus the driving force can always be represented by (DO_{sat} – DO).

2.2.5 Steady State Method Conventional Data Analysis

For SSM, the conventional approach is to calculate $K_L a$ analytically solving Equation 2.5, which was derived from Equation 2.2 by assuming steady state conditions ($\frac{dDO}{dt} = 0$).

$$K_L a = \frac{F_L}{V_R} \ln\left(\frac{DO_{sat} - DO_{in}}{DO_{sat} - DO_{ss}}\right) \qquad Equation\ 2.5$$

2.2.6 Measurement of DO Probe Response Time

To correct for any potential error caused by probe lag [54], the probe lag constant (T_P) was measured and then accounted for in calculations. The probe lag constant was determined experimentally by quickly transferring the DO probe from a beaker with deoxygenated water to a well-mixed beaker with air-saturated water and the experimental data were fit to a first-order lag equation by fitting T_P to Equation 2.6 [55].

$$\frac{dDO_{probe}}{dt} = \frac{DO_L - DO_{probe}}{T_P} \qquad Equation\ 2.6$$

Equation 6 illustrates that the DO measured at the surface of the DO probe, lags from the true DO in the liquid phase of the DO sampling container. A first order response is assumed between the true liquid DO concentration and the DO probe reading [54].

2.3 Model Development

2.3.1 Theory and Approach

A mathematical model of G/L transfer in the microreactor was developed in this work and adapted to each mass transfer coefficient determination method. The modeling approach attempts to improve the accuracy of K_La determination compared to the conventional data analysis approaches by adding details that capture the full complexity of the reactor and DO measurement systems. The model was based on advection along the reactor and gas-liquid mass transfer, represented by the fundamental mass balance on the DO concentration (Equation 2.2). The model was based on the same assumptions listed for Equation 2.4 with the following exceptions or additions (i) ideal plug flow through the reactor; (ii) the air flow is one-pass, exiting through the top of the DO probe sampling

container; (iii) the DO is constant throughout the ancillary system (i.e. complete mixing in the DO probe sampling container and concentration remains constant in the recycle tubing).

Model variations for each determination method were based on the same set of mass balance equations for the DO in the reactor, the DO in the liquid DO sampling container, and at the probe itself, but different boundary conditions. The model equations were solved numerically. The reactors were discretized in the axial direction using an array, as is often done with plug flow reactors [55], [56] which entailed discretizing the reactor volume into ten finite elements, as shown in Figure 2.3. The number of finite elements (N) to use was determined by a simple sensitivity analysis, resulting in a N large enough to accurately approximate plug flow and additional finite elements did not significantly change the resulting values from the model simulations.

For the mathematical models, the K_La value was determined by fitting the model equations and outputs to the experimental DO probe data by adjusting the value of K_La. For the dynamic method, time series of DO increase were used for K_La fitting, while in the steady state method, the model was fitted to steady state DO values after the model was allowed to reach steady state. A schematic representation of the mathematical model is shown in Figure 2.3, and mass balances are developed next.

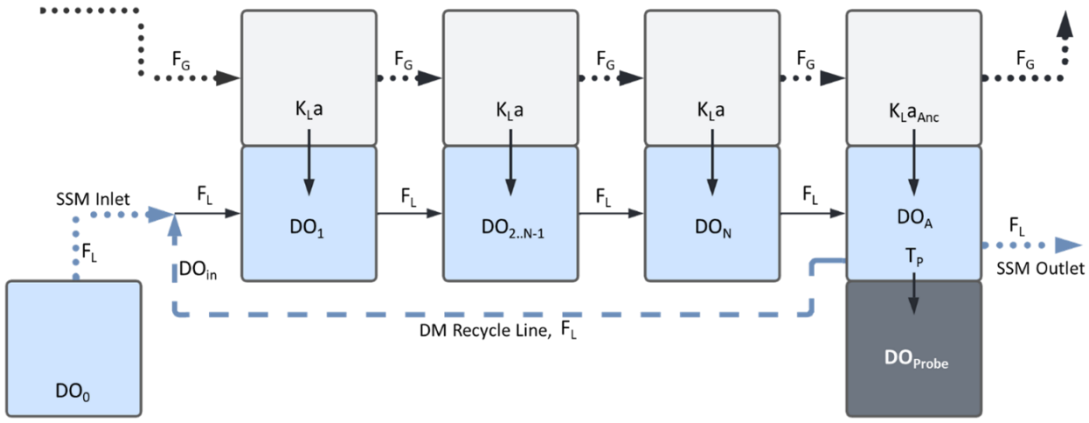

Figure 2.3: Generalized conceptual schematic of the mathematical model. The difference between the models for the two methods is shown with the dotted and dashed lines. The dashed line represents the DM liquid recycle line, part of the DM ancillary system, that transports liquid from the DO probe sampling container back to the inlet. Dotted lines represent the SSM liquid inlet and outlet lines. Light gray boxes represent the gas phase, blue boxes the liquid phase, and the dark gray box represents the DO probe. The gas and liquid phases are shown here as fully separate for simple schematic purposes, and more closely resemble slug flow or annular flow [57] depending on the operational conditions.

2.3.2 Mass Balances on DO in the Reactor System

Equation 2.7 describes the DO in the liquid phase in the first finite element of the reactor, where the water enters the reactor. For the DM, water enters the reactor from the ancillary system liquid recycle line such that $DO_{in} = DO_A$. For the SSM, water enters the reactor from a beaker constantly sparged with N_2 gas, such that $DO_{in} = DO_0$.

$$V_{L,i}\frac{dDO_{i=1}}{dt} = F_L \cdot (DO_{in} - DO_1) + K_L a \cdot (DO_{sat} - DO_1) \cdot V_{R,i} \qquad Equation\ 2.7$$

Equation 2.8 describes the DO in the liquid phase through the subsequent finite elements of the reactor, until the final, or N^{th}, element.

$$V_{L,i}\frac{dDO_{i=2..N}}{dt} = F_L \cdot (DO_{i-1} - DO_i) + K_L a \cdot (DO_{sat} - DO_i) \cdot V_{R,i} \qquad Equation\ 2.8$$

2.3.3 Mass Balances on DO in the Ancillary System

DO mass balances on the ancillary system differ slightly depending on the experiment. When the reactor is used, Equation 2.9 describes the DO in the liquid phase of the ancillary system, consisting of the DO probe sampling container and the liquid recycle line for DM, or the DO probe sampling container only for SSM.

$$V_{L,A}\frac{dDO_A}{dt} = F_L \cdot (DO_N - DO_A) + K_L a_{Anc} \cdot (DO_{sat} - DO_A) \cdot V_A \qquad Equation\ 2.9$$

To model experiments used to characterize the ancillary system alone (i.e., without the reactor) in the DM, the DM ancillary system is modeled as an ideally mixed system and represented by Equation 2.10.

$$V_{L,A}\frac{dDO_A}{dt} = K_L a_{Anc} \cdot (DO_{sat} - DO_A) \cdot V_A \qquad Equation\ 2.10$$

For the characterization of the ancillary system using the SSM, it is modeled as a plug flow system, with water and gas entering the system at the inlet and exiting after the DO probe sampling container. The SSM ancillary system is represented by Equation 2.11. Experimentally, the DO_{in} value was measured in the inlet beaker with an additional DO probe.

$$V_{L,A}\frac{dDO_A}{dt} = F_L \cdot (DO_{in} - DO_A) + K_L a_{Anc} \cdot (DF_{LM}) \cdot V_A \qquad Equation\ 2.11$$

Note that in Equation 2.11, a log mean of the DO at the inlet and outlet (DF_{LM}) is used for simplicity, though the ancillary system could equally be modeled using finite elements.

2.3.4 Including DO Probe Response Time in Each Model

In the system of equations for the model, Equation 2.6 is the final equation, with the liquid DO from the ancillary system (DO_A) as the input instead of DO_L, and DO_{probe} is

the parameter fitted to experimental data. Thus, the ancillary system model consists of an ancillary equation (2.9, 2.10 or 2.11) and the probe lag equation (2.6). The reactor system model consists of a reactor equation (2.7-2.8), an ancillary equation (2.9-2.11), and the probe lag equation (2.6). The ancillary systems were measured experimentally and the K_La_{Anc} values determined before analyzing the reactor data, so that the K_La_{Anc} value could be used as a fixed parameter for the reactor models.

2.3.5 Model Evaluation

The model outputs were evaluated using the Standard Error of Prediction (SEP, %), also referred to as a Normalized Root Mean Squared Error (NRMSE), which was calculated according to Equation 2.12. The Root Mean Squared Error (RMSE) is normalized by the range of DO values measured.

$$SEP\ (\%) = \frac{RMSE}{(DO_{max} - DO_{min})} \times 100\% \qquad Equation\ 2.12$$

2.4 Results and Discussion

2.4.1 Evaluation of Experimental and Data Analysis Methods

Typical oxygenation curves for both experimental methods are shown in Figure 2.4. The typical DM curve, shown in Figure 2.4 (Left), starts at a low DO (0.1-0.5 mg L^{-1}) and increases until reaching DO_{sat}. DM DO curves typically featured a delay of a few seconds when the gas was switched from N_2 to air before the DO probe recorded an increase in the oxygen concentration. This delay was partly due to the physical delay of transit time, approximately 2.7 s, for the gas to travel from the inlet tee to the DO probe sampling container, and partly due to probe lag. The DO profile increases more rapidly for tests operated at higher liquid flow rates, reaching DO_{sat} more quickly. Alternatively for SSM, DO had various initial values, depending on the previous measurement. Regardless

of the initial value, the DO would increase or decrease to reach the new steady state value for that condition, as seen Figure 2.4 (only the steady state is shown). It was observed that the DO_{ss} value was higher for lower liquid flow rates and lower for higher liquid flow rates (not shown), as expected from a simple mass balance (see Equation 2).

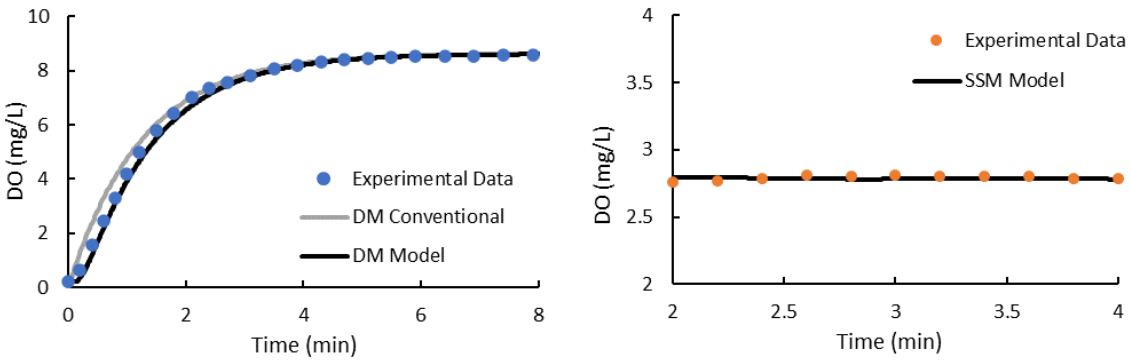

Figure 2.4: Typical fits of models and data analysis to experimental data. (Left) A typical fit of the conventional DM data analysis (NLR, Equation 4) and the DM model to DM experimental data (F_L=40 mL min^{-1}) and (Right) A typical fit of the SSM model to SSM experimental data (F_L=88 mL min^{-1}). All tests were conducted with a gas flow rate of 100 mL min^{-1}. SSM conventional data analysis (Equation 5) is not shown because it is only one point. Experimental data (collected at 1 datum/s) were trimmed for the graph to show individual data points.

Figure 2.4 also shows the fit for the mathematical models to the experimental data. The average standard error of prediction (SEP) for the DM model to experimental data was 1.4% (± 0.3%). A conventional NLR also fits the DM experimental data well (average SEP 1.4% ± 0.5%), but the initial lag data must be trimmed, and the NLR-fitted K_La values are 1.5 – 2 times those fitted by the DM model. SSM data were fit to the steady state portion of the data with average SEP of 5.1%. One of the benefits of the SSM is that, once at steady state, lags no longer have any effect, so probe lag is not a concern.

The G/L K_La of the reactor at various flow conditions determined by each experimental method and data analysis approach are shown in Figure 2.5. In general, the K_La increased roughly linearly with increasing liquid flow rates, the same trend as seen in other studies [31], [55]. When the data were analyzed by conventional data analysis approaches (Equation 2.3-2.4), the reactor K_La values were significantly different between the experimental methods ($p=0.03, 0.01, 0.02$ at $Q_L=40, 70, 88$, respectively), using paired 2-tailed t-test. Conventionally analyzed SSM data produced a K_La of 600 h^{-1} at the highest liquid flow rate tested (88 mL min^{-1}), while conventional analysis of DM data at the same conditions determined the K_La to be only 387 h^{-1}. Using conventional data analyses, SSM K_La values were substantially higher than DM K_La values, as shown in Figure 2.5 and Figure 2.6. Since the flow conditions through the reactor were the same for each experimental method, the same mass transfer coefficient should have been obtained.

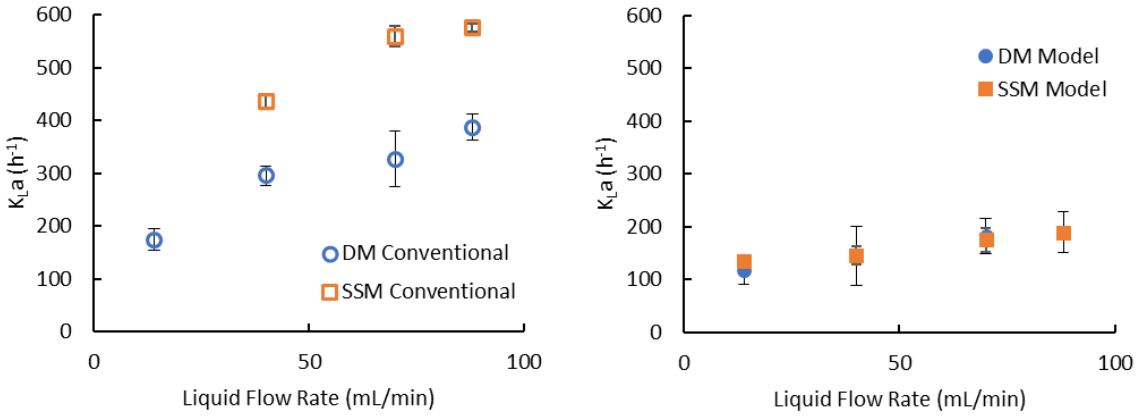

Figure 2.5: Comparison of the reactor K_La values determined by each data analysis method. Conventional (open symbols) or mathematical model (solid symbols) for DM (blue circles) and SSM (orange squares).

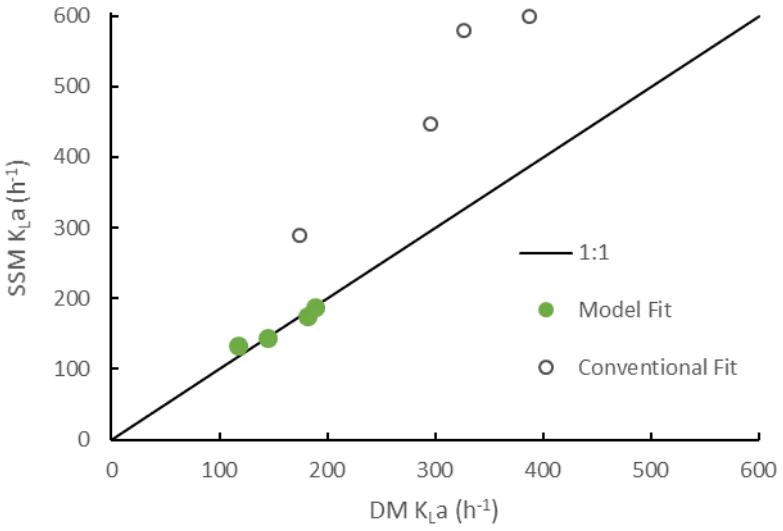

Figure 2.6: Comparison of K_La values between the two experimental methods when the data are analyzed by conventional methods (open circles) or fitted to the models developed here (green circles).

Alternatively, the K_La values obtained from both experimental methods were very similar when the K_La values were fit using the mathematical model ($p=0.99, 0.43, 0.41$ at Q_L (ml min^{-1}) =40, 70, 88, respectively, using paired 2-tailed t-test). At the highest liquid flow rate, the model fit of SSM data resulted in an average K_La of 203 h^{-1}, while fitting of DM data yielded an average value of 189 h^{-1}, i.e., not statistically different. This observation was valid at all tested flow rates: model-fit values of K_La were consistent between experimental methods, as shown in Figure 2.6.

The agreement between each experimental method when using the model to determine K_La values strongly supports the findings that both experimental methods are valid and that model-fit values are accurate, whereas conventional data analysis does not allow accurate determination of K_La values at this scale.

2.4.2 Importance of the Ancillary System

Results for the G/L MTC for the ancillary systems (K_La_{Anc}) are shown in Figure 2.7. The values of K_La_{Anc} increased linearly with increased liquid flow rate, up to 70 h^{-1} for DM ancillary. Two sets of experiments are shown for SSM ancillary: one set of experiments conducted with a V_L of 10 mL, which corresponds to the SSM reactor experimental system, and the other at 17 mL, which was the liquid volume used in DM ancillary experiments, in order to facilitate comparison between the two ancillary systems. The value for the SSM ancillary K_La_{Anc} peaked at 133 h^{-1} for a V_L of 10 mL and 108 h^{-1} for a V_L of 17 mL at the second highest liquid flow rate (70 mL min^{-1}) and then slightly decreased to 165 h^{-1} and 101 h^{-1}, respectively, at 88 mL min^{-1}, which is a trend that was also observed in our other microbioreactor study [20]. In microchannels, it has been shown that K_La can decrease at higher liquid velocities due to change in flow pattern [58] or slug size [34], which affects interfacial area, though the specific reason here was not evaluated. In contrast to the reactor results shown in Figure 2.5, K_La_{Anc} results presented in Figure 2.7 show that there was no significant difference between the K_La_{Anc} values determined by conventional or model data analysis. This was because the ancillary system was modeled as one control volume (see Equation 2.9), like a simple batch or plug flow reactor, which is modeled with only one equation. The model-fit values for the ancillary DM may be slightly more accurate than the NLR as the model accounted for probe lag. The K_La_{Anc} values from the SSM experiments were higher than the K_La_{Anc} values from the DM experiments at all test conditions and even at the same overall liquid volume. The difference between the experimental method K_La_{Anc} values was smallest at the lowest liquid low rate and greatest at 70 mL min^{-1}. Despite attempts to make the experimental systems as similar as possible, there were minor differences between the experimental configurations (e.g., in tubing

volume and configuration) and the values of K_La_{Anc} reflect these differences between the methods. This highlights the importance of measuring, as well as minimizing, the K_La_{Anc} of the ancillary system for each experimental set up, so that any differences in the ancillary system are accounted for and will not be mistaken for differences in the K_La of the reactors.

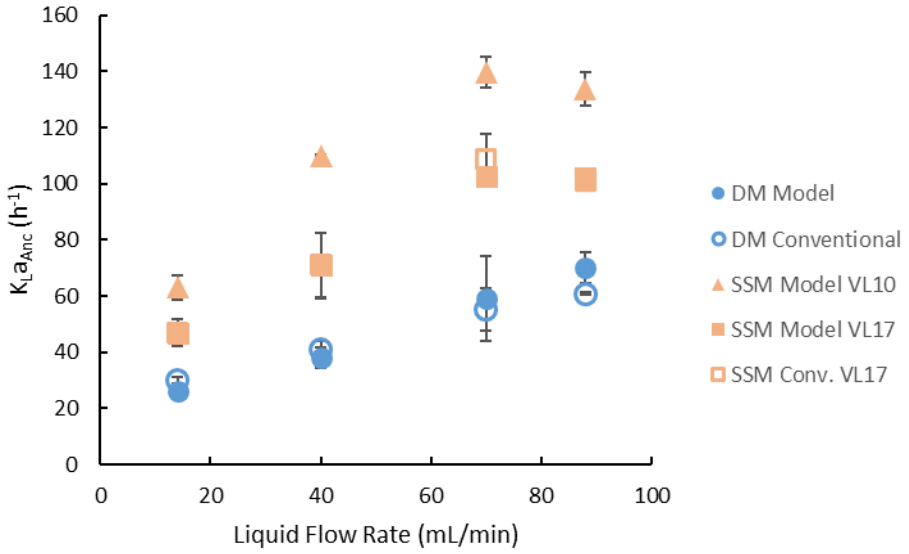

Figure 2.7: Comparison of the K_La_{Anc} values for the ancillary system determined by conventional data analysis or model-fitting for both experimental methods. Values are also reported for SSM ancillary systems of different liquid volumes.

The importance of accounting for the ancillary system to accurately characterize the G/L MTC is illustrated in Figure 2.8, which shows K_La values obtained from SSM experiments, but determined using various data analysis approaches. Using the exact same data set, the conventional SSM analytical equation (Equation 2.5) resulted in a K_La value of 600 h^{-1} at the highest flow rate, while the SSM model-determined K_La value was only 203 h^{-1}. However, if the value of K_La_{Anc} in the SSM model was manually changed from 133 h^{-1} to 0 h^{-1} (in effect neglecting mass transfer in the ancillary system), the model

predicted the K_La of the reactor to be 570 h^{-1}, a much closer value to that determined by the conventional equation. This indicated that the conventional analysis overestimated the reactor's K_La by not accounting for the aeration contributed by the ancillary system. This also clarifies that the DM model-fit and NLR-fit values for K_La were different despite both having a good fit to the data (see Figure 2.4) because the NLR incorrectly attributes all of the oxygen transfer to the reactor volume.

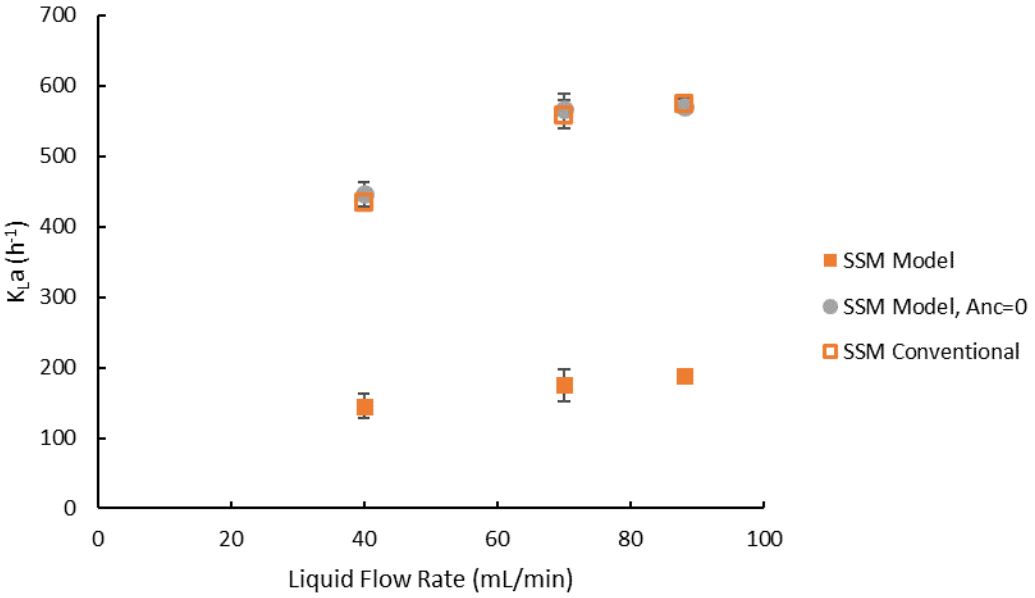

Figure 2.8: Comparison of the reactor K_La values from different data analysis methods of the same SSM experimental data.

A discussion comparing the ancillary and reactor MTC values is warranted. As discussed previously, at the highest flow rate tested, the K_La_{Anc} value for the ancillary system was 70 h^{-1} when using the DM and 133 h^{-1} when using the SSM, compared to the reactor K_La of 189 h^{-1} and 203 h^{-1}, for the DM and SSM, respectively. Based on the MTC alone, the reactor appears to surpass the ancillary system. However, to determine the Oxygen Transfer Rate (OTR), the volumetric rate must be multiplied by the reactor or

ancillary volume. If taking the maximum K_La values and assuming a DO of zero, considering the reactor and ancillary volumes, the max OTR of the reactor is 6.1 mg h^{-1}, compared to 10.7 mg h^{-1} and 12 mg h^{-1} for the ancillary system, using DM or SSM values, respectively. Thus, although the ancillary system has a lower overall volumetric MTC, a greater total mass of oxygen can be transferred within the ancillary system than in the reactor due to the much larger volume of the ancillary system. This is consistent with our observation that the gas-liquid flow through the inlet and outlet tubing strongly resembles a slug flow pattern, which is characterized by high G/L mass transfer rates [40], [48].

Several microfluidic studies have highlighted for the importance of the ancillary system in mass transfer coefficient measurements, which in microfluidic contexts is often referred to as “end effects” of the inlet and outlet to a microfluidic channel. For example, one recent study by Li et al (2018) investigated the contribution of each segment of their liquid-liquid capillary microreactor system: the inlet T-micromixer, the capillary reactor, and the sampling zone, determining a coefficient for each section as well as an overall volumetric mass transfer coefficient for the entire system [59]. They found that each section contributed significantly to the transfer between phases, with the inlet T-micromixer contributing between 34-78% to the mass transfer [59]. Therefore, the large contribution of the ancillary system here is consistent with prior findings. Further, it is reasonable to assume that the majority of the mass transfer within the ancillary system happens in the inlet and outlet tubing, rather than the DO probe sampling container and recycle tubing, which are mostly free of gas bubbles.

Alternatively, most studies determining mass transfer coefficients in lab- and large-scale reactors have ignored the ancillary system or assumed that it did not contribute to mass transfer. For example, in one of the first papers to determine mass transfer

coefficients in biofilters by Kim & Deshusses (2008), the inlet and outlet of the ancillary system was not considered in calculations [31]. In a more recent paper by Estrada et al (2014), a mathematical model was used to determine K_La by fitting the model to experimental data of DO concentration in a lab-scale biotrickling filter [35]. This model assumed that all oxygen absorption took place within the biotrickling filter (4 L volume) and that no mass transfer took place within the mixing tank or liquid recycle tubing (1 L volume) [35]. A major difference between these lab-scale studies and the study presented here is the relative volume of the reactor to the ancillary system, which was 4:1 for the lab-scale system by Estrada et al., compared to 1:5 for the microchannel reactor studied here. It is not clear at what ratio the ancillary system can be safely ignored. As a simple demonstration of OTR, with a theoretical reactor of 100 mL and K_La of 100 h^{-1}, a reasonable MTC for stirred tanks or biofilters, with an ancillary system of only 10 mL with a max K_La of 50 h^{-1}, which is a reasonable value as shown here, the ancillary system could still provide as much as 5% of the oxygen transferred in the system. A theoretical 50 mL bioreactor with the same K_La of 100 h^{-1} and the same ancillary system might attribute 10% of the oxygen transferred to the ancillary system, which is certainly too large to ignore. Analysis of bioreactors with higher MTCs or larger reactor to ancillary volume ratios may be able to neglect the contribution of the ancillary system. Ultimately, it will depend on how much G/L mass transfer is occurring in parts other than the actual reactor, which must be experimentally measured before safely making further assumptions. Furthermore, it is reasonable to assume there is a lower limit to the microreactor volume that can be studied with typical lab-scale DO probes, even with fast response times.

2.5 Conclusions and Recommendations for Best Practices

Steady-state and dynamic gassing-in mass transfer methods were shown to be valid for use in flow-through miniature and microbioreactors when the data were analyzed with a mathematical model accounting for the mass transfer contribution of ancillary systems, i.e., parts other than the actual reactor. In order to obtain accurate MTCs for any reactor type with ancillary volumes, there must be precise measurements of the ancillary volume, the ancillary MTC, and the DO probe lag (for the DM), in addition to the typical measurements of the reactor. It should be best practice for studies to clearly state the reactor K_La and the ancillary system K_La_{Anc} separately, along with their respective volumes. Authors must also clearly specify how each volume is defined, for example if V_L refers to the volume of liquid within the reactor itself or within the entire system.

This work shows that conventional lab-scale and large-scale mass transfer characterization methods can be accurately adapted at small-scales, giving researchers the ability to adapt familiar methods to miniaturized prototypes, rather than employ methods more commonly used in lab-on-a-chip and microfluidics studies, which might not be directly applicable to larger systems. However, the conventional data analysis methods must be corrected for implementation at smaller scales. The improvements and adaptations of classic methods shown here, along with clarifications of the ancillary, reactor, and whole system MTCs will allow for clear comparisons of reactor designs and new technologies.

3 Evaluation of Microbioreactor Design on Performance: Mass Transfer and Continuous Biological Operation

3.1 Introduction

The study of key parameters influencing design and manufacturing of microbioreactors is critical to achieving high performance with these devices. Design parameters such as microchannel size, geometry, and length are factors that require thorough study for their impact on microbioreactor performance and function. However, testing each possible design combination in full, long-term operation with microorganisms would be a massive undertaking. Therefore, it is important to be able to rapidly test design prototypes for abiotic performance indicators that can serve as predictors of microbioreactor performance.

Mass transfer is typically a key parameter for predicting a bioreactor's performance for cultures treating volatile pollutants. High mass transfer rates between the gas and liquid phase are a critical requirement to ensuring that microorganisms are supplied with sufficient oxygen and gaseous or vapor substrate. Many reactor systems operating with suspended growth or two-phase flow are mass transfer-limited, so attempts to increase performance often focus on mechanisms to increase the rates of mass transfer [60]. The capacity for mass transfer in a reactor is characterized by the mass transfer coefficients (MTCs): $1/k_Ga$ represents the gas-side resistance to mass transfer and $1/k_La$ represents the liquid side resistance to mass transfer. For air-water two-phase flows, the resistance to transfer for oxygen and other sparingly soluble compounds is generally dominated by the liquid side and thus, the overall mass transfer coefficient, K_La, can be assumed to be approximately equal to the liquid side coefficient. K_La can be rapidly and easily determined with oxygen absorption experiments in lab-scale and large-scale bioreactors [61]. The K_La

of these conventional-scale reactors can now be directly compared to the K_La of microbioreactors using the adapted methods described here in Chapter 2 [62]. The fundamental contribution of mass transfer to performance and the ease of determining K_La makes it an ideal parameter for predicting biological performance of microbioreactor prototypes.

Several studies have examined the effect of microfluidic channel design on two-phase transfer phenomena. The majority of studies on mass transfer in microchannels have focused on two-phase flow in single channels [40]. One study found that mixing (which enhances transfer *via* convection) was eight times higher for gas-liquid two-phase flow in meandering channels than in straight channels [63]. Another study found that the cross sectional geometry of the microchannels (square, round, trapezoidal) and the configuration of the inlet where the gas and liquid flows meet also have a major impact on the mass transfer coefficients by impacting the flow regime [13]. Flow patterns have been shown to be related to mass transfer, with slug flow or Taylor flow typically found to be associated with higher K_La [58]. In a study of liquid-liquid two phase flow in capillary reactors with internal diameter of 0.8, 1.6, and 3.0 mm, higher MTCs were inversely correlated with channel diameter when controlled for liquid velocity [64].

The majority of studies on mass transfer in microbioreactors have been abiotic. There remained a gap in the literature connecting the increase of mass transfer coefficients with improvement of microbial cultivation outcomes. Therefore, the objective of this study was to evaluate the effects of important design parameters on the performance of microbioreactors featuring a monolithic bed of parallel microchannels. Performance of the microreactors was evaluated based on the overall mass transfer coefficient of oxygen (K_La), and biodegradation rates of toluene as a model hydrophobic

VOC. Furthermore, microbioreactor designs were assessed for the feasibility of continuous microbial cultivation and toluene vapor biodegradation, with the aim of finding designs and operation yielding minimal clogging and minimizing the need for operational intervention.

3.2 Methods

3.2.1 Microbioreactor Design and 3D Printing

The overarching goal of the design was to have a rapid prototyping platform where new reactor designs could be quickly exchanged and tested. This was achieved by designing and constructing microbioreactors consisting of two main parts: an outer gas-tight case that easily connected to the experimental system and an inner microbioreactor bed of varying dimensions that could be swapped in and out. An image of a selection of the microbioreactors system is shown in Figure 3.1.

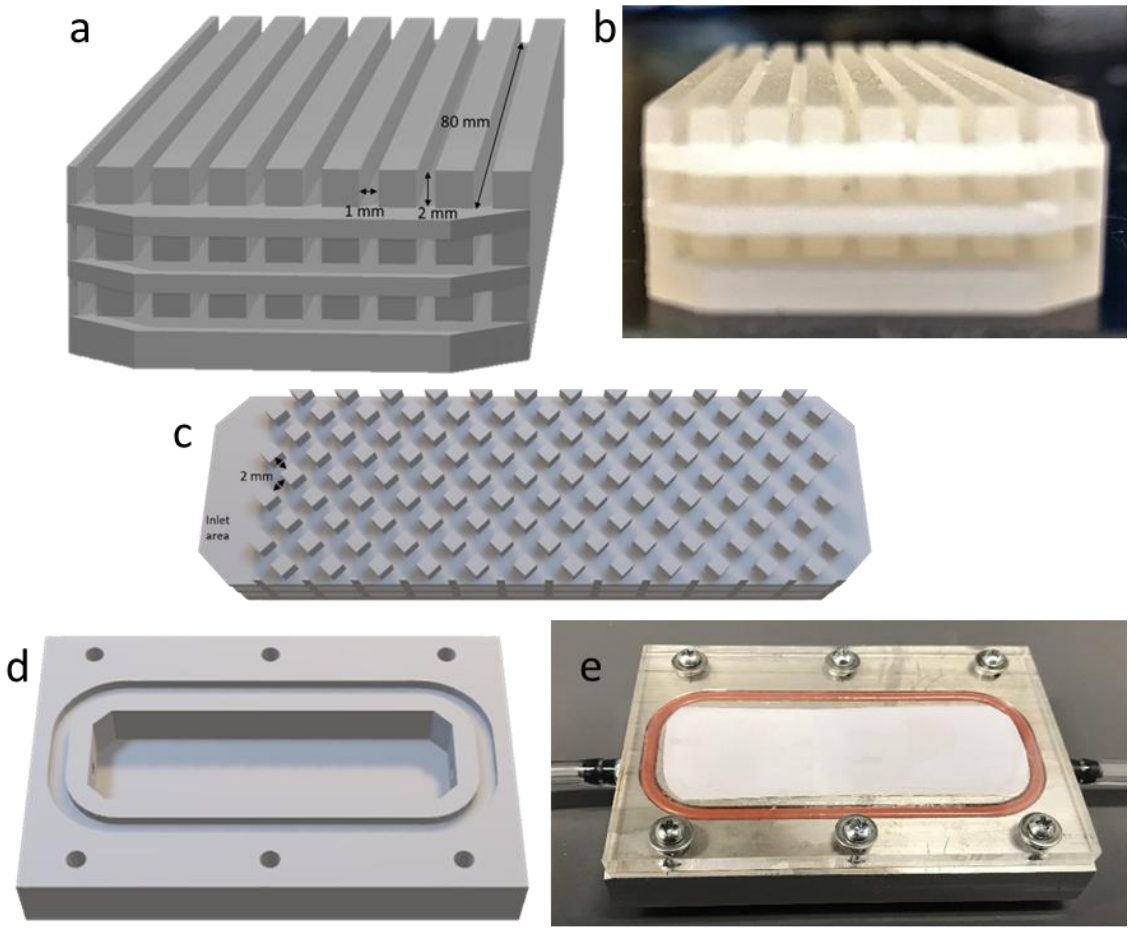

Figure 3.1 CAD designs and photos of microbioreactors. a) CAD design of Reactor 2-S (1x2 mm straight channels) b) 3D print of Reactor 2-S, c) CAD design of Reactor 4-P (2x2 mm patterned channels), d) CAD design of the reactor case bed, and e) the machined case with a microbioreactor sealed by waterproof tape and the acrylic lid for operation.

The microbioreactor beds used in this study were designed as a monolith piece with 21 to 72 parallel microchannels through the bed. The microbioreactor beds were designed using AutoCAD Inventor with either straight rectangular channels or with a zig-zagged channel pattern, and with channel dimensions varying from 0.5 mm to 10 mm in width and height. The cross-sectional area of a single channel (A) was defined as the width x height (mm^2) and the total area was single channel A x the number of channels.

The specifications of all microbioreactor beds tested experimentally are given in Table 3.1. The microbioreactor beds were 3D-printed using a 3D Systems Multijet MJP3600 3D printer with a polycarbonate-like filament, VisiJet M3 Crystal (3D Systems, Rock Hill, SC). The post-processing of 3D-prints first consisted of incubation at 30ºC, at which temperature the Crystal polymer remained solid but the support material would melt out. For microbioreactor beds with channel A ≤ 1 mm^2, manual removal of support material was needed, which was done by scraping out channels using 26 to 30 gauge metal wire and flushing with alternate rinses of warm water and isopropyl alcohol.

Table 3.1: Specifications of the various microbioreactor beds.

Reactor ID	Channel Geometry	Channel A (mm^2)	Total A (mm^2)	V_R (mL)
0.5 S	Straight	0.5	36	3.4
1 S	Straight	1	48	4.5
1 P	Patterned	1	21	5.6
2 S	Straight	2	48	4.5
2 P	Patterned	2	48	9.0
4 S	Straight	4	72	6.2
4 P	Patterned	4	54	9.1
8.5 P	Patterned	8.5	51	10.2

The outer cases were also designed using AutoCAD inventor. The case consists of two halves, a bottom base in which the reactor bed is placed and a top lid. All parts for the case were from McMaster-Carr (Elmhurst, IL). The bottom base was machined out of a ½" sheet of multipurpose 6061 aluminum. An ultra-chemical resistant silicone O-ring was placed in a groove machined into the aluminum around the void in which the reactor is placed. The top lid was cut from a sheet of clear polycarbonate. A 10-32 threaded hole was tapped at both lengths of the base for the inlet and outlet, into which a plastic barbed tube fitting was connected and sealed with epoxy resin. Five replicate cases were made.

A piece of waterproof tape was placed over the reactor to seal the small gap between the reactor bed and the base. The lid was then placed on top of the taped reactor and the lid and base were closed with screws, forming a gas-tight seal with the O-ring. The parts were removable and the microbioreactor beds were interchangeable in the case.

3.2.2 Mass Transfer Coefficient Determination

The overall gas-liquid (G/L) volumetric MTCs (K_La) were experimentally determined using the Dynamic Method and corresponding mathematical model described previously in Chapter 2 [62], which includes detailed accounting of mass transfer each component in the experimental system: the mass transfer in the reactor and contribution of the ancillary system, the effect of probe lag, and flow description. Here, the “ancillary system” refers to all liquid-containing volumes excluding the microbioreactor. Thus, it includes the inlet, outlet, and recycle tubing and the liquid volume of the liquid sampling container, i.e., the entire experimental setup excluding the microbioreactor itself. The ancillary system was measured separately as it was previously found to substantially contribute to the G/L mass transfer of the experimental system [62]. A schematic of the experimental set up is shown in Figure 3.2. Briefly, water is recirculated from the reactor exit, through the liquid sampling container and back to the inlet, creating a closed loop. Before each test, the dissolved oxygen (DO) was reduced to 0.1 – 0.3 mg/L by sparging with nitrogen gas. The gas inlet was then switched to air, and the DO increase was continuously monitored by an optical DO probe (Vernier, Beaverton, OR) in the sampling chamber until the DO reached saturation. To account for the mass transfer contribution of the ancillary system, the same tests were run on the ancillary system to determine its mass transfer coefficient (K_La_{Anc}). The data were analyzed and the MTCs were determined

by fitting the Dynamic Method model to experimental data using the K_La as the fitting parameter.

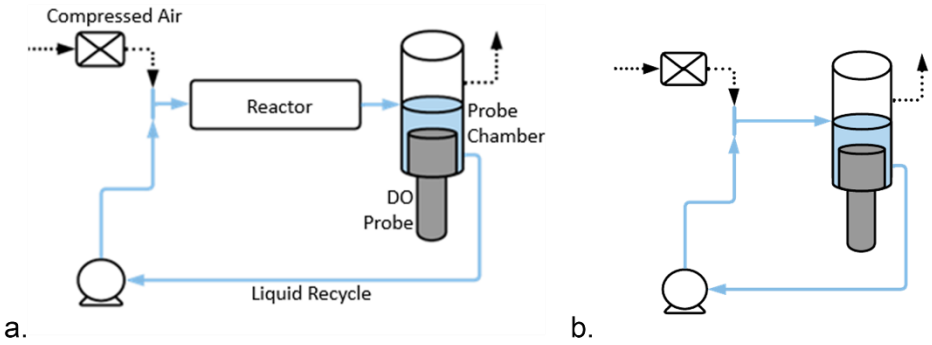

Figure 3.2 Diagrams of the abiotic experimental setups for mass transfer testing. The dotted lines represent gas flow and solid lines represent liquid flow. (a) Set up for the microbioreactor. (b) Set up for testing the ancillary system. From [62].

Mass transfer determinations were conducted at a constant gas flow rate of 90 mL min^{-1}, with air used for aeration and nitrogen gas used for oxygen depletion. The gas flow was controlled with a mass flow controller (Alicat Scientific, Tucson, AZ). Liquid flow rates ranged from 16 mL min^{-1} to 116 mL min^{-1}, which were controlled by a peristaltic pump (Masterflex, Vernon Hills, IL). All tests were conducted at room temperature (22 ºC).

3.2.3 Biological Performance

Five of the microbioreactors were selected for biodegradation investigations. The reactors were chosen to cover a range of channel dimensions from A of 0.5 – 4 mm^2 for both straight and patterned. Additionally, a setup of the ancillary system alone was also investigated. A diagram of the biological test system is shown in Figure 3.3. The gas inlet consisted of a humidified air stream controlled by a mass flow controller (Alicat Scientific, Tucson, AZ), which was spiked with toluene vapors by combining with a second stream

of air that passed through the headspace of a vial of pure toluene, which was controlled by a second mass flow controller. The combined air stream was then distributed to each microbioreactor through a manifold and five flowmeters (Dwyer, Michigan City, IN) to ensure equal flows. The flowmeters for each microbioreactor were set to 75 mL min^{-1}. The synthetic contaminated air stream combined with the liquid medium at each microbioreactor inlet tee. The microbioreactors were operated at a liquid flow rate of 75 mL min^{-1}. After passing through each microbioreactor, the gas and liquid were passed through a 50 mL centrifuge tube which served as the gas-liquid separator and the liquid sampling container. A DO probe (Vernier, Beaverton, OR) was inserted through a hole in the centrifuge tube cap and sealed with parafilm. The liquid DO was continuously measured throughout the experiment and recorded using a data logger (Vernier, Beaverton, OR). From the liquid sampling container, the effluent gas was passed through a polycarbonate sampling bottle fitted with an NDIR CO_2 probe, (Vernier, Beaverton, OR) which continuously recorded CO_2 concentration in the effluent gas with a data logger. A GC septum (Restek Thermolite, Shimadzu, Kyoto, Japan) was inserted into the effluent gas sampling bottle, through which a gas-tight syringe was inserted to take samples for analysis of gaseous toluene concentration. The liquid phase was continuously recirculated using a peristaltic pump (Masterflex, Vernon Hills, IL).

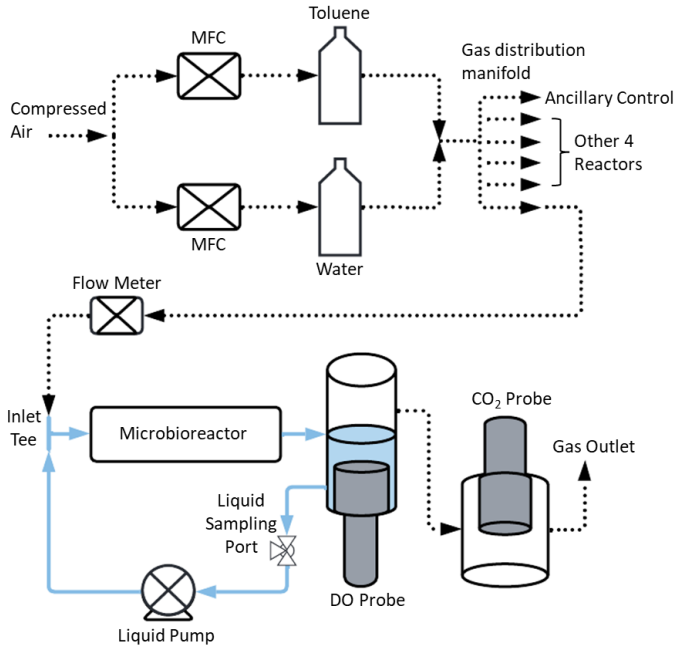

Figure 3.3: Diagram of the experimental setup for biological experiments. The system includes five equivalent systems, each with a different microbioreactor, and one ancillary-only control. Only one microbioreactor setup is shown in the diagram. A photo of the experimental setup is shown in Figure S1.

The microbioreactors and ancillary-only control were inoculated with a culture dominated by *Pseudomonas putida BBC443*, which had been cultivated continuously in a toluene-fed 500 mL suspended growth stirred vessel (Chemglass Life Sciences, Vineland, NJ) in non-aseptic conditions for several months in mineral medium [19] with toluene (liquid concentration 50-200 mg L^{-1}) as the sole carbon and energy source. Culture growth was monitored with optical density (OD) at 600 nm using a spectrophotometer (BioRad SmartSpec 3000, Hercules, CA). The microbioreactors were inoculated at an OD of 0.35, by centrifuging and resuspending cells in fresh mineral medium which was added to the liquid sampling container of each system.

The microbioreactors were operated continuously for 14 days. The liquid phase was sampled roughly every 24 hours by removing 10 mL through a three-way sampling valve in the recycle tubing. The liquid was analyzed for OD and toluene concentration. Liquid samples for toluene analysis were filtered with an 0.2 µm syringe filter to remove biomass prior to analysis. Toluene concentration in the liquid phase was measured using direct injection of aqueous samples into a GC-FID (Shimadzu, Kyoto, Japan) fitted with an Agilent HP-INNOWAX column (30 m × 0.25 mm ID, 0.25 µm film) and an autosampler and using an FID detector. Immediately after sampling, fresh mineral medium was added to through the recycle line to replace the removed liquid volume. The gas effluent was sampled once to three times per day, using a gas-tight syringe (Hamilton Company, Reno NV) to collect 0.5 mL gas samples from the gas sampling bottle through the septum, and immediately analyzed by GC-FID (Shimadzu, Kyoto, Japan) fitted with an Agilent DB-624 column (30 m × 0.32 mm ID, 1.8 µm film) and an FID detector.

The biological performance of the microbioreactors was evaluated by the Removal Efficiency (RE), Elimination Capacity (EC), and Mineralization Percentage (MP), defined in Equations 3.1 – 3.3.

$$RE = \frac{(C_{in} - C_{out})}{C_{in}} \cdot 100\% \qquad Equation\ 3.1$$

$$MP = \frac{(C.CO_{2,out} - C.CO_{2,in})}{(C.toluene_{in} - C.toluene_{out})} \cdot 100\% \qquad Equation\ 3.2$$

$$EC = \frac{F_G \cdot (C_{in} - C_{out})}{V_L} \qquad Equation\ 3.3$$

Where C_{in} refers to the concentration of toluene in the gas inlet, C_{out} is the concentration of toluene in the gas effluent, $C.CO_2$ refers to the mass of carbon as CO_2 (g) and C.toluene refers to the mass of carbon in the form of toluene (g), F_G is the gas flow rate, V_L is the total liquid volume in one microbioreactor system including the ancillary system, V_R is the internal reactor volume (see Table 3.1). An additional parameter, the Reactor-only elimination capacity, or R.EC, was calculated using Equation 3.4, which subtracts the removal measured in the ancillary-only system and is normalized to the volume of the microbioreactor. The R.EC represents the additional elimination capacity contributed by the microbioreactor.

$$R.EC = \frac{F_G \cdot \left(C_{in} - C_{out,Ancillary} - C_{out,Reactor}\right)}{V_R} \qquad Equation\ 3.4$$

The microbioreactors were imaged with a high-resolution x-ray computed tomography scanner or “MicroCT” (XTH 225 ST, Nikon, Japan) before biological experiments to assess the fidelity of 3D prints to CAD designs and after biological experiments to evaluate the accumulation of biomass within the reactor channels.

3.2.4 Data Analysis

Mass transfer coefficients were determined using Berkeley Madonna as detailed in Chapter 2 [62]. Statistical analyses of data from mass transfer and biological experiments were performed using Microsoft Excel and RStudio (R version 4.2.2). Results were reported with the mean and standard error of experimental replicates. Statistical

significance was determined using one-way or multi-way ANOVAs with post-hoc Tukey's HSD tests with a 95% confidence interval.

3.3 Results

3.3.1 Evaluation of Microbioreactor Design and 3D-Printing

Initial reactor prints in PLA were not gas-tight, and were weak prone to leaks and cracks. This led to machining the case out of aluminum and using "Crystal" polymer which resulted in gas-tight reactors, though the reactor beds could also crack or break if not handled delicately or with difficult post-processing of tiny channels. MicroCT scans revealed that actual printed dimensions matched expectations. The 0.5 x 1 mm channel reactor (0.5-S) did have some residual support material that was unable to be removed in post-processing, as shown in CT scans (see Figure 3.10). Post-processing of prints was more difficult for patterned channels than for straight prints, which limited the patterned prints to a minimum A of 1 mm^2 whereas a straight channeled reactor of 0.5 mm^2 was possible. A straight 0.5x0.5 mm reactor was printed, but support material could not be removed. Overall, it was feasible to 3D print and iterate on design of the reactor beds. The case was more difficult to produce and achieve gas tight conditions, while maintaining the ability to interchange reactor beds. Sealing with waterproof tape was needed to prevent leaks.

3.3.2 Mass Transfer Coefficients

The maximum K_La for each microbioreactor are shown in Figure 3.4, which were all from tests conducted at the highest liquid flow rate of 116 mL min^{-1}. As expected, the K_La of the microbioreactor with the smallest channels ("Reactor 0.5-S" with 0.5 x 1 mm^2

channels) was significantly higher than all other microbioreactors at 644 h^{-1} ($p < 0.001$), while the microbioreactor with the largest channels had the lowest K_La of 127 h^{-1}. The increase in K_La from microbioreactors with larger to smaller channels was not linear, but rather increased exponentially as the channels got smaller. The K_La of Reactor 0.5-S was almost 300 h^{-1} higher than the K_La of either microbioreactor with A of 1 mm^2. In comparison, the maximum K_La of patterned and straight microbioreactors with A of 2 mm^2 were 86 to 200 h^{-1} higher, respectively, than their patterned and straight counterparts with A of 4 mm^2, though only the difference between Reactor 2-S and those at A=4 was statistically significant ($p = 0.001 - 0.002$).

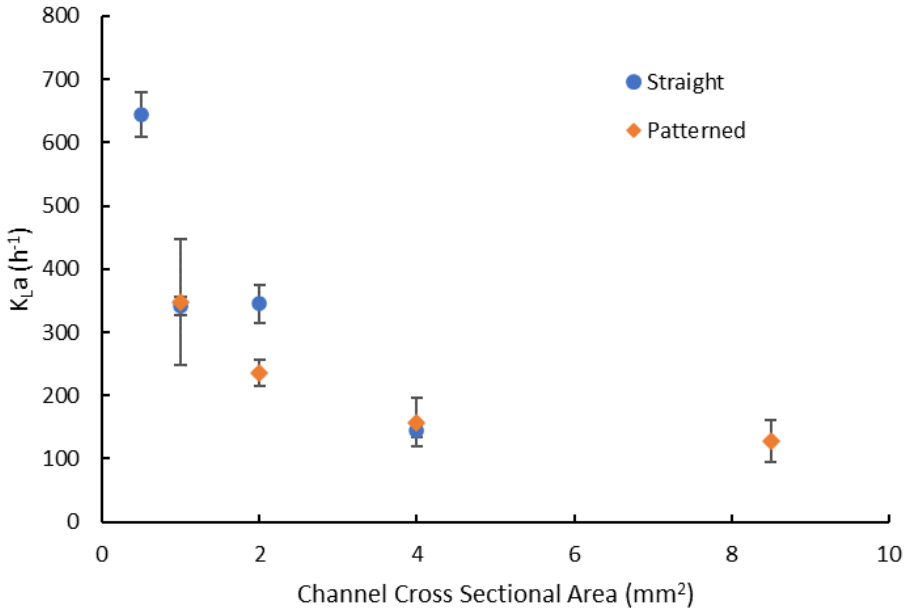

Figure 3.4: Maximum K_La for all reactor beds of varying microchannel cross-sectional area (A). Tests were conducted at Q_L = 116 mL min^{-1}.

The MTC in each microbioreactor followed the expected trend of higher MTCs with increasing liquid flow rates, shown in Figure 3.5. The overall trend of higher MTC values

for smaller channeled microbioreactors can also be seen at all flow conditions tested. The difference in K_La between each incremental increase in A was only significant between A of 0.5 to 1 mm^2 and between 2 to 4 mm^2 (for 2-S only). For instance, the K_La of microbioreactors with A of 1 mm^2 and 2 mm^2 were not significantly different at any flow rate for either straight or patterned reactors ($p = 0.09 – 1$), though potentially due to high variability for some of the reactors, as the K_La for the A=1 mm^2 microbioreactors were seen to be slightly higher at most flow rates, as shown in Figure 3.5. However, the difference in K_La was always significant when comparing microbioreactors with larger differences in A (i.e. between 0.5-S and 2-S, $p < 1\times10^{5}$). Overall, these results are consistent with other studies that have found higher MTCs with smaller channels [64]. Alternatively, the differences between the average K_La for straight and patterned were not significant for reactors with the same A (e.g. 2-S and 2-P) at any flow conditions, indicating there was no significant difference between the mass transfer in straight and patterned microbioreactors.

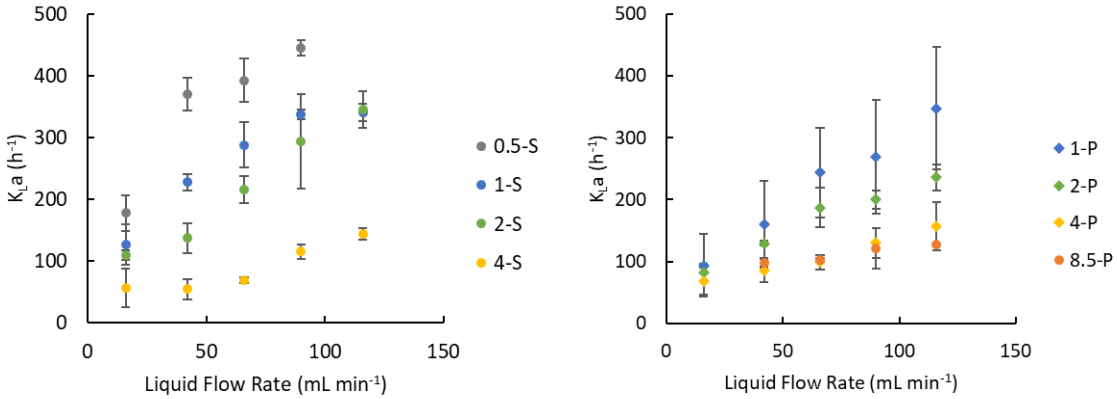

Figure 3.5 Overall volumetric MTCs of microbioreactors of varying channel size (A) with straight channels (Left) and patterned channels (Right) as a function of liquid flow rate. All tests were conducted at gas flow rate of 90 mL min^{-1}.

3.3.3 Biodegradation Performance

The biological removal of toluene was evaluated in five microbioreactors as well as the ancillary system alone. The maximum elimination capacities (EC) and average EC after a start-up period of three days are shown in Figure 3.6. The biological performance of the microbioreactors resembles the MTC results shown in Figure 3.4, showing that there was more toluene removal in microbioreactors with smaller channels, though the results were not statistically significant due to the high variability over the course of the experiment. Similarly to the mass transfer results, there was no difference between the average EC of patterned and straight microbioreactors at equivalent channel size. For the reactors with A=2 mm^2 and A=4 mm^2, the patterned channel microbioreactors had a greater maximum EC than the straight channel microbioreactors over the course over the experiment. However, as each Max EC was from a single time point, the statistical significance could not be tested. It is important to note that the EC was calculated as removal per volume of liquid in the entire system (microbioreactor + ancillary), which was kept equal for each microbioreactor system. Thus, the ECs were normalized to the same volume to facilitate comparison.

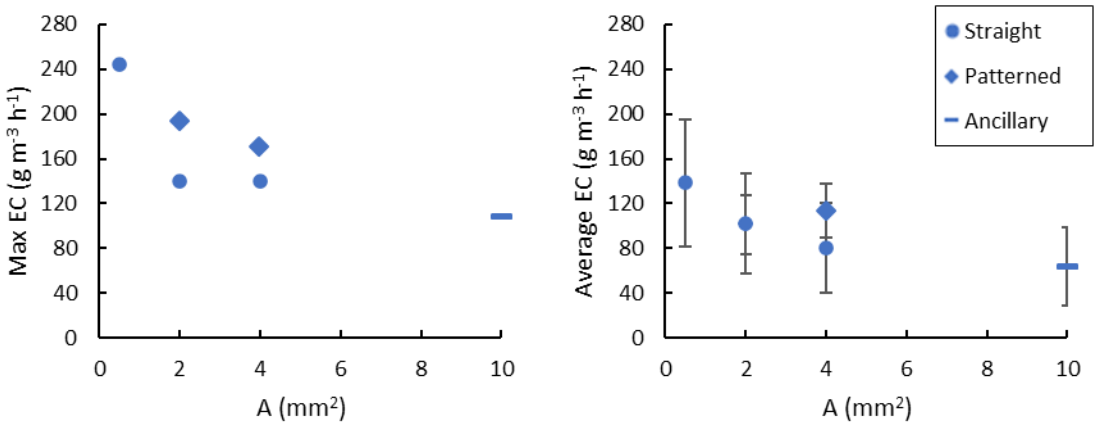

Figure 3.6: Elimination capacities from days 4-12. (Left) Maximum EC (Right) Average EC, with results pruned to only include the afternoon samples when reactors were not nutrient-limited. The ancillary system was arbitrarily set at A=10 mm^2 for display purposes. Note that all ECs are normalized to the liquid volume (18 mL), which was the same for each microbioreactor system as well as the ancillary system.

The ECs for each microbioreactor at increasing loading rates (LR) are depicted in Figure 3.7. While toluene elimination in the ancillary system was generally less than 100 g m^{-3} h^{-1}, toluene elimination in the microbioreactors was consistently higher. Figure 3.7 shows that reactors with smaller channel size generally had higher ECs than microbioreactors with larger channels across LRs. The improved performance of the microbioreactors over the ancillary system alone, and in particular of microbioreactors with smaller channels, was more pronounced at higher toluene LRs. Furthermore, these results show the microbioreactors capacity to achieve a substantial removal of toluene, even at higher LRs. The greater performance of microbioreactors with smaller channels highlights the importance of higher mass transfer. The microbioreactor with the smallest channels (0.5-S), was the top performer throughout most of the experiment, despite having the smallest working volume.

The EC of the ancillary system alone averaged 63 g m^{-3} h^{-1} between days 4-12, which substantiates the finding from Chapter 2 that the ancillary system is an important contributor to the performance of the overall system. The maximum K_La of the ancillary system was 45 h^{-1} which substantially contributes to the overall oxygen transfer rate of the total microbioreactor system (see Section 2.4.2). Furthermore, the majority of the liquid volume, and therefore the biomass, was within the ancillary system, and so it is reasonable to expect the ancillary system to significantly contribute to the overall performance.

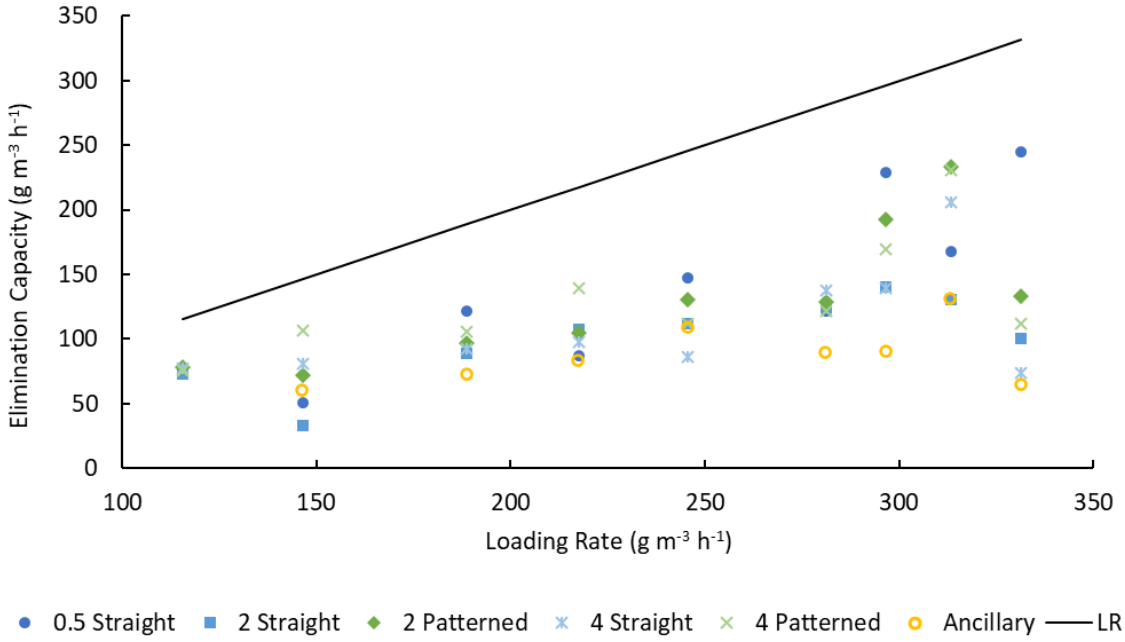

Figure 3.7: Comparison of the EC at increasing LR for each microbioreactor. The diagonal line represents 100% removal.

Alternatively, it is common to normalize ECs to the working volume of the bioreactor. Figure 3.8 shows the Reactor-Only EC (R.EC) for the microbioreactors, which represents the toluene removal rate of the microbioreactor alone (Equation 3.4). The

average R.EC for 0.5-P from days 4-12 was 405 g $m^{-3}_{reactor}$ h^{-1}, much higher than for the others which ranged from 83-151 g $m^{-3}_{reactor}$ h^{-1}. The standard deviations of all average R.ECs were quite high due to the variability during the experiments. However, during most of the operation, the AEC for the smallest reactor ranged from about 200 to almost 1000 g m^{-3} h^{-1}, which is very high compared to conventional bioreactors [19]. The other reactors had average R.ECs between 100-166 g m^{-3} h^{-1}, which are also higher than volumetric removal rates seen in most conventional reactors, highlighting the value of process intensification due to the miniaturization of the bioreactors.

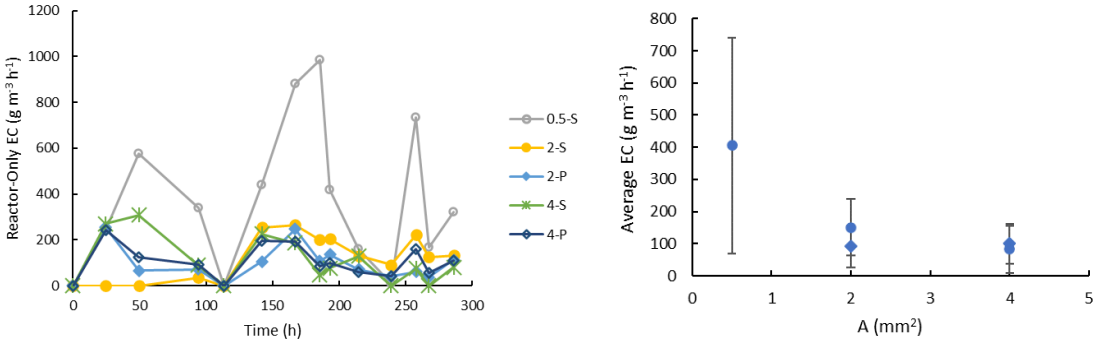

Figure 3.8: Reactor-only EC (R.EC) of the microbioreactors. EC was normalized to the microbioreactor volume with the ancillary contribution subtracted. (Left) AEC over time. (Right) Average R.EC from days 4-12 vs. channel area.

Detailed evaluation of on-line monitoring data offered insight into the performance of the microbioreactors as well as opportunities for optimization. Here, this is illustrated for one of the microbioreactors. The continuous operation of Reactor 0.5-S is shown in Figure 3.9, in which key parameters (DO, EC, CO_2 production, and MP) are reported. The production of CO_2 was measured to track the biodegradation of toluene, and determine whether there was complete mineralization to CO_2, as opposed to the accumulation of

metabolic intermediates. Figure 3.9 shows that the CO_2 concentration in the gas effluent stream largely tracks with removal efficiency, and thus was a strong indicator of toluene elimination and confirmed that toluene removal was the result of biodegradation.

The DO was also an informative parameter for monitoring the microbial community as well as overall system conditions. In Figure 3.9 it can be seen that the DO could have been limiting during the first two days of operation, indicated by DO values occasionally declining to 0 mg/L. In order to address this, air flow rates at the MFCs were increased after hour 50 to provide sufficient oxygen. The DO was observed to increase after fresh, oxygenated medium was added (once daily) and then to decline over the next several hours, indicating oxygen consumption from microbial growth. At certain time periods before medium addition, such as between hours 160-180, the DO leveled off or slightly increased, which could potentially indicate that growth was leveling off due to depletion of mineral nutrients in the medium. During the times with strongest biological performance (hours 75-95 and 160-186), as indicated by both high RE and EC, the DO would decline to a below 4 mg/L, which indicated growth, but DO was kept from being fully depleted with high enough air flow rates. Alternatively, poor overall performance and need for microbioreactor maintenance was indicated by sustained high DO measurements (4-8 mg/L) after medium replacement, as was observed after hour 100 and again after hour 200, which also corresponded to low RE and effluent CO_2 concentrations below 1000 ppm. When these conditions were observed at hour 114, the reactors were taken offline for maintenance.

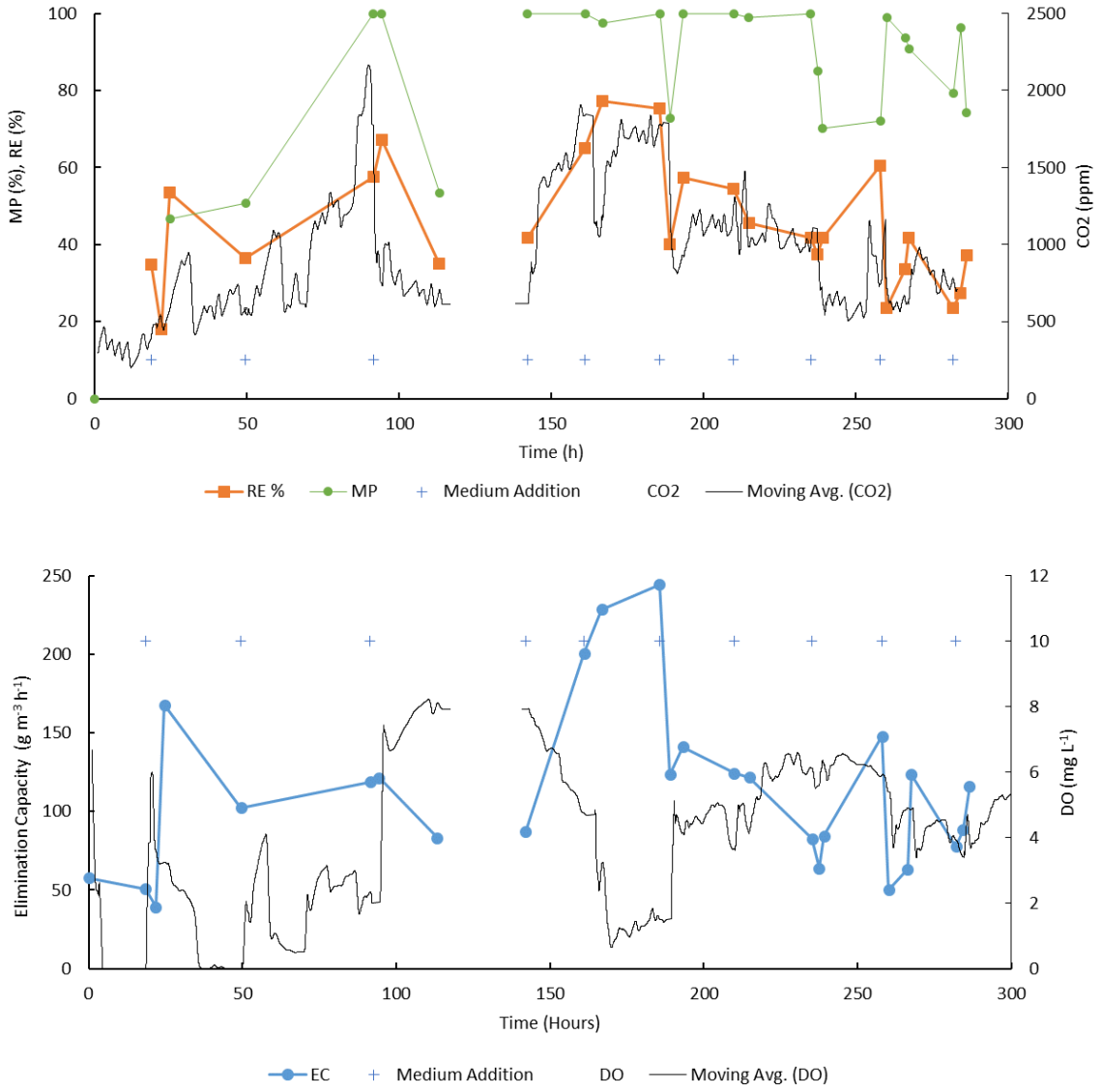

Figure 3.9 Continuous operation of microbioreactor 0.5-S. (Top) moving average (avg. per 60 minutes) of CO_2 production, and toluene removal as RE and MP. (Bottom) moving average (avg. per 60 minutes) of the DO and toluene EC. Reactors were operated continuously from hours 0-114 and 142-300. The reactors were offline between hours 114 – 142 for maintenance.

When the microbioreactors were restarted at hour 142, reactor performance improved and reached the highest ECs of the operating period and high toluene removal

was maintained until hour 182. DO consumption was high and CO_2 production reached 1920 ppm, similar to the peak during the first week of operation. During this time, RE increased from 42% to 77% with 100% of the toluene removed fully mineralized to CO_2. However, performance began to decline by hour 200, indicated by DO concentrations between 4-6 mg/L, low CO_2 production, and RE eventually dropped to only 37%. Elevated back pressure at the MFCs indicated high levels of clogging. The experiment was stopped at hour 300 to assess the biomass accumulation.

The clogging of channels from biomass was evaluated using microCT scans, shown in Figure 3.10. It was expected that there would be a correlation between channel size and biomass clogging, with smaller channels becoming more clogged during biological experiments. However, Figure 3.10 shows that this was not entirely the case. All reactors had at least some minor buildup of biofilm on the inner walls of the channels, though few were fully blocked. The lack of clogging within the channels could be due to the high two-phase flow velocities, which ranged from 17 mm s^{-1} for Reactor 4-S to 35 mm s^{-1} for Reactor 0.5-S, and the resulting high shear stress, which has been shown to cause cell and biofilm detachment [65]. However, significant biomass blockage occurred for all microbioreactors at the inlet area leading into the channels rather than within the channels themselves (highlighted in Supplementary Figure 6.1). A thick coating of biomass was found at the channel inlet area in all microbioreactors by the end of the experiment. This thick biomass plug at the inlet area could have blocked more biomass from traveling into and clogging within the channels. Therefore, due to the design of the microbioreactor inlet area, which had a larger cross-sectional area than the individual channels, all of the microbioreactors were similarly clogged at the inlet, regardless of channel dimensions. The major issue presented by the clogging was the significant pressure (110-131 kPa)

needed to maintain the gas flow rate through the microbioreactors, which was especially pronounced for the smaller microbioreactors. Given that the flow meters were set manually, this occasionally caused variability in gas flow rates between the microbioreactors. After 300 hours of operation, the gas flow rates could not be maintained due to clogging from excess biomass.

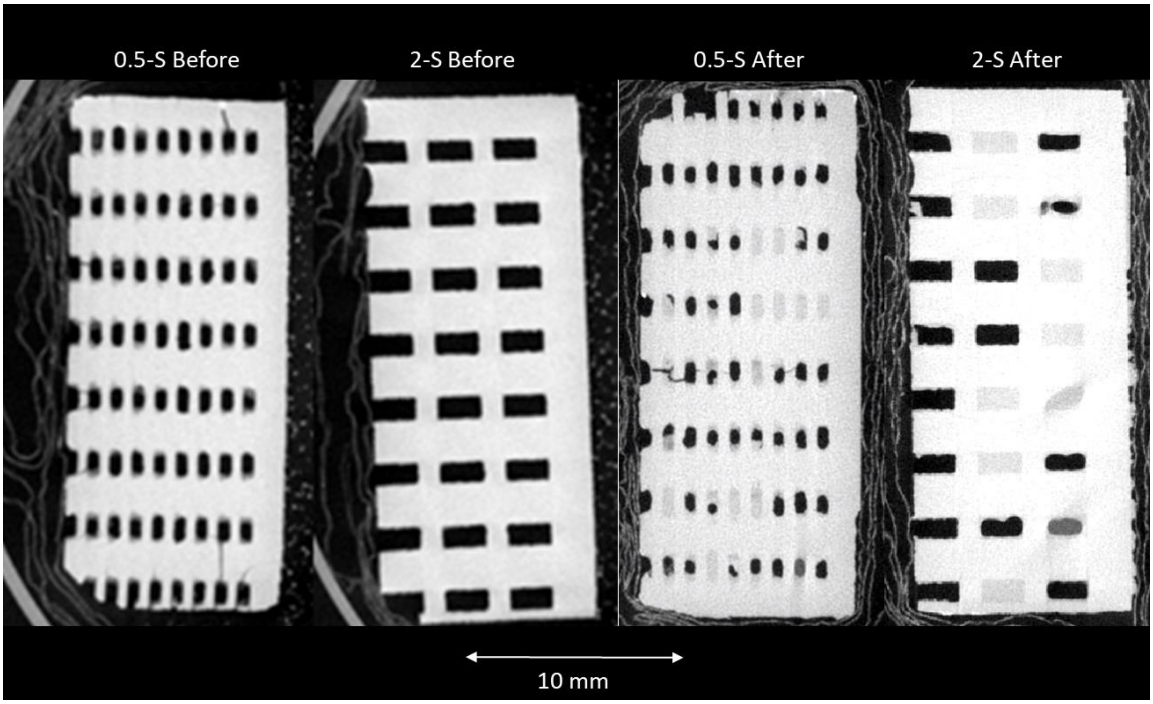

Figure 3.10 MicroCT scans of microbioreactor cross sections before (left) and after (right) toluene vapor biodegradation experiments for the straight-channeled reactors. Note that a dim, uniform haze over a channel likely shows water, whereas the non-uniform and darker haze is likely biofilm. In the before image of Reactor 0.5-S (smallest channels) the rounded internal channels show 3D-printing support material that was unable to be removed.

A number of biomass control strategies could prolong the microbioreactor operation, ideally indefinitely. A simple option could be to periodically pause operation to manually clear biomass accumulation from the inlet, which would be simple given the

reactor case was designed for easy interchange of reactor beds. An equivalent clean bed could immediately be inserted into the case, or replaced with another encased reactor already prepared, thus only pausing operation for a minute to reconnect the tubing. The microbial community present in the liquid phase of the ancillary system would be sufficient to maintain performance. Additionally, these microbioreactors are equivalent at either end, so the reactors could be periodically rotated or the direction of the flows reversed such that the inlet is now the outlet, which could push any accumulated biomass through the outlet into the liquid sampling container. High flow rates could help shear biomass through the channels and dislodge biofilm accumulation at the inlet chamber. Another option could be to have the reactor outlet flow to the sampling container through the bottom and the liquid phase recycled from the top. This reorientation could offer two advantages, the first by keeping more of the biomass in the liquid sampling container with most biomass setting to the bottom and recycling the medium from the top of the liquid phase. The settled biomass could also be periodically purged from the system. This would be similar to the operation of the capillary microbioreactor from our preliminary work [66] (Section 1.4) which reported very high toluene removal (4000 - 9000 g m^{-3} h^{-1}) during continuous operation of 300 hours. Additionally, by having the reactor effluent enter the liquid sampling container at the bottom, it would effectively prolong the gas phase retention time in the system, for example from 2.7 s to 10.7 s for Reactor 0.5-S, and allow more opportunity for mass transfer of toluene to the liquid phase.

3.4 Conclusions

The overall gas to liquid MTC was determined for several microbioreactors with parallel channels of varying dimensions. It was shown here that microbioreactors with

smaller channels had higher K_La. The incremental increase in K_La from one channel size to the next was most pronounced between the smallest channel area of 0.5 mm^2 to 1 mm^2, perhaps reflecting an inflection point where the dimensions cross from above to below 1 mm. However, there was no significant difference between the K_La of microbioreactors with straight and patterned channels of the same channel size.

Several of the microbioreactors were then evaluated for biological removal of toluene vapors in continuous operation for 300 hours. The microbioreactor with the smallest A (0.5 mm^2) had the greatest capacity to eliminate toluene, with the highest maximum and average EC over the course of the experiment after an initial startup period. The greater performance was attributed to the higher mass transfer coefficient. This was somewhat unexpected, as it was originally hypothesized that biomass clogging could have a more negative impact on reactors with smaller channels, reducing their toluene elimination capacity. However, all reactors experienced substantial accumulation of biomass at the reactor inlet while the internal microreactor channels were much less clogged than expected. The most noticeable impact of biomass accumulation was the need for greater pressure to maintain gas flow through the reactors and manual adjustment of the flowmeters to ensure equal gas flow distribution to each reactor. Future work should aim to overcome the negative effects of biomass accumulation with simple operational strategies in order to achieve longer continuous operation. The results shown here demonstrate that the increased mass transfer rates of smaller microfluidic-scale microbioreactors do translate to better biological performance.

4 Comparison of Microbial Community Design Approaches for Biodegradation of Multiple VOCs

4.1 Introduction

Our work so far has demonstrated the successful biological treatment of toluene and methanol as model single substrates using microbioreactors. In the first study, it was demonstrated that a capillary microbioreactor could achieve greater elimination of model VOCs compared to miniaturized biotrickling filters [19]. During a following two-month study on operational optimization, the capillary microbioreactors were capable of continuous operation with efficient treatment and minimal clogging [20]. The microchannel reactors discussed in Chapter 3 demonstrated the utility of 3D-printing for rapid prototyping and evaluation of microbioreactor designs.

Just as we have demonstrated the value of optimizing microbioreactor design and operation, there is also a need to optimize the microbial culture. In a typical indoor environment or other realistic treatment scenario, the microbioreactor system will have to treat a large number of VOCs, instead of just methanol or toluene. As mentioned in the overall introduction, indoor environments are likely to have many common VOCs such as benzene, toluene, ethylbenzene, xylene, styrene, naphthalene, α-pinene [2]. The presence of many different VOCs is likely to pose a challenge for the microbioreactor's microorganisms. Previous studies have shown that biological removal of VOCs can be impaired when treating mixtures of VOCs compared to single compounds [67]. For example, one study found that the removal efficiency of n-hexane alone was 76%, but dropped to 21% when treated in with a mixture of BTEX compounds [68]. In a study of the biotrickling filtration of benzene, toluene, xylene, and styrene (BTXS), it was found that while removal efficiencies over 90% were achievable for single substrates or combinations

of two substrates, the removal of total BTXS decreased with the increased complexity of pollutants in the gaseous influent [69]. In this study, a high relative of *Achromobacter* were suggested to be of particular importance for VOC removal of single or binary substrates while *Burkholderia* was suggested to be particular important for removal of ternary and quaternary VOC mixtures, which suggests these could be important taxa to target in the enrichment or rational design of VOC-degrading communities [69].

Some studies have found improved multi-VOC removal by using mixed cultures or a natural enrichment [70]. However, typical enrichments do not always produce the desired results [71]. Adaptive laboratory evolution, or directed evolution experiments, which involves subjecting microbial cultures to a set of environment pressures and allowing natural selection to increase the community fitness over time, can be time and labor intensive [72]. The success of directed evolution can also be dependent on minute methodological details such as transferring cultures at an optimal stage of growth and in a quantity of an optimal proportion to the community, where the optimum may be different for each community or desired outcome [72].

Prior attempts to rationally design microbial consortia for pollutant remediation have been limited, but indicate promising results. Typically, when treating a single pollutant, the easiest choice is to choose a single species known for its ability to degrade that substrate. This was the case in our own work, when *Pseudomonas putida* (*P. putida*) greatly outperformed activated sludge enrichments on toluene as sole carbon and energy source (unpublished). One approach to improving pollutant removal is to add multiple microbial species that are all individually capable of degrading the single target pollutant. For example, one study found better biodegradation of pentachlorophenol by a three-species consortium compared to each species alone [73]. When treating multiple

pollutants, a consortium can be designed by adding one known degrader of each target pollutant. In a study on biofiltration of styrene and vinyl acetate, two pure strains of Pseudomonas that had each shown evidence of treating one of the pollutants, with steady state removal efficiencies of over 78-94% and 80-98%, respectively [74]. Another study on biodegradation of various aromatic hydrocarbons evaluated two species that produce different dioxygenases responsible for initiating biodegradation for successful biodegradation of a mixture of toluene and phenol [75]. These initial efforts at rational design have often resulted in improved performance, which encourages further efforts at rational consortia design.

There are various approaches to the rational design of microbial communities [76]. Enrichment cultures are the classic example of a “top-down” approach, which involves taking a natural, diverse community and subjecting it to environmental pressures, letting natural selection take its course to eventually develop a community with higher fitness and hopefully the intended functionality [77]. Alternatively, a “bottom-up” approach involves building a community with individual components, each hand-picked or bioengineered to contribute a specific functional role to the community [78]. A blended or iterative approach, such as the development of a consortium composed of species isolated from an enrichment culture, was shown to be promising for the degradation of phenanthrene [79].

Metabolic modeling offers great promise as a new approach to rationally designing microbial consortia. Not only the main target pollutants are considered, but also the metabolic intermediates that are often underestimated in importance, if not neglected entirely. Accumulation of metabolic intermediates in the degradation of VOCs like toluene and hexane can cause inhibition and decreased performance over time [80]. More importantly, metabolic modeling is a tool that could take out much of the guess and check

that goes into so much experimental work. For example, one study focused on finding consortia for lignocellulose degradation experimentally tested 65 different combinations of species, which revealed that combinations with metabolic complementarity exhibited better performance [81]. With increasing capabilities of *in silico* modeling, many potential consortia could be rapidly screened before experimental testing, potentially enabling better choices and more efficient research. In one study, metabolic network modeling was used to predict combinations of species for algae-bacteria communities, and it was found that the communities selected by modeling grew significantly more algal biomass than controls [82]. Though there are numerous review papers calling for efforts at engineering microbiomes [83], and several papers on tools [84] and best practices [76], the number of studies applying these new theories and tools are few. Moreover, the utilization of the concepts to an actual application, not just an artificial situation, is quite rare.

With advances and growing availability of high-throughput sequencing and modeling of metabolic networks, the rational design of microbial communities has now emerged as a realistic possibility [76]. Therefore, I aimed to develop a methodology that will enable the engineering of microbial consortia that can efficiently degrade a given mixture of VOCs and for the members of the consortium to stably coexist long-term. Ultimately, the goal is to utilize a blend of top-down and bottom-up design to engineer a mixed culture that could potentially outperform pure cultures or simple enrichments for long-term biodegradation of VOC mixtures. To that end, I aimed to evaluate the feasibility of using metabolic network modeling to rationally design minimal microbial consortia for biodegradation of multiple VOCs, in comparison with pure cultures and an enrichment culture, using the combination of toluene and styrene as a model scenario.

4.2 Methods

4.2.1 Metabolic Network Modeling and Species Selection

Preliminary modeling was carried out using annotated genome assemblies from a collection of over 1000 high-quality metagenome-assembled genomes (MAGs) from the activated sludge (AS) of wastewater treatment plants [85]. Given the lack of species resolution, these results were used to inform the curation of genome assemblies with resolved taxonomy. A collection of annotated genome assemblies was retrieved from the NCBI database for in silico modeling. The database was searched for available assemblies from various taxonomic groups that had been identified in preliminary modeling of the AS MAGs, or in the literature as being associated with biodegradation of various pollutants, being present in activated sludge, or specifically identified to metabolize toluene or styrene (see Table 4.1). The genome assemblies were further curated based on several criteria: i. the assembly level was for the complete genome, with the aim of fuller and more accurate modeling; ii. annotation was available in GenBank format, which was required by the modeling platform; iii. “OK” taxonomy check status, which would allow for obtaining specific strains.

Table 4.1 Curation of annotated genome assemblies as inputs for metabolic network modeling.

Group	Level	Number of Genomes	Reason / Reference
Actinomycetales	order	50	[86], preliminary modeling with MAGs
Burkholderiales	order	1635	[87], [88], preliminary modeling with AS MAGs
Celeribacter	genus	3	NCBI keyword search “styrene”
Microbacterium	genus	21	[89]
Mycobacterium	genus	356	[88]
Propionibacteriaceae	family	95	preliminary modeling with AS metagenome
Pseudomonas	genus	708	[87], [90], [91]
Rhodococcus	genus	71	[92], [93]
Rhodocyclaceae	family	9	preliminary modeling with AS metagenome
Sphingopyxis	genus	8	NCBI keyword search “styrene”

The metabolic network modeling was completed with Metage2Metabo (M2M) [94], a Python3-based pipeline for the automated, parallel reconstruction and analysis of metabolic network models. In the first step of the pipeline, genome scale metabolic networks (GSMNs) were reconstructed using the PathoLogic algorithm from Pathway Tools [95] and applying the PathoLogic pathway hole-filling program PHFiller to infer reactions and pathways that were potentially unidentified in the genome annotation [95]. The collection of GSMNs were then analyzed with M2M to compute the individual metabolic capabilities, or potential to produce metabolites, for each GSMN and the collective metabolic potential of each possible community. The community model takes a “mixed-bag” approach which assumes the potential for cooperation and metabolite exchange by simulating the community as a single “meta-organism” composed of the GSMNs of all community members. Inputs to M2M included the GSMNs and an SBML file

of input metabolites, representing nutrients available from the minimal medium as well as common currency metabolites that are generally present in cells (see Appendix Table 7.1).

The model objective was to predict all possible "minimal communities," representing the combinations of GSMNs with the fewest number of members that has the collective metabolic potential to reach a given set of target metabolites. The model was first run without specific metabolic targets, which set the model objective to find minimal communities that achieved the greatest "added value," defined as the number of additional metabolites that have the potential to be produced through community cooperation. The model was then run with the objective set to determine minimal communities with the collective metabolic potential to produce specific target metabolites: the degradation pathway intermediates of toluene and styrene, shown in (listed in Appendix Table 7.2). The degradation pathway metabolites were identified from the MetaCyc database [96]. Styrene had one degradation pathway characterized in MetaCyc (Figure 4.1), while there were five degradation pathways characterized for toluene, which make up the "superpathway" of aerobic toluene biodegradation (Figure 4.2). The model was run separately for each set of toluene degradation pathway targets in combination with the one set of styrene targets. From here on, each target set will be referred to by the toluene pathway number, e.g. the target set with degradation products of styrene and toluene degradation pathway I will be referred to as Target Set I. The model identified each possible minimal community, or combination of species' GSMNs, that could potentially produce the maximum number of target metabolites. A list of "key species" was compiled of each GSMN included in at least one minimal community solution. These key species were considered as candidates for inclusion in experiments.

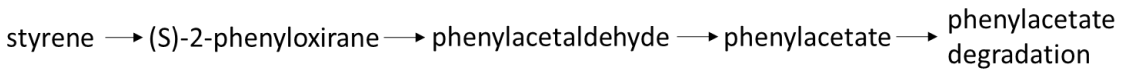

Figure 4.1 MetaCyc styrene degradation pathway.

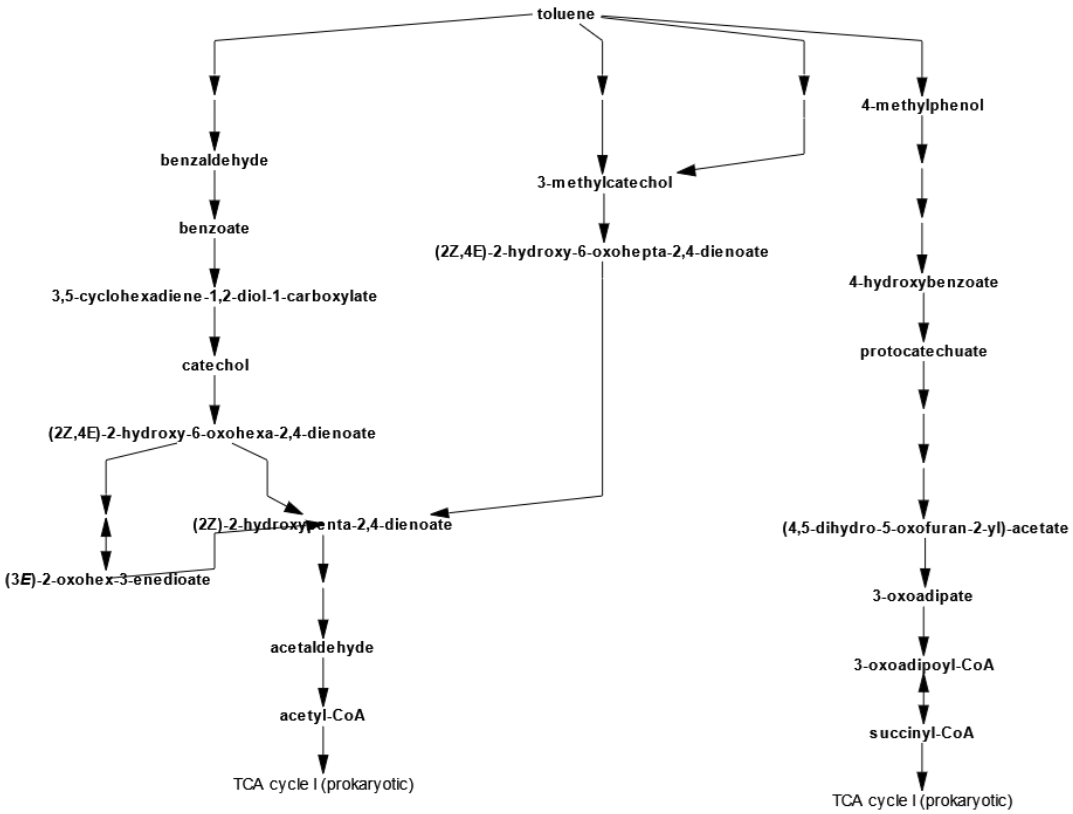

Figure 4.2 MetaCyc superpathway of aerobic toluene degradation.

4.2.2 Microbial Cultivation

Five of the minimal community candidate species were chosen for experimental testing: *Pseudomonas putida G7* (ATCC 17485) *(PPG7), Cupriavidus metallidurans CH34 (CM), Sphingopyxis lindanitolerans WS5A3p (SL), Novosphingobium aromaticivorans (NA),* and *Pseudomonas fluorescens NCTC10038 (PF)*. A positive control strain known to

grow in minimal medium using toluene as the sole carbon and energy source, *Pseudomonas putida BBC443 (BBC)*, was also included in biodegradation experiments. Pure cultures of the strains were generously provided by the Gunsch lab (Duke University). Each strain was grown as a pure culture in minimal medium with either toluene or styrene as the sole carbon and energy source. Each strain was also grown separately as pure culture using LB medium and streaked on LB agar plates.

The pure strains were cultivated in 240 mL serum bottles using PTFE-lined silicone septa. The VOCs were added using a microliter syringe to achieve an initial liquid concentration of 50 mg L^{-1} of the respective VOC, calculated according to Equation 4.1 (thus taking into account partition into the gas phase).

$$M = V_L C_L + V_G C_G = V_L C_L + V_G \frac{C_L}{K_H} \qquad \text{Equation 4.1}$$

Where V_L is the liquid volume, C_L is the concentration in the gas phase, V_G is the gas volume, C_G is the concentration in the gas phase, K_H is the dimensionless Henry's law constant (3.69 for toluene and 8.9 for styrene at 25ºC [97]).

The bottles were shaken at 150 rpm and incubated at 30ºC. The growth of the cultures was monitored by optical density (OD) at 600 nm using a spectrophotometer (BioRad SmartSpec 3000, Hercules, CA) and the consumption of VOC, which was monitored by collecting 0.5 mL gas samples through the septum, and immediately analyzing them by GC-FID (Shimadzu, Kyoto, Japan) fitted with an Agilent DB-624 column (30 m × 0.32 mm ID, 1.8 µm film) and an FID detector. For strains that showed low or no biomass growth on VOC alone, the minimal medium was supplemented with 5% (v/v) LB. Cultures were transferred to a new bottle with fresh medium and VOC when OD reached above 0.5 or the concentration of VOC in the headspace was depleted.

An enrichment culture (E) was cultivated separately. A sample of activated sludge was collected from the activated sludge return line of the North Durham Water Reclamation Facility (Durham, NC). Three replicate activated sludge samples were initially incubated in serum bottles with 20 mL minimal medium and shaken at 150 rpm at room temperature (22ºC). They were dosed with both toluene and styrene as the sole carbon source, at initial liquid concentrations of 25 mg L^{-1} each, or 50 mg L^{-1} total VOCs (TVOC). Subsequent transfers were dosed with 100 mg L^{-1} to 200 mg L^{-1} TVOC. Eventually, the enrichment cultures were combined and transferred to a 500 mL suspended growth stirred vessel to streamline culture maintenance.

4.2.3 Biodegradation Experiments

Biodegradation experiments were conducted using the same cultivation conditions described in section 4.2.2. Pure cultures were tested with initial liquid concentrations of 50 mg L^{-1} of either toluene or styrene, depending on the predictions of their individual metabolic potential. Thus, CM, NA, PPG7, and SL were grown in pure culture with toluene, and only PF was grown in pure culture with styrene. Cultures were incubated with low starting liquid concentrations ($C_{L,0}$) of 50 mg L^{-1} toluene or styrene, as growth rates of various bacteria have been shown to decline at higher concentrations [19], [92]. Additionally, some strains were combined to form the minimal community cultures identified by the model, as will be discussed in detail in Results. Minimal consortia, the enrichment culture (E), and BBC, were dosed with initial concentrations of 50 mg L^{-1} of both toluene and styrene, for total VOC (TVOC) of 100 mg L^{-1}. In preparation for the experiments, fresh liquid cultures were started from a colony and incubated for 1-2 days. Cultures were centrifuged in 50 mL tubes at 3000 RCF and resuspended in minimal medium. The cultures were transferred to serum bottles at starting OD of 0.02 – 0.05.

Culture bottles were initially sampled prior to incubation and periodically over 20 – 48 hours. Gas samples were analyzed for VOC consumption as previously described. A 1.0 mL liquid sample was collected with a sterile syringe for immediate analysis of OD and 0.8 mL was stored in sterile 1.5 mL tube and immediately frozen for later qPCR analysis. Sampling frequency was minimized to decrease the potential for VOC leaks, which could increase due to sampling with a needle through the cap septum. Cultures were monitored until VOC consumption was complete or up to 48 hours.

4.2.4 DNA Extraction, qPCR, and Amplicon Sequencing

DNA was isolated from activated sludge and enrichment culture samples using the Qiagen DNeasy PowerSoil Kit (Hilden, Germany) following manufacturer's instructions, using 1 mL sample volumes of activated sludge slurry or liquid culture. Aliquots of extracted DNA were sent to the Duke Sequencing and Genomic Technologies core facility (Duke University, Durham, NC) for library preparation and sequencing, following the Earth Microbiome Project protocol (http://www.earthmicrobiome.org/). PCR amplicon libraries targeting the V4 region of the 16s rRNA gene were produced using 515F and 806R barcoded primers. Sequencing was performed on an Illumina MiSeq instrument with 250 base-pair paired-end sequencing runs. Demultiplexed sequencing data were processed in Rstudio with the DADA2 Bioconductor R package [98, p. 2]. Taxonomy was assigned to operational taxonomic units (OTUs) using the Silva 132 classifier version 138.1 [99]. Statistical analysis of taxonomic data was performed using with the phyloseq R package [100]. Additional processing of data and generation of figures were performed using Tidyverse R packages [101].

The absolute and relative abundance of each strain in a minimal consortium was determined using multiplex qPCR. Assays were performed using direct aliquots of

samples subjected to quick lysis so that abundance could be directly converted to concentration. The use quick lysis on direct samples was validated in comparison to isolated DNA and DNA standards before application to experimental samples. The starting quantity (SQ) per sample volume of each strain was calculated with a 6-point standard curve and normalized by their respective number of 16s rRNA gene copies. Primers, probes and DNA standards were developed by Paige Varner [102] except for those for *Pseudomonas fluorescens NCTC10038,* which were designed to be used in multiplex qPCR with the others. Standards for absolute quantification were generated using gBlock™ Gene Fragments (Integrated DNA Technologies, Coralville, Iowa) corresponding to the V3 region of their 16s rRNA genes. PrimeTime™ probes for each strain were developed targeting the variable V3 region of the 16S rRNA genes, while primers were developed targeting the conserved area of the V3 region. All qPCR assays were performed on a BioRad CFX96 Touch Real-Time PCR Detection System (Hercules, CA, USA) in a total reaction volume of 20 µL. Primers and probes were added to 250 µM final concentration, with 1 µL liquid culture and using BioRad SsoAdvanced Universal Probes Supermix. The reaction conditions consisted of initial heating at 98 °C for 10 minutes for lysis, followed by 39 cycles of denaturation at 95 °C for 20 seconds and annealing/extension at 60 °C for 30 seconds. Reactions were performed in triplicate and included negative controls. Statistical significance was determined by performing a two-way repeated measures ANOVA using the rstatix package (rpkgs.datanovia.com/rstatix/) in R studio. P-values were adjusted using the Bonferroni multiple testing correction method.

Table 4.2 Primer and probe sequences for qPCR assays.

Primer/Probe	Sequence
V3 Forward Primer	AKGAATTGACGGGGRCCY
V3 Reverse Primer	TCACRACACGAGCTGACG
C. metallidurans probe	ACGAAGCAGAGATGCATTAGGTGCCCG
N. aromaticivorans probe	CCAGAGATGGAAAGGTTCCCTTCGGG
P. fluorescens probe	TAGATTGGTGCCTTCGGGAACATTGAG
P. putida G7 probe	CAGAGAACTTTCCAGAGATGGATTGGTGC
S. lindanitolerans probe	CAGAACCTTACCAGCGTTTGACATCCTTG

4.3 Results and Discussion

4.3.1 M2M Modeling and Identification of Minimal Communities

The full M2M analysis pipeline was applied to the curated dataset of 2870 GSMNs. The model computed the minimal community solutions for each target set, which ranged from 26 to 860 possible minimal communities. The model identified 194 GSMNs as key species, meaning they were identified in one or more minimal consortia with the metabolic potential to produce degradation metabolites of toluene and styrene. Of the key species, 12 were predicted to have the individual metabolic potential to produce the degradation products of styrene. There were 83 key species predicted to have the individual metabolic potential to reach all of the degradation products in at least one of the toluene degradation pathways. The remaining 99 key species were predicted to have the metabolic potential to reach some, but not all of the targets in any of the degradation pathways, and were therefore in a minimal community requiring cooperation and exchange of metabolites.

A network graph was generated for the solution for each set of targets that illustrates the association between key species in minimal communities. The solution

graph of minimal communities for Target Set I is shown in Figure 4.3. The solution graphs show key species as nodes (circles), that are grouped into power nodes, and associations are represented by edges (lines). The power nodes indicate functional redundancy, such that the minimal community can be composed of one species from each connected power node. Figure 4.3 illustrates that a minimal community for Target Set I could be composed two key species only: one species from the left power node and one species from the right power node would have the collective metabolic potential to reach all given targets. By mapping which species were able to reach each target (see Appendix Table 7.4), Figure 4.3 can be understood to show one power node with potential producers of all toluene degradation products along one toluene biodegradation pathway and the other with potential producers of all styrene degradation products along the styrene biodegradation pathway.

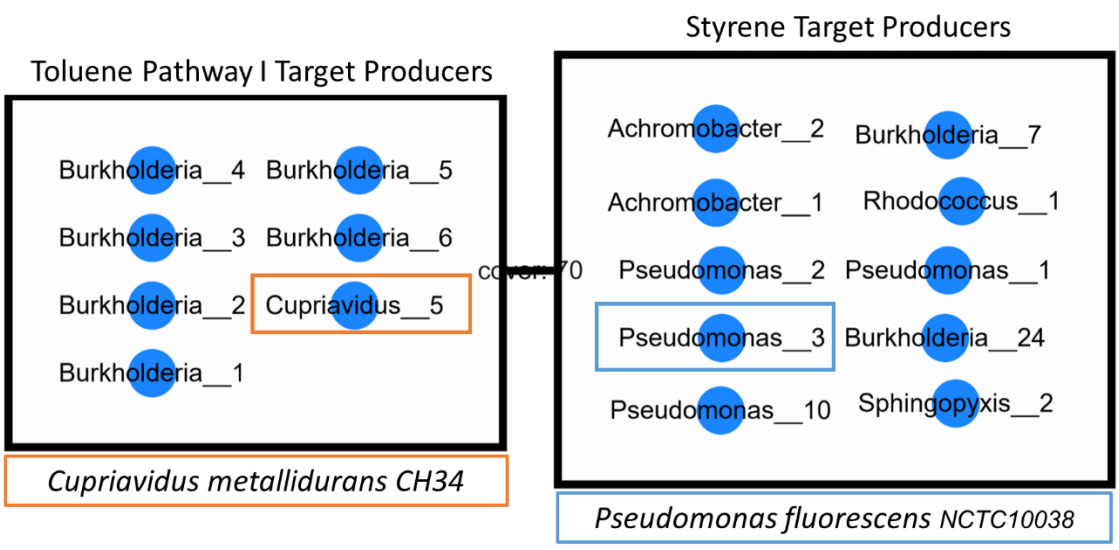

Figure 4.3 Solution graph of the minimal communities and key species for toluene (pathway I) and styrene degradation products. Key species are shown by their genus and a numerical identifier used to distinguish unique key species within the same genera. Two of the key species chosen for experimentation are boxed and the species name is displayed below the power nodes.

The solution graphs for the other four target sets are shown in Appendix Section 7.3. The minimal communities for each set of targets could be reduced to only two members, except for Target Set II, which was also predicted to be reachable by a single species, *Achromobacter xylosoxidans R4*. The structure of the solution graph for the two-species minimal community solutions for Target Set II closely resembles that of Target Set I, with two power nodes each corresponding to potential degraders of one VOC, though the key species for the toluene-target power node are not the same. The solution graph for Target Set III has three power nodes, with one power node of styrene-target producers and two separate power nodes of toluene-target producers. One of the groups of toluene-target producers have the individual metabolic potential to reach all targets in the toluene III biodegradation pathway, however, the other group were only predicted to be in a minimal community when paired with one specific styrene-target producing species: *Achromobacter xylosoxidans strain R4,* which was predicted to be able to produce the first metabolic product of toluene biodegradation, but not the rest of the pathway, while the paired species, such as *Novosphingobium aromaticivorans DSM 12444*, were predicted to have the potential to produce the toluene biodegradation targets in the rest of the pathway, but not to complete the first step. The solution graphs for Target Sets IV and V have several power nodes indicating specific associations for minimal community formation. These specific associations were required because no species was predicted to have the individual metabolic potential to degrade all of the targets in the toluene degradation pathways IV or V. Thus, the minimal community required cooperation between the styrene-degrading species and the species predicted to reach most of the toluene degradation targets. The model assumed that cooperation was possible, and the

import and export of metabolites in and out of cells was not considered. Therefore, cooperation and exchange of metabolites may or may not occur *in vivo.*

The key species identified by the model were then evaluated for suitability in experimental tests of the predicted minimal communities. The number of key species that could be included in experiments needed to be narrowed down from 194 to less than 10 in order to have a manageable number of experimental treatments. A summary of the key species, grouped by genus level, is shown in Table 4.3. An additional summary table with genus level taxonomy of key species is included in Appendix Table 7.3. The taxonomic group with the largest number of key species belonged to the genus *Bordetella* (*Alcaligenaceae*), with 77 key species. *Bordetella* was also the group with the greatest representation in the curated genome inputs to the model, with over 1,000 complete and annotated genome assemblies available in the NCBI database, due to the importance of several *Bordetella* strains as human pathogens [103]. While studies on *Bordetella* almost exclusively focus on its role as a pathogen, in one study on the biodegradation of toluene and naphthalene, a suspended-growth enrichment culture dominated by *Bordetella petrii* and *Bacillus sphericus* was found to degrade the combination of pollutants [104]. In a genomic analysis of *Bordetella holmesii*, sequencing results revealed the presence of a gene encoding for a toluene-4-monooxygenase system [105]. While pathogenic species are not ideal for use in treatment of air pollutants, particularly due to the risk of releasing bioaerosols, the identification of *Bordetella* species as potential degraders of toluene was verified to be a reasonable prediction.

Table 4.3 Taxonomic summary of the key species identified through metabolic network modeling, grouped by genus. N represents the number of key species belonging to each taxonomic group.

Order	Family	Genus	N
Burkholderiales	*Alcaligenaceae*	*Bordetella*	72
Burkholderiales	*Burkholderiaceae*	*Burkholderia*	27
Pseudomonadales	*Pseudomonadaceae*	*Pseudomonas*	26
Burkholderiales	*Burkholderiaceae*	*Cupriavidus*	11
Burkholderiales	*Burkholderiaceae*	*Paraburkholderia*	10
Burkholderiales	*Burkholderiaceae*	*Ralstonia*	6
Burkholderiales	*Comamonadaceae*	*Comamonas*	5
Burkholderiales	*Alcaligenaceae*	*Achromobacter*	4
Burkholderiales	*Burkholderiaceae*	*Pandoraea*	4
Burkholderiales	*Comamonadaceae*	*Acidovorax*	4
Sphingomonadales	*Sphingomonadaceae*	*Sphingopyxis*	3
Burkholderiales	*Comamonadaceae*	*Alicycliphilus*	2
Burkholderiales	*Comamonadaceae*	*Hydrogenophaga*	2
Pseudomonadales	*Pseudomonadaceae*	*Stutzerimonas*	2
Corynebacteriales	*Nocardiaceae*	*Rhodococcus*	1
Micrococcales	*Microbacteriaceae*	*Microbacterium*	1
Rhodobacterales	*Roseobacteraceae*	*Celeribacter*	1
Sphingomonadales	*Sphingomonadaceae*	*Novosphingobium*	1
Burkholderiales	*Alcaligenaceae*	*Kerstersia*	1
Burkholderiales	*Comamonadaceae*	*Delftia*	1
Burkholderiales	*Comamonadaceae*	*Diaphorobacter*	1
Burkholderiales	*Comamonadaceae*	*Melaminivora*	1
Burkholderiales	*Comamonadaceae*	*Polaromonas*	1
Burkholderiales	*Comamonadaceae*	*Simplicispira*	1
Burkholderiales	*Sphaerotilaceae*	*Ideonella*	1
Burkholderiales	*Sphaerotilaceae*	*Methylibium*	1
Burkholderiales	*Sphaerotilaceae*	*Schlegelella*	1
Burkholderiales	*Sphaerotilaceae*	*Sphaerotilus*	1
Rhodocyclales	*Rhodocyclaceae*	*Aromatoleum*	1
Rhodocyclales	*Rhodocyclaceae*	*Rugosibacter*	1

Key species identified as potential producers of toluene degradation targets belonged to many taxonomic groups, with the most numerous belonging to *Burkholderia*

and *Pseudomonas*, both of which have been documented in the literature as having aromatic pollutant-degrading species [69], [106], [107]. There were only 12 key species identified as potential producers of styrene degradation products. Three strains of *Pseudomonas fluorescens* were predicted to be styrene degraders, which should be expected given that the genes coding for styrene degradation were first sequenced and characterized from a *P. fluorescens* strain [91]. Additionally, three strains of *Achromobacter xylosodixans* were predicted to degrade styrene, and *Achromobacter* has also been associated with degradation of styrene [108]. Therefore, the modeling predictions of key species for minimal communities of toluene and styrene degradation was verified to be reasonable.

Ultimately, the narrowing down of which key species to include in minimal community experiments was decided by two factors: 1. Preference for non-pathogenic strains; and 2. feasibility of obtaining the specific strains identified by the model. The five species chosen for experimentation are detailed in Table 4.3. Four key species predicted to degrade toluene in minimal communities were selected, with each predicted to degrade toluene by different pathways, which are listed in Table 4.3 as the respective Target Sets. *Pseudomonas fluorescens NCTC10038* (PF) was the only key species predicted to degrade styrene that was included in experiments. Notably, *Novosphingobium aromaticivorans DSM 12444* (NA) was only identified in one minimal community with *Achromobacter xylosoxidans strain R4* as previously mentioned, however, NA has been documented to contain genes for toluene degradation on the pNL1 plasmid [109], and thus was determined to be suitable for use in experiments, with particular interest of evaluating if the prediction for the lack of individual potential for degrading toluene was a false negative.

Table 4.4 Strains chosen for minimal consortia experiments. Details for each target set are given in Supplementary Table 7.2 and illustrated in Figure 4.1 and Figure 4.2.

Strain	ID	GenBank	Target Sets
Cupriavidus metallidurans CH34	CM	GCA_000196015	I, II
Pseudomonas fluorescens NCTC10038	PF	GCA_900475215	All
Pseudomonas putida G7	PPG7	GCA_023221695	II, III, IV, V
Novosphingobium aromaticivorans DSM 12444	NA	GCA_000013325	II (cooperative)
Sphingopyxis lindanitolerans WS5A3p	SL	GCA_002993885	II, III

4.3.2 Evaluation of the Enrichment Culture Composition

The relative abundances (RA) of taxa (operational taxonomic units or "OTUs") at the order level for samples from activated sludge and the resulting enrichment cultures are shown Figure 4.4. Alternative depictions of RA grouped by class and genus are shown in Supplementary Figure 7.6 and Figure 7.10. Both enrichment cultures were dominated by OTUs from Pseudomonadales, specifically the genera *Pseudomonas* (41 and 69%). While the two enrichment cultures shared most of the same taxa, Enrichment "A" had a larger RA of Burkholderia and Chitinophagales, while there was a larger RA of OTUs belonging to Flavobacteriales, Shingobacteriales, and Xanthomodales in Enrichment "B." In a study of petroleum-degrading enrichment communities, Pseudomonadales were also found to be the dominant order, followed by Burkholderia, Xanthomodales, Rhizobiales, and Flavobacerales [110], all of which were found in the enrichment cultures here except for Rhizobiales, which noticeably lost from the AS community. OTUs belonging to the genera *Cupriavidus* were present in Enrichment A at almost 5%. Therefore, three of the species chosen for minimal community experiments (PF, PPG7, and CM) belonged to genera also identified in the enrichment cultures.

The microbial community sequenced from the original AS samples was notably different from the resulting enrichment cultures, as shown in Figure 4.4. The order with the largest RA in the activated sludge (AS) samples was Cornybacteriales, with the genera *Mycobacterium* comprising an average 11% of the AS sample community. Notably, the average relative abundance of *Pseudomonadales* taxa was only 0.045%. The AS community was composed of many low-abundance taxa, with 27% of the AS samples' sequence reads comprised of OTUs each with a relative abundance of less than 1%, in comparison to less than 5% for the enrichment cultures. This was reflected in the alpha diversity measures for the communities, shown in Figure 4.5, which was much higher in samples of activated sludge compared to the enrichment communities. The observed richness in activated sludge samples ranged from 304-389 compared to 58-106 for all enrichment culture samples.

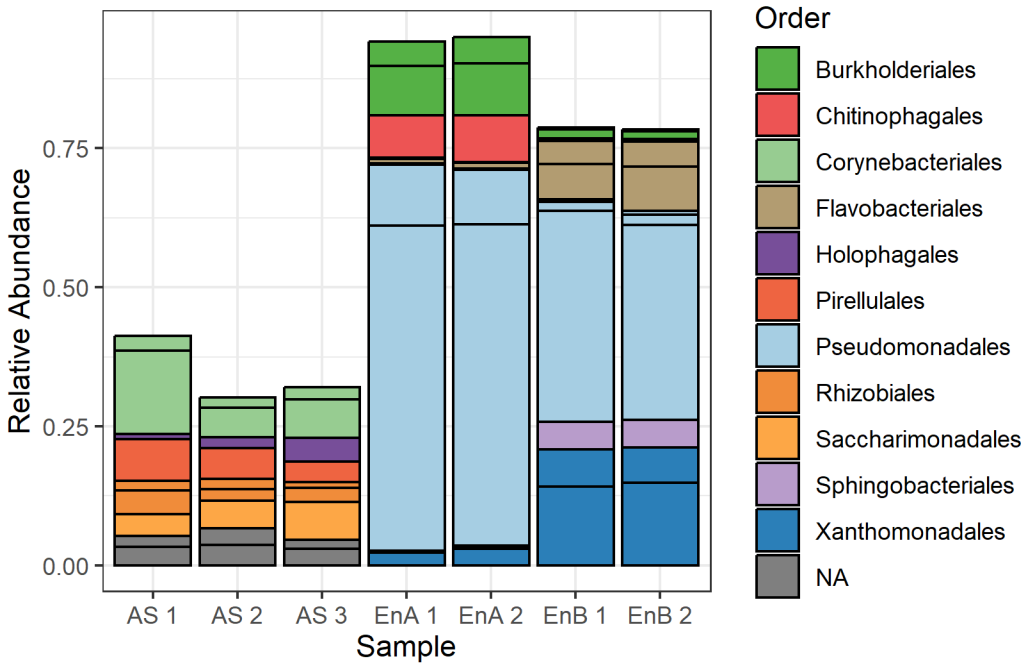

Figure 4.4 Relative abundance of OTUs at the order level determined by 16s rRNA gene sequencing from samples of activated sludge and enrichment cultures. Samples labeled "AS" were from fresh activated sludge. Samples labeled "EnA"

and "EnB" were from two separate enrichment cultures. The sample numbers refer to DNA isolation replicates that were submitted for sequencing.

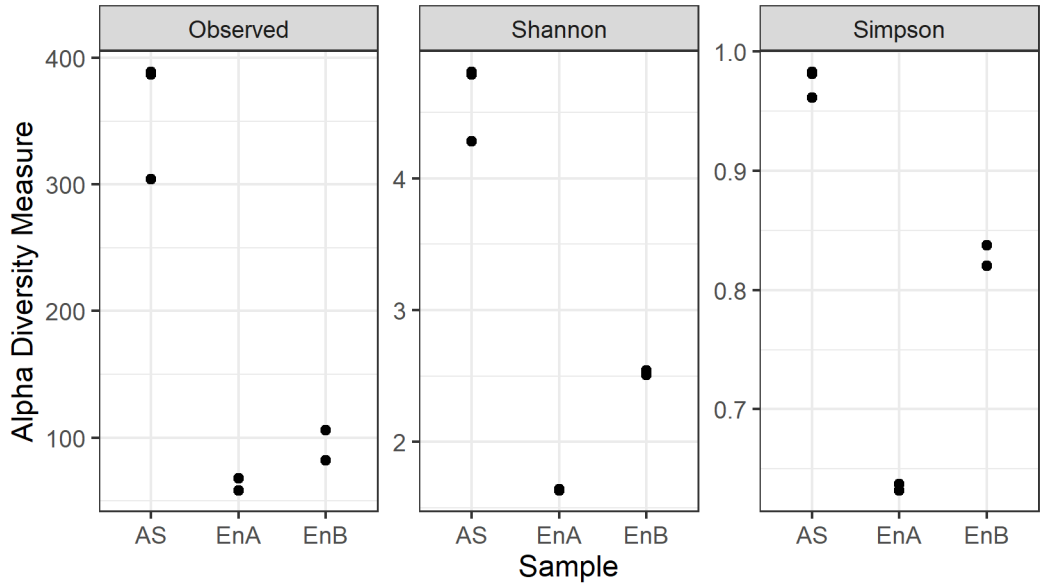

Figure 4.5 Alpha diversity measures of community richness for activated sludge (AS) and enrichment culture (EnA & EnB) samples.

4.3.3 VOC Biodegradation

The chosen key species were evaluated experimentally for their individual ability to degrade either toluene or styrene, based on the respective modeling predictions of their individual metabolic potential. Of the five model-predicted strains, only two were able to utilize toluene or styrene as their sole carbon source. As shown in Figure 4.6, PF was able to degrade styrene and NA was able to degrade toluene, while CM, PPG7, and SL were not. CM, PPG7, and SL were able to grow in minimal medium supplemented with LB in the presence of toluene, indicating toluene tolerance, however, the consumption of toluene was negligible, indicating that supplementing with an additional rich carbon substrate and nutrient source did not result in simultaneous or sequential biodegradation

of toluene, though, since significant growth occurred, it was possible that a nutrient limitation prevented the utilization of toluene. The growth of SL was slow and minimal even in LB supplemented conditions and was excluded from experiments due to insufficient biomass growth for inoculation. During the experimental testing of pure cultures, the OD of NA increased from 0.06 to 0.17, indicating growth, while the OD of CM and PPG7 stayed constant or declined. The OD of PF increased over the first 10 hours from 0.08 to 0.13, during which all of the styrene was consumed, and consequently the OD slightly decreased to 0.11 by the next sampling point, likely due to cell decay caused by the lack of substrate. The ODs for all cultures were expected to be low given the dose of VOC. The OD to cell concentration (g dry weight L^{-1}) can vary for each culture and the increase would also be affected by each culture's yield. While these correlations were not measured here, given theoretical numbers from similar cultures, for an OD:TSS ratio of 0.4 [111] and yield of 0.2 gVSS/gVOC [20], the expected OD increase for $C_{L,0}$ 100 mg L^{-1} TVOC would be about 0.15, while the expected OD increase for $C_{L,0}$ 50 mg L^{-1} styrene alone (2.0 mg styrene total) would be 0.06, indicating that the observed densities here are within expectation.

The above results point to discrepancies between model predictions and experiments. CM and PPG7 were found to not degrade toluene individually or in a minimal community with PF, while NA was not predicted to degrade toluene, yet it was observed to consume toluene in pure cultures. The discrepancy between model predictions of individual metabolic potential and experimental observations could be due to a number of factors. The genome annotation of CM identified the gene for toluene-4-monooxygenase and toluene-2-monooxygenase, which indicated it should be able to metabolize toluene. Alternatively, the genome annotation of PPG7 did not identify a toluene monooxygenase

or toluene dioxygenase [112]. However, the gap-filled GSMN predicted it had the individual metabolic potential to produce the degradation products of toluene in four of the five pathways. It is unclear why those pathways were identified as likely to be present, though the degradation of toluene by various *P. putida* strains has been widely reported in the literature [107], [113]. There could be a tendency to make assumptions for the presence of certain phenotypes based on species-level characteristics or those of higher taxonomic groups. In an evaluation of gap filling for metabolic model for a case scenario, the authors of PathwayTools found that the predictions of automated computational gap filling were 66%, with a similar tendency to predict false positives as false negatives. The discrepancy between the experimental results here and the model predictions could indicate shortcomings of automated gap filling methods for generating metabolic models and these were false positive predictions of functionality. However, the discrepancy could also indicate non-ideal cultivation conditions in the current experiments, which could take extensive experimental work to optimize. Most likely, these results indicated a need for manual curation of the metabolic models as well as optimization of cultivation conditions.

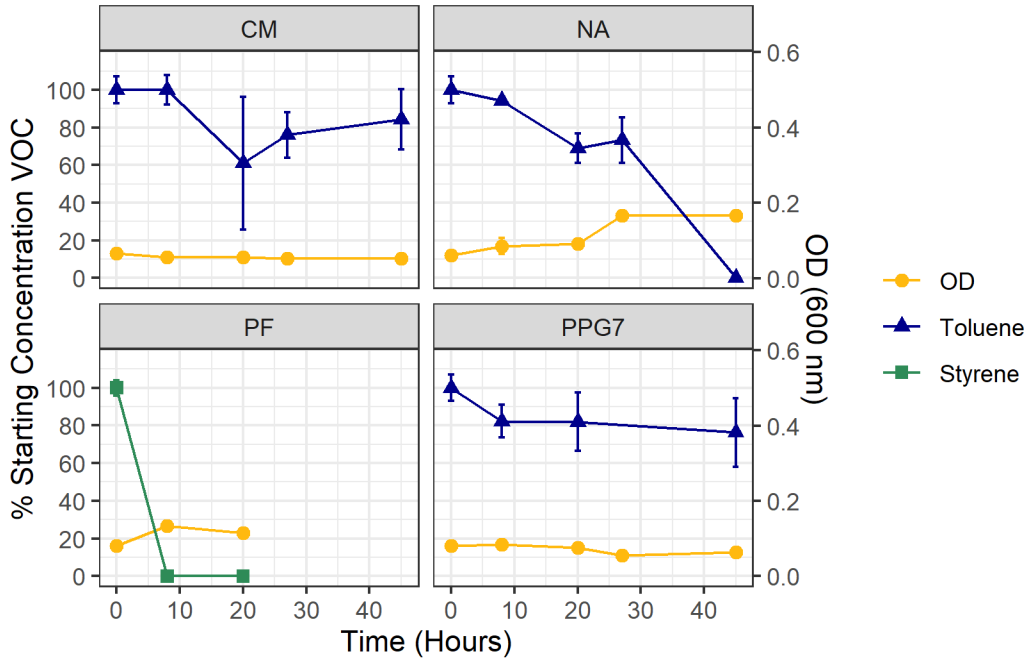

Figure 4.6 VOC removal and growth of pure cultures on 50 mg L^{-1} toluene or styrene.

Two synthetic consortia were then created from the chosen pure strains for biodegradation of both toluene and styrene. A consortium consisting of PF and NA (PF+NA) and another consortium of PF and CM (PF+CM) were tested experimentally in comparison with the BBC pure culture and enrichment (E), shown in Figure 4.7. All cultures were dosed with toluene and styrene to reach initial liquid concentrations ($C_{L,0}$) of 50 mg L^{-1} each (100 mg L^{-1} TVOC). In both minimal consortia, the styrene was fully consumed within 8 hours, which can be attributed to PF, which also completely degraded styrene within 8 hours in pure culture (Figure 4.6). However, neither minimal consortium completely removed toluene after 48 hours. The average concentration of toluene decreased to 46% of $C_{L,0}$ in the PF+NA consortium, The incomplete toluene consumption by the PF+NA consortium was surprising given that NA had been shown to degrade an equivalent concentration of toluene in pure culture. A possible explanation is that NA did

not tolerate styrene. Prior studies also indicate that NA is a slow growing strain [102]. Both synthetic consortia also showed smaller increase in OD than BBC or E, likely due to low growth of CM and NA. The OD of each minimal consortium (PF+NA and PF+CM) increased by 0.04 compared to 0.12 for BBC and 0.16 for E.

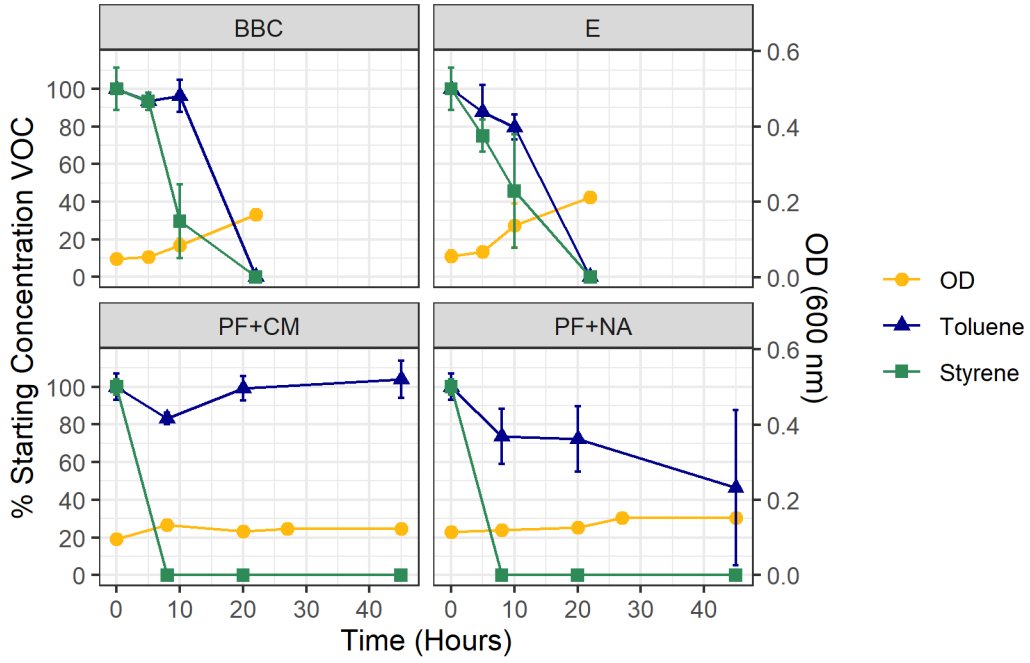

Figure 4.7 VOC removal and growth by cultures with 100 mg L^{-1} TVOC.

In comparison, BBC and E each completely degraded both toluene and styrene within 22 hours. Both BBC and E showed a preference for styrene, as the concentration of styrene decreased first and more rapidly than that of toluene. The consumption of styrene and toluene was sequential for BBC, which only began to degrade toluene after the concentration of styrene reached 30% of the initial concentration. Interestingly, E consistently developed a bright yellow color (see Supplementary Figure 7.8), which indicated the accumulation of a metabolic intermediate in the liquid medium, likely a

catechol compound [114]. The yellow color would decrease after complete consumption of styrene and toluene from the gas phase, (Supplementary Figure 7.9) indicating that the compound was eventually degraded.

4.3.4 Minimal Community Stability

Multiplex qPCR was carried out to monitor the growth of pure cultures and composition of synthetic consortia in biodegradation experiments. The quantification of 16s rRNA genes for NA and PF from experimental samples of the NC+PF minimal consortium is shown in Figure 4.8. The results show that the relative abundance of NA was almost 80% in the samples of the experimental inoculum (p.adj = 0.005). This could have been because the inoculum was not homogenous, or that NA has a lower OD to cell concentration than PF. The abundance of 16s genes for both species increased in the first 10 hours, from $3.0x10^6\ \mu L^{-1}$ to $4.9x10^6\ \mu L^{-1}$ normalized gene copies for NA and more than doubling from $1.4x10^6\ \mu L^{-1}$ to $3.2x10^6\ \mu L^{-1}$ for PF, though these were not statistically significant for either strain due to high variability in the qPCR results for NA.

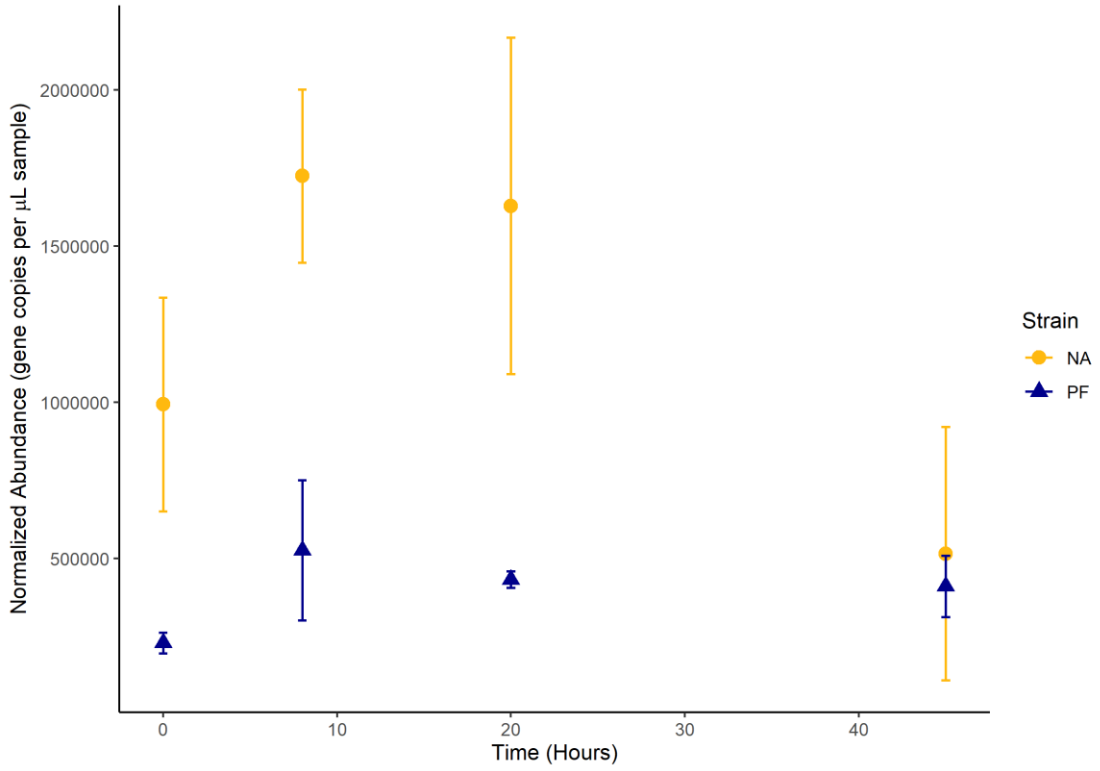

Figure 4.8 Quantification of 16s genes for NA and PF in a minimal consortium over the course of the experiment.

Monitoring the culture with qPCR analysis alongside OD and VOC removal offered additional insight into the minimal community. The abundance of NA and PF both increased from hours 0 to 8, which coincided with the complete degradation of styrene and removal of 26% of toluene, though the OD did not increase during this time. In the rest of the experiment, toluene was further removed to 46% of the starting concentration by hour 45 and the OD increased from 0.11 to 0.15, while the gene abundance of NA and PF did not increase significantly, though the error for NA was quite large. Altogether, these results indicate that monitoring of cultures using qPCR can be informative for growth when cell densities are very low and reveal the individual growth of each species in a minimal

community. However, the multiplex qPCR analysis of PF and NA may have needed better optimization or increased number of sample replicates to minimize analytical error.

4.4 Conclusion

The use of community metabolic network modeling was evaluated for use in the rational design of minimal microbial communities for VOC biodegradation. Over 2,700 individual metabolic network models were generated for use in community modeling. The model identified 95 key species with the individual metabolic potential to degrade either toluene or styrene and over 1,000 combinatoric possibilities for two-member minimal communities with the collective metabolic potential to degrade both toluene and styrene.

A selection of five key species were evaluated experimentally as pure cultures and in minimal communities for toluene and styrene degradation. Two of the five key species were able to degrade toluene or styrene as single substrates as predicted by the individual metabolic network models, while three of the five were unable to utilize their respective VOC as the sole carbon and energy source. Subsequently, only two minimal communities were able to be tested experimentally. Of those, one minimal community composed of *P. fluorescens* and *N. aromaticivorans* was able to fully degrade styrene and partially degrade toluene at the given low concentrations.

The minimal communities were compared experimentally with a pure culture of *P. putida BBC443* and a mixed culture enriched from activated sludge on toluene and styrene as the sole sources of carbon, which were both able to fully degrade toluene and styrene at the given concentrations. The enrichment culture accumulated a bright yellow metabolic product that was excreted from the cells into the liquid medium, which was eventually degraded, however, could potentially be an issue if the culture was grown with a continuous VOC feed. Ultimately, the pure culture of *P. putida BBC443* and the enrichment

culture were better able to degrade a combination of toluene and styrene than the minimal communities tested here. However, the *P. fluorescens* (PF) strain proved able to degrade styrene as well as the BBC and E. Future research should explore the metabolic potential of PF to degrade styrene and potentially other pollutants, alone or in a community with other species.

These results indicate that community metabolic network modeling could be a valuable tool for screening candidate species for inclusion in minimal consortia, but that the approach needs to be combined with additional steps of manual curation and quantitative modeling. Specifically, the predictions must be evaluated for models run with and without metabolic pathway gap filling and manually curated with an eye for false positives. Furthermore, the results are not quantitative, nor do they provide insight on the necessary cultivation conditions that would enable the target metabolism. The modeling approach would be best used as an initial screening step followed by manual curation of metabolic models for the key species of interest, and finally with flux balance analysis modeling of minimal communities, which can give quantitative estimates of metabolic functions.

5 Conclusions

The research presented in this dissertation contribute valuable scientific insights into the engineering of microbioreactors and the microbial communities cultivated within them. In Chapter 2, an experimental method and mathematical model were developed for accurate determination and characterization of mass transfer in microbioreactors, which can be used in future studies to improve the accuracy of mass transfer coefficient determinations and allow for comparison of mass transfer across scales. Results revealed that both experimental methods can be equally accurate and applicable at small scales provided that there is careful consideration of mass transfer and volumes peripheral to the reactor itself.

The method developed in Chapter 2 was then applied to characterize the mass transfer coefficients of several microbioreactor prototypes, which were used to evaluate the impact of several design parameters on performance. In particular, this study focused on the effect of microchannel size and configuration on the mass transfer coefficient and on continuous biological removal of toluene vapors as a model VOC. It was found that microbioreactors with smaller channel dimensions had greater mass transfer coefficients, regardless of microchannel configuration. Furthermore, microbioreactors with smaller channels had greater removal of toluene in continuous biodegradation experiments. All microbioreactors tested in biological experiments were found to have good toluene removal rates (elimination capacities between 100 – 400 g m^{-3} h^{-1}). Overall, Chapter 2 illustrated the value of a rapid prototyping platform for development and optimization of microbioreactors, and provided new information on the relationships between microbioreactor design and performance.

Finally, metabolic network modeling was applied to assist in the engineering of minimal microbial communities for degradation of toluene and styrene as a model system for mixed pollutant biodegradation. It was found that the modeling predictions were reasonable based on general taxonomic traits. However, the models were only partially successful in predicting the performance of strains in experiments. Additionally, a pure culture of *Pseudomonas putida BBC443* and an enrichment culture were observed to degrade both toluene and styrene. In future work, it would be valuable to sequence the whole genome of *P. putida BBC443* and isolates from the enrichment culture, which could be evaluated with metabolic modeling. Metabolic network modeling could prove a valuable screening tool when followed by manual curation of metabolic models and combined with quantitative metabolic modeling of minimal microbial communities.

The ultimate goal of this dissertation was to engineer microbioreactors and microbiomes for biodegradation of VOCs. To this end, methods were developed to characterize key performance indicators, iterate and evaluate microbioreactor design parameters, and rationally design VOC-degrading microbial communities. The research presented here addressed knowledge gaps in the literature connecting microbioreactor design and long-term, biological performance. Future research will benefit from the insights gained here into the value and limitations of automated metabolic network modeling for the engineering of microbiomes.

6 Appendix A. Supplementary Material for Chapter 3.

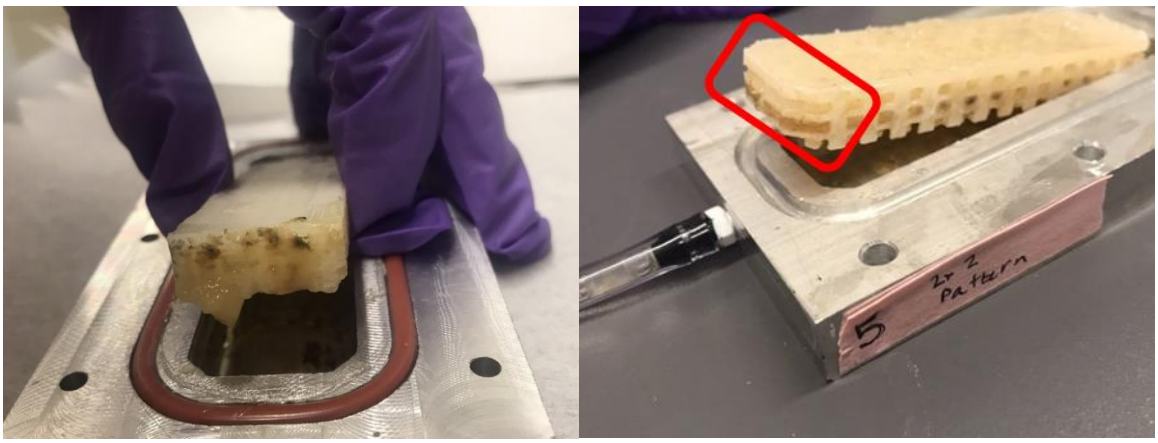

Figure 6.1 Images of two microbioreactors at the end of over 300 hours of operation. (Left) Reactor 0.5-S, (Right) Reactor 4-P. The inlet or "entrance" area to the channels is highlighted in the Right image. The images show microbial biomass agglomerated at the inlet. The presence of dark spots may indicate fungal growth.

Figure 6.2 Experimental set up for biological performance experiments. One of the microbioreactors is circled.

7 Appendix B. Supplementary Material for Chapter 4.

7.1 Inputs to M2M Model

Table 7.1 M2M model "seeds" or metabolite inputs to the model.

Compound	BioCyc ID	Role
water	WATER	Nutrient / Medium component
H^+	PROTON	Nutrient / Medium component
carbon dioxide	CARBON DIOXIDE	Nutrient / Medium component
oxygen	OXYGEN MOLECULE	Nutrient / Medium component
chloride	CL	Nutrient / Medium component
magnesium	MG+2	Nutrient / Medium component
sulfate	SULFATE	Nutrient / Medium component
dihydrogen phosphate	CPD-16459	Nutrient / Medium component
potassium	K	Nutrient / Medium component
phosphate	Pi	Nutrient / Medium component
ammonium	AMMONIUM	Nutrient / Medium component
ammonia	AMMONIA	Nutrient / Medium component
nitrate	NITRATE	Nutrient / Medium component
NADH	NADH	Currency metabolite
NADPH	NADPH	Currency metabolite
NAD+	NAD	Currency metabolite
NADP	NADP	Currency metabolite
FADH2	FADH2	Currency metabolite
an oxidized ferredoxin [iron-sulfur] cluster	Oxidized ferredoxins	Currency metabolite
extracellular repeat	Reduced ferredoxins	Currency metabolite
an oxidized azurin	Oxidized Azurins	Currency metabolite
coenzyme A	CO A	Currency metabolite
succinyl-CoA	SUC-COA	Currency metabolite
ATP	ATP	Currency metabolite
diphosphate	PPI	Currency metabolite
ADP	ADP	Currency metabolite
FAD	FAD	Currency metabolite
Toluene	TOLUENE	Primary substrate (carbon source, electron donor)
Styrene	CPD-1092	Primary substrate (carbon source, electron donor)

Table 7.2 Target metabolites of toluene and styrene degradation pathways.

Degradation Pathway	Common Name	BioCyc ID
Toluene I (*via o-cresol*)	2-methylphenol	CPD-109
	3-methylcatechol	CPD-111
	(2Z,4E)-2-hydroxy-6-oxohepta-2,4-dienoate	CPD-8782
	(2Z)-2-hydroxypenta-2,4-dienoate	CPD-14447
	(S)-4-hydroxy-2-oxopentanoate	4-HYDROXY-2-KETOVALERATE
	acetaldehyde	ACETALD
	acetyl-CoA	ACETYL-COA
Toluene II (*via 4-methylcatechol*)	4-methylphenol	CPD-108
	4-methylcatechol	4-METHYLCATECHOL
	(2Z,4E)-2-hydroxy-5-methyl-6-oxohexa-2,4-dienoate	CPD-8781
	(2Z)-2-hydroxyhexa-2,5-dienoate	CPD-22385
	(S)-4-hydroxy-2-oxohexanoate	CPD-13722
	1-propanal	CPD-665
	pyruvate	PYRUVATE
Toluene III (*via p-cresol*)	4-methylphenol	CPD-108
	4-hydroxybenzyl alcohol	4-HYDROXY-BENZYL-ALCOHOL
	4-hydroxybenzaldehyde	4-HYDROXYBENZALDEHYDE
	4-hydroxybenzoate	4-hydroxybenzoate
	protocatechuate	3-4-DIHYDROXYBENZOATE
	3-carboxy-cis,cis-muconate	CPD-245
	(2-carboxy-2,5-dihydro-5-oxofuran-2-yl)-acetate	CPD-7737
	(4,5-dihydro-5-oxofuran-2-yl)-acetate	3-OXOADIPATE-ENOL-LACTONE
	3-oxoadipate	3-KETO-ADIPATE
	3-oxoadipyl-CoA	3-KETO-ADIPYL-COA
	succinyl-CoA	SUC-COA
Toluene IV (*via catechol*)	benzyl alcohol	BENZYL-ALCOHOL
	benzaldehyde	BENZALDEHYDE
	benzoate	BENZOATE

	3,5-cyclohexadiene-1,2-diol-1-carboxylate	CPD-290
	catechol	CATECHOL
	(2Z,4E)-2-hydroxy-6-oxohexa-2,4-dienoate	HYDROXYMUCONATE-SALD
	(2Z,4E)-2-hydroxyhexa-2,4-dienedioate	CPD-13339
	(3E)-2-oxohex-3-enedioate	CPD-8742
	3-oxoadipate	3-KETO-ADIPATE
	3-oxoadipyl-CoA	3-KETO-ADIPYL-COA
	succinyl-CoA	SUC-COA
Toluene IV (*via toluene-cis-diol)*	(1S,2R)-3-methylcyclohexa-3,5-diene-1,2-diol	TOLUENECISDHDIOL
	3-methylcatechol	CPD-111
	(2Z,4E)-2-hydroxy-6-oxohexa-2,4-dienoate	HYDROXYMUCONATE-SALD
	(2Z)-2-hydroxypenta-2,4-dienoate	CPD-14447
	(S)-4-hydroxy-2-oxopentanoate	4-HYDROXY-2-KETOVALERATE
	acetaldehyde	ACETALD
	acetyl-CoA	ACETYL-COA
Styrene	(S)-2-phenyloxirane	CPD-13773
	phenylacetaldehyde	PHENYLACETALDEHYDE
	phenylacetate	PHENYLACETATE

7.2 Supplementary Model Results

Table 7.3 Taxonomic classification of key species for toluene and styrene degradation targets.

Class	Order	Family	Genus	N
Actinomycetia	*Corynebacteriales*	*Nocardiaceae*	*Rhodococcus*	1
Actinomycetia	*Micrococcales*	*Microbacteriaceae*	*Microbacterium*	1
Alphaproteobacteria	*Rhodobacterales*	*Roseobacteraceae*	*Celeribacter*	1
Alphaproteobacteria	*Sphingomonadales*	*Sphingomonadaceae*	*Novosphingobium*	1
Alphaproteobacteria	*Sphingomonadales*	*Sphingomonadaceae*	*Sphingopyxis*	3
Betaproteobacteria	*Burkholderiales*	*Alcaligenaceae*	*Achromobacter*	4
Betaproteobacteria	*Burkholderiales*	*Alcaligenaceae*	*Bordetella*	72
Betaproteobacteria	*Burkholderiales*	*Alcaligenaceae*	*Kerstersia*	1
Betaproteobacteria	*Burkholderiales*	*Burkholderiaceae*	*Burkholderia*	27
Betaproteobacteria	*Burkholderiales*	*Burkholderiaceae*	*Cupriavidus*	11
Betaproteobacteria	*Burkholderiales*	*Burkholderiaceae*	*Pandoraea*	4
Betaproteobacteria	*Burkholderiales*	*Burkholderiaceae*	*Paraburkholderia*	10
Betaproteobacteria	*Burkholderiales*	*Burkholderiaceae*	*Ralstonia*	6
Betaproteobacteria	*Burkholderiales*	*Comamonadaceae*	*Acidovorax*	4
Betaproteobacteria	*Burkholderiales*	*Comamonadaceae*	*Alicycliphilus*	2
Betaproteobacteria	*Burkholderiales*	*Comamonadaceae*	*Comamonas*	5
Betaproteobacteria	*Burkholderiales*	*Comamonadaceae*	*Delftia*	1
Betaproteobacteria	*Burkholderiales*	*Comamonadaceae*	*Diaphorobacter*	1
Betaproteobacteria	*Burkholderiales*	*Comamonadaceae*	*Hydrogenophaga*	2
Betaproteobacteria	*Burkholderiales*	*Comamonadaceae*	*Melaminivora*	1
Betaproteobacteria	*Burkholderiales*	*Comamonadaceae*	*Polaromonas*	1
Betaproteobacteria	*Burkholderiales*	*Comamonadaceae*	*Simplicispira*	1
Betaproteobacteria	*Burkholderiales*	*Sphaerotilaceae*	*Ideonella*	1
Betaproteobacteria	*Burkholderiales*	*Sphaerotilaceae*	*Methylibium*	1
Betaproteobacteria	*Burkholderiales*	*Sphaerotilaceae*	*Schlegelella*	1
Betaproteobacteria	*Burkholderiales*	*Sphaerotilaceae*	*Sphaerotilus*	1
Betaproteobacteria	*Rhodocyclales*	*Rhodocyclaceae*	*Aromatoleum*	1
Betaproteobacteria	*Rhodocyclales*	*Rhodocyclaceae*	*Rugosibacter*	1
Gammaproteobacteria	*Pseudomonadales*	*Pseudomonadaceae*	*Pseudomonas*	26
Gammaproteobacteria	*Pseudomonadales*	*Pseudomonadaceae*	*Stutzerimonas*	2

7.3 Solutions graphs for model runs with styrene and toluene degradation pathways II – V as targets

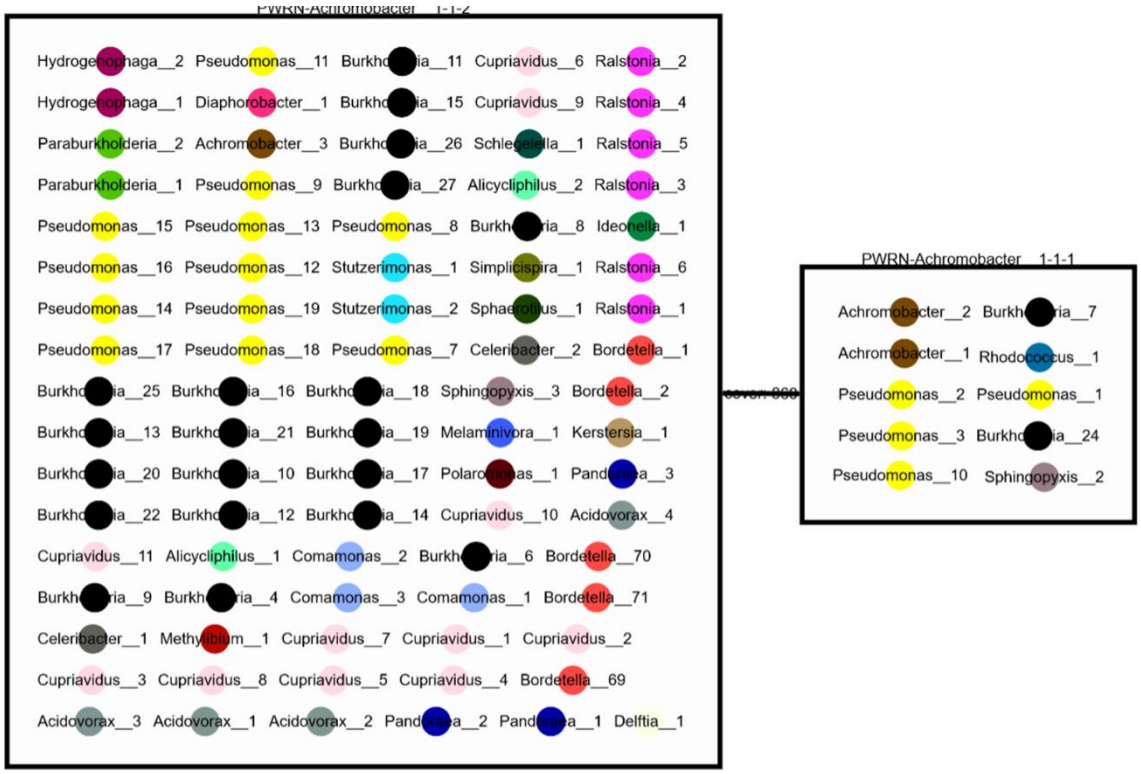

Figure 7.1 Solution graph of the minimal communities and key species for toluene (degradation pathway II) and styrene degradation products. The solution graph shown here was generated from a model run without the GSMN for *Achromobacter xylosoxidans R4,* which was predicted to be able to reach all metabolites in Target Set II individually. Key species are colored by genus. Black circles correspond to *Burkholderia*.

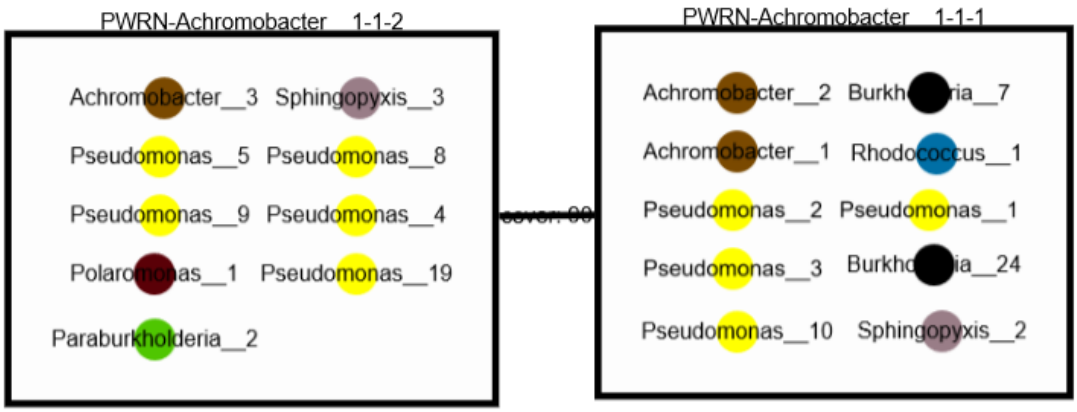

Figure 7.2 Solution graph of the minimal communities and key species for toluene (degradation pathway III) and styrene degradation products. Key species are colored by genus.

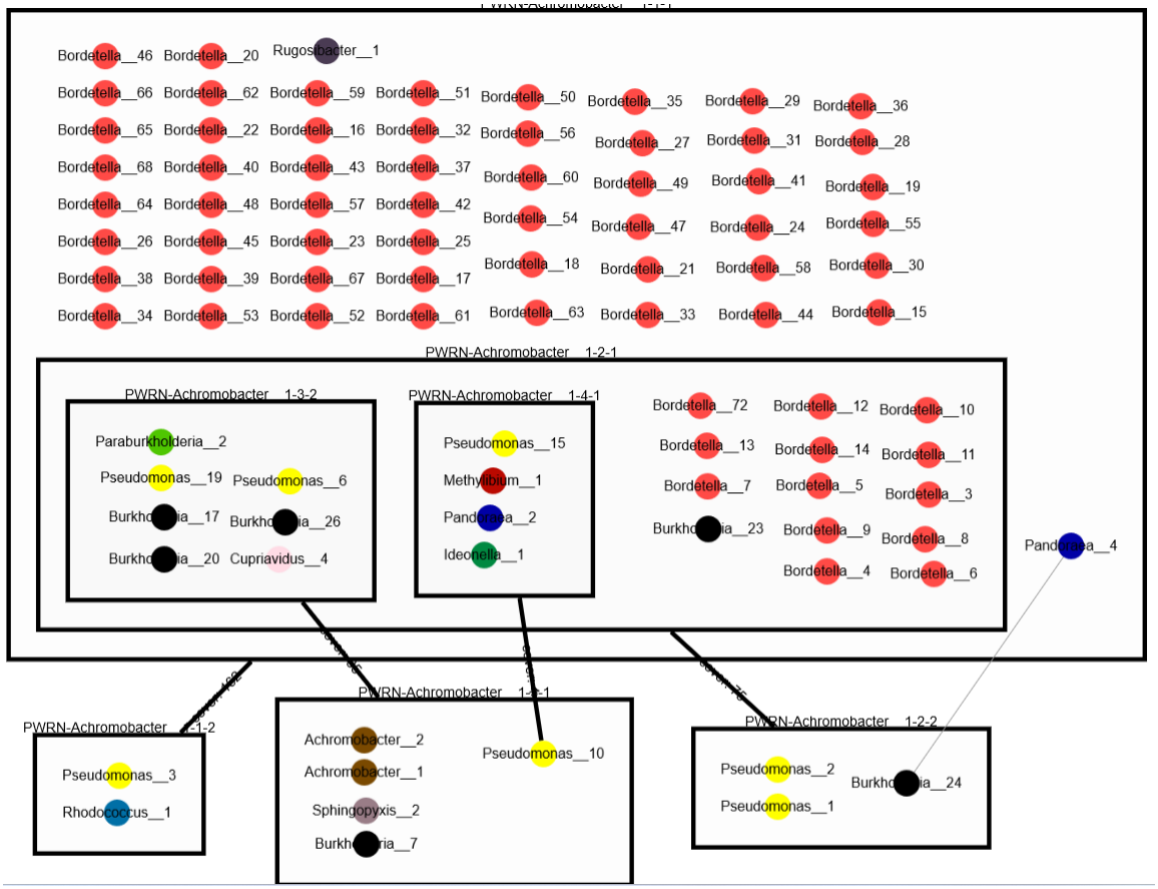

Figure 7.3 Solution graph of the minimal communities and key species for toluene (degradation pathway IV) and styrene degradation products. Key species are colored by genus.

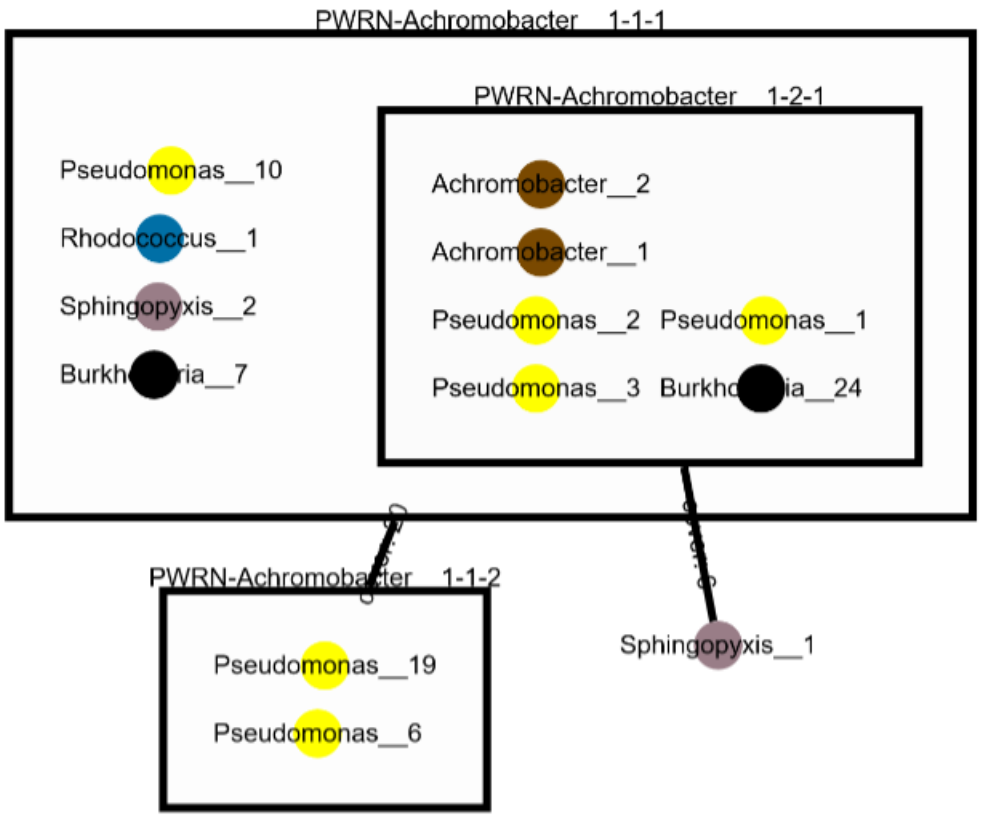

Figure 7.4 Solution graph of the minimal communities and key species for toluene (degradation pathway V) and styrene degradation products. Key species are colored by genus.

7.4 Producers of each target metabolite in example minimal communities.

Table 7.4 Producers of metabolic targets for Target Set I

Target Metabolite	Specific pathway	Target Producer(s)
2-methylphenol	Toluene I	GCA_000196015 (CM)
3-methylcatechol	Toluene I	GCA_000196015 (CM)
(2Z,4E)-2-hydroxy-6-oxohepta-2,4-dienoate	Toluene I	GCA_000196015 (CM)
(2Z)-2-hydroxypenta-2,4-dienoate	Toluene I	GCA_900475215 (PF)
		GCA_000196015 (CM)
(S)-4-hydroxy-2-oxopentanoate	Toluene I	GCA_000196015 (CM)
acetaldehyde	Toluene I	GCA_900475215 (PF)
		GCA_000196015 (CM)
acetyl-CoA	Toluene I	GCA_900475215 (PF)
		GCA_000196015 (CM)
(S)-2-phenyloxirane	Styrene	GCA_900475215 (PF)
phenylacetaldehyde	Styrene	GCA_900475215 (PF)
		GCA_000196015 (CM)
phenylacetate	Styrene	GCA_900475215 (PF)
		GCA_000196015 (CM)

This shows which species in a 2-member minimal community (here PF & CM) has the metabolic potential to reach each metabolic target. Some are producible by one species while others are producible by both.

Table 7.5 Producers of metabolic targets for Target Set III


```
"1": {
    "M_3__45__4__45__DIHYDROXYBENZOATE_c": [
      "GCA_000013325",
      "GCA_900009125"
    ],
    "M_3__45__KETO__45__ADIPATE_c": [
      "GCA_900009125",
      "GCA_000013325"
    ],
    "M_3__45__KETO__45__ADIPYL__45__COA_c": [
      "GCA_900009125",
      "GCA_000013325"
    ],
    "M_3__45__OXOADIPATE__45__ENOL__45__LACTONE_c": [
      "GCA_000013325",
      "GCA_900009125"
    ],
    "M_4__45__HYDROXYBENZALDEHYDE_c": [
      "GCA_000013325"
    ],
    "M_4__45__HYDROXY__45__BENZYL__45__ALCOHOL_c": [
      "GCA_000013325"
    ],
    "M_4__45__hydroxybenzoate_c": [
      "GCA_900009125",
      "GCA_000013325"
    ],
    "M_CPD__45__108_c": [
      "GCA_900009125"
    ],
    "M_CPD__45__13773_c": [
      "GCA_900009125"
    ],
    "M_CPD__45__245_c": [
      "GCA_900009125"
    ],
    "M_CPD__45__7737_c": [
      "GCA_900009125"
    ],
    "M_PHENYLACETALDEHYDE_c": [
      "GCA_900009125"
    ],
    "M_PHENYLACETATE_c": [
      "GCA_900009125"
    ],
    "M_SUC__45__COA_c": [
      "GCA_900009125",
      "GCA_000013325"
    ]
```


Target Set III: Producers of metabolic targets in the minimal community of GCA_000013325 (NA) and GCA_900009125 (*Achromobacter xylosoxidans R4*), as direct output from M2M.

7.5 Quality profile of activated sludge forward and reverse reads for 16s rRNA gene amplicon sequencing.

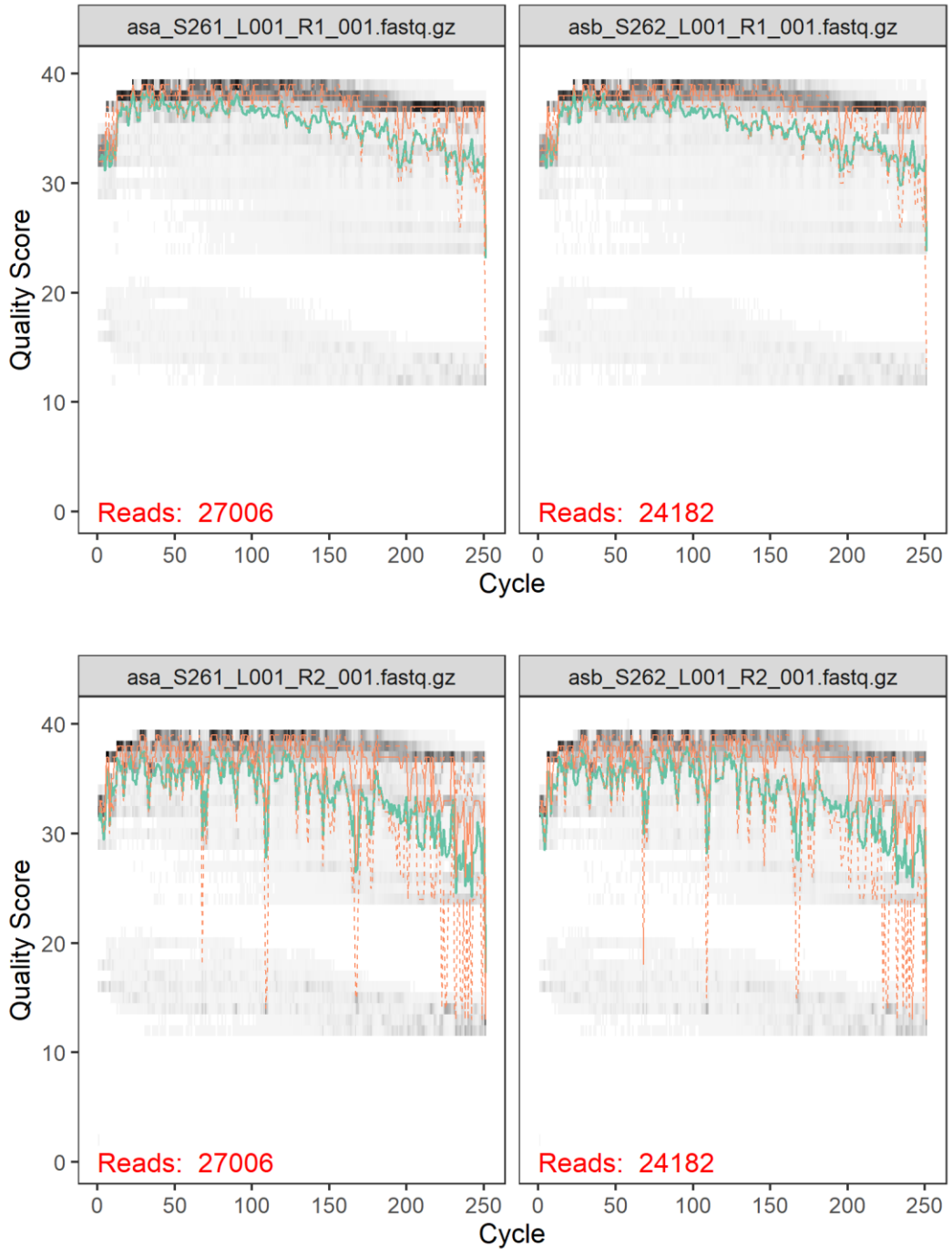

Figure 7.5 Forward (top) and reverse (bottom) read quality profiles.

7.6 Alternative Presentations of Relative Abundance

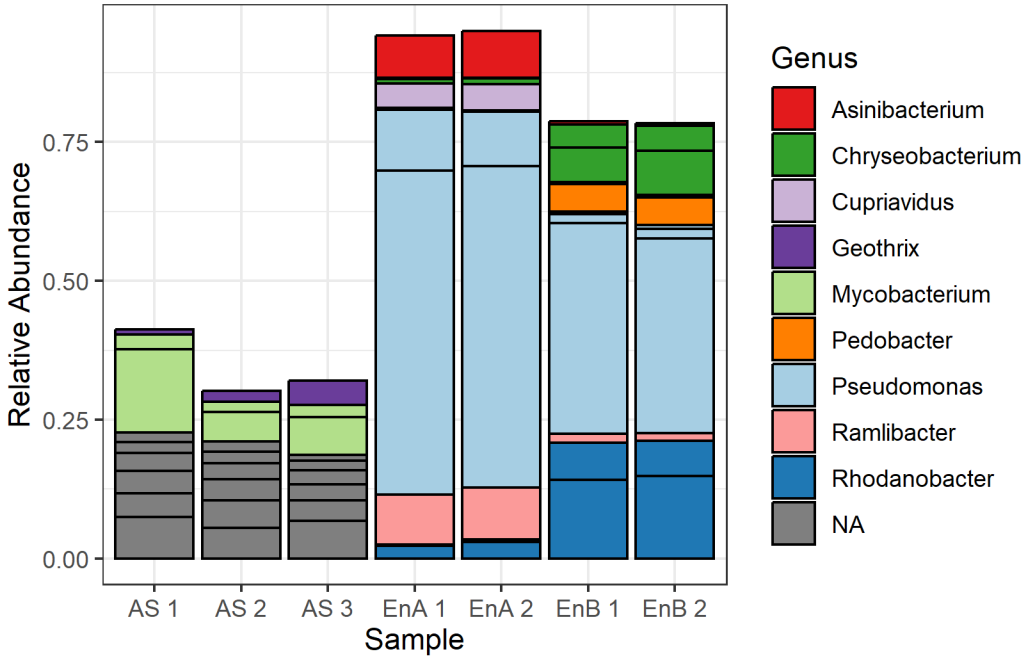

Figure 7.6 Relative abundance of OTUs at the genus level.

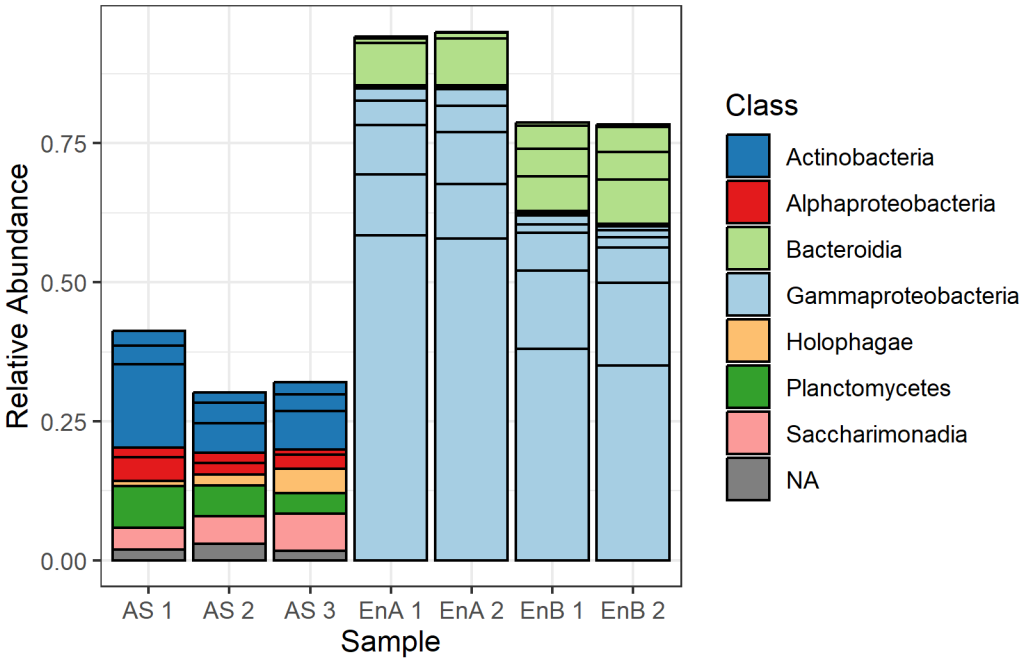

Figure 7.7 Relative abundance of OTUs at the class level.

7.7 Accumulation of Yellow Compound in Enrichment Culture

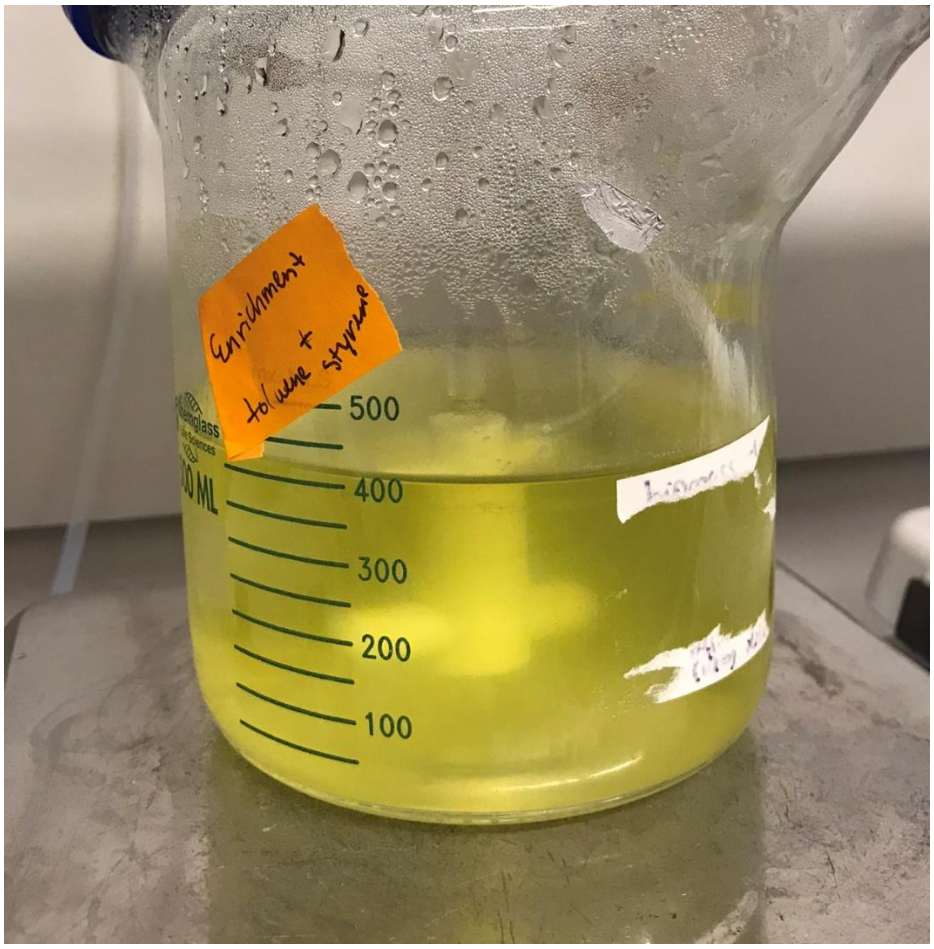

Figure 7.8 Yellow color of the enrichment culture 2 hours after dosing with 100 mg/L (initial liquid concentration) of toluene and styrene each.

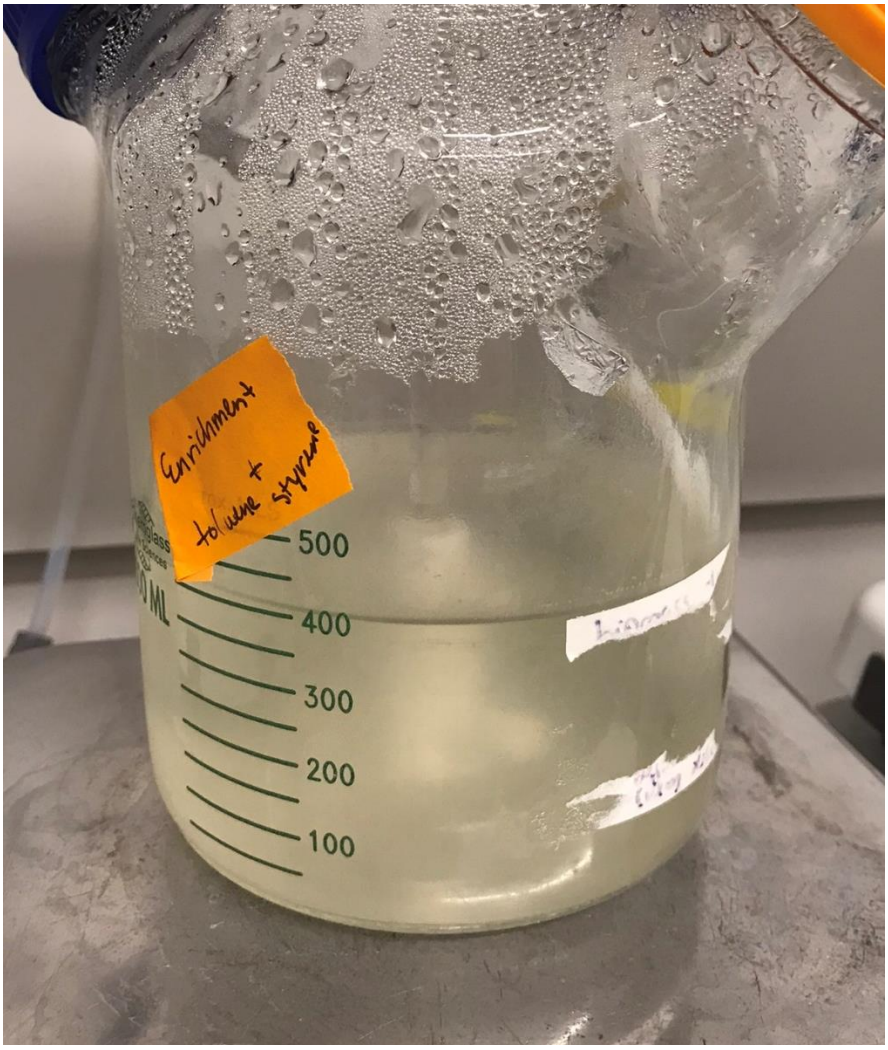

Figure 7.9 Color of the enrichment culture 19 hours after dosing with 100 mg/L (initial liquid concentration) of toluene and styrene each.

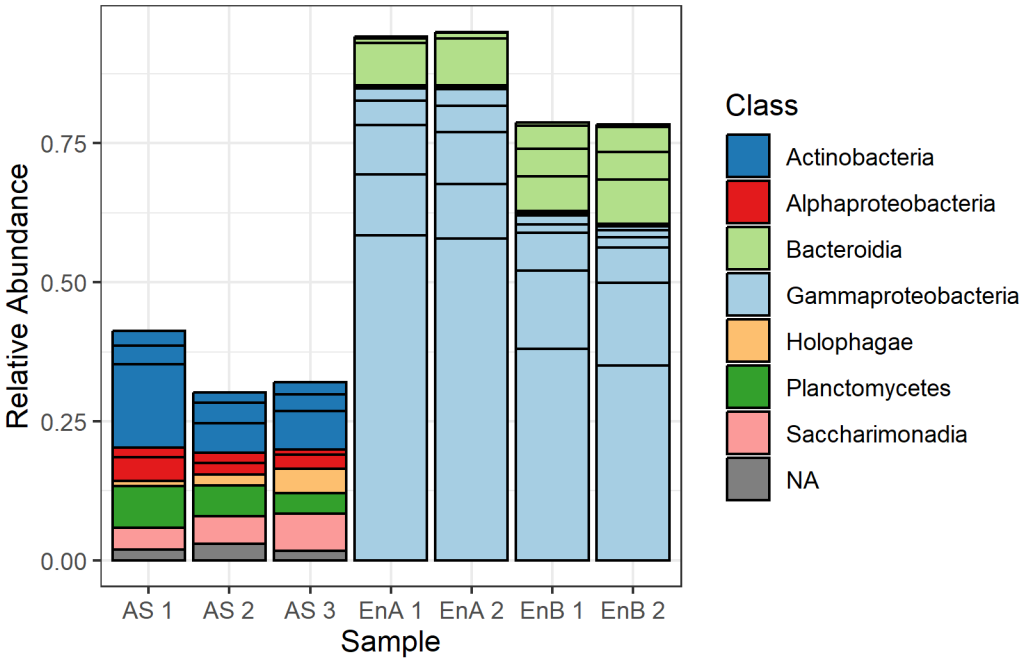

Figure 7.10 Relative abundance of OTUs at the class level.

References

[1] U.S. EPA, “Volatile Organic Compounds’ Impact on Indoor Air Quality,” 2012. https://www.epa.gov/indoor-air-quality-iaq/volatile-organic-compounds-impact-indoor-air-quality

[2] C. Jia, S. Batterman, and C. Godwin, “VOCs in industrial, urban and suburban neighborhoods, Part 1: Indoor and outdoor concentrations, variation, and risk drivers,” *Atmospheric Environment*, vol. 42, no. 9, pp. 2083–2100, 2008, doi: 10.1016/j.atmosenv.2007.11.055.

[3] F. C. Su, B. Mukherjee, and S. Batterman, “Determinants of personal, indoor and outdoor VOC concentrations: An analysis of the RIOPA data,” *Environmental Research*, vol. 126, pp. 192–203, 2013, doi: 10.1016/j.envres.2013.08.005.

[4] B. Grajewski and J. Deddens, “Measurements of Indoor Air Quality on Commercial Transport Aircraft,” *Indoor Air*, pp. 782–787, 2002.

[5] J. T. James, T. F. Limero, P. F. Cheng, V. J. De Vera, J. Hand, and A. Macatangay, “International Space Station Air Quality Assessed According to Toxicologically-Grouped Compounds”.

[6] Y. D. Severs, “A baseline air quality assessment onboard a Victoria class submarine: HMCS Windsor,” no. May, 2006.

[7] S. Cakmak *et al.*, “Residential exposure to volatile organic compounds and lung function: Results from a population-based cross-sectional survey,” *Environmental Pollution*, vol. 194, pp. 145–151, 2014, doi: 10.1016/j.envpol.2014.07.020.

[8] W. Chen *et al.*, “Performance of air cleaners for removing multi- volatile organic compounds in indoor air,” *ASHRAE Transactions.*, no. 111(1), pp. 1101–1114, 2005.

[9] L. Yang, A. Cai, C. Luo, Z. Liu, W. Shangguan, and T. Xi, “Performance analysis of a novel TiO 2 -coated foam-nickel PCO air purifier in HVAC systems,” *Separation and Purification Technology*, vol. 68, no. 2, pp. 232–237, 2009, doi: 10.1016/j.seppur.2009.05.008.

[10] U.S. EPA, “Residential Air Cleaners (Second Edition): A Summary of Available Information,” 2009. https://www.epa.gov/indoor-air-quality-iaq/residential-air-cleaners-second-edition-summary-available-information

[11] D. Gabriel and M. a Deshusses, “Retrofitting existing chemical scrubbers to biotrickling filters for H2S emission control.,” *Proceedings of the National Academy of Sciences of the United States of America*, vol. 100, no. 11, pp. 6308–6312, 2003, doi: 10.1073/pnas.0731894100.

[12] “Deshusses, M. A., Biological waste air treatment in biofilters. Current Opinion in Biotechnology 1997, 8, (3), 335-.pdf.”

[13] M. N. Kashid, A. Renken, and L. Kiwi-Minsker, “Gas-liquid and liquid-liquid mass transfer in microstructured reactors,” *Chemical Engineering Science*, vol. 66, no. 17, pp. 3876–3897, 2011, doi: 10.1016/j.ces.2011.05.015.

[14] L. Shui, J. C. T. Eijkel, and A. van den Berg, “Multiphase flow in microfluidic systems - Control and applications of droplets and interfaces,” *Advances in Colloid and Interface Science*, vol. 133, no. 1, pp. 35–49, 2007, doi: 10.1016/j.cis.2007.03.001.

[15] A. Zanzotto, N. Szita, P. Boccazzi, P. Lessard, A. J. Sinskey, and K. F. Jensen, “Membrane-aerated microbioreactor for high-throughput bioprocessing,” *Biotechnology and Bioengineering*, vol. 87, no. 2, pp. 243–254, 2004, doi: 10.1002/bit.20140.

[16] K. Jensen, “Microreaction engineering—is small better?,” *Chemical Engineering Science, 2001*, vol. 56, pp. 293–303, 2001, doi: 10.1016/S0009-2509(00)00230-X.

[17] B. Damit, “Droplet-based microfluidics detector for bioaerosol detection,” *Aerosol Science and Technology*, vol. 51, no. 4, pp. 488–500, 2017, doi: 10.1080/02786826.2016.1275515.

[18] B. Guieysse, C. Hort, V. Platel, R. Munoz, M. Ondarts, and S. Revah, “Biological treatment of indoor air for VOC removal: Potential and challenges,” *Biotechnology Advances*, vol. 26, no. 5, pp. 398–410, 2008, doi: 10.1016/j.biotechadv.2008.03.005.

[19] L. R. López De León, K. E. Deaton, and M. A. Deshusses, “Miniaturized Biotrickling Filters and Capillary Microbioreactors for Process Intensification of VOC Treatment with Intended Application to Indoor Air,” *Environmental Science and Technology*, vol. 53, no. 3, pp. 1518–1526, 2019, doi: 10.1021/acs.est.8b05209.

[20] L. R. López de León, K. E. Deaton, J. Junkin, and M. A. Deshusses, “Capillary microbioreactors for VOC vapor treatment: Impacts of operating conditions,” *Chemosphere*, vol. 258, pp. 1–9, 2020, doi: 10.1016/j.chemosphere.2020.127286.

[21] F. Garcia-Ochoa and E. Gomez, “Bioreactor scale-up and oxygen transfer rate in microbial processes: An overview,” *Biotechnology Advances*, vol. 27, no. 2, pp. 153–176, 2009, doi: 10.1016/j.biotechadv.2008.10.006.

[22] L. R. López, T. Bezerra, M. Mora, J. Lafuente, and D. Gabriel, “Influence of trickling liquid velocity and flow pattern in the improvement of oxygen transport in aerobic biotrickling filters for biogas desulfurization,” *Journal of Chemical Technology and Biotechnology*, vol. 91, no. 4, pp. 1031–1039, 2016, doi: 10.1002/jctb.4676.

[23] G. Skouteris, G. Rodriguez-Garcia, S. F. Reinecke, and U. Hampel, “The use of pure oxygen for aeration in aerobic wastewater treatment: A review of its potential and limitations,” *Bioresource Technology*, vol. 312, no. May, p. 123595, 2020, doi: 10.1016/j.biortech.2020.123595.

[24] N. J. R. Kraakman, J. Rocha-Rios, and M. C. M. Van Loosdrecht, “Review of mass transfer aspects for biological gas treatment,” *Applied Microbiology and Biotechnology*, vol. 91, no. 4, pp. 873–886, 2011, doi: 10.1007/s00253-011-3365-5.

[25] R. Lebrero, J. M. Estrada, R. Muñoz, and G. Quijano, “Toluene mass transfer characterization in a biotrickling filter,” *Biochemical Engineering Journal*, vol. 60, pp. 44–49, 2012, doi: 10.1016/j.bej.2011.09.017.

[26] W. G. Whitman, “The two film theory of gas absorption,” *International Journal of Heat and Mass Transfer*, vol. 5, no. 5, pp. 429–433, May 1962, doi: 10.1016/0017-9310(62)90032-7.

[27] K. Van’T Riet, “Review of Measuring Methods and Results in Nonviscous Gas-Liquid Mass Transfer in Stirred Vessels,” *Industrial and Engineering Chemistry Process Design and Development*, vol. 18, no. 3, pp. 357–364, 1979, doi: 10.1021/i260071a001.

[28] S. Suresh, V. C. Srivastava, and I. M. Mishra, “Techniques for oxygen transfer measurement in bioreactors: A review,” *Journal of Chemical Technology and Biotechnology*, vol. 84, no. 8, pp. 1091–1103, 2009, doi: 10.1002/jctb.2154.

[29] ASCE Oxygen Transfer Standards Subcommittee, “Standard Guidelines for In-Process Oxygen Transfer Testing.” doi: 10.1061/9780784414958.

[30] M. K. Stenstrom, S.-Y. (Ben) Leu, and P. Jiang, “Theory to Practice: Oxygen Transfer and the New ASCE Standard,” in *WEFTEC*, 2006, pp. 4838–4852.

[31] S. Kim and M. A. Deshusses, “Determination of mass transfer coefficients for packing materials used in biofilters and biotrickling filters for air pollution control. 1. Experimental results,” *Chemical Engineering Science*, vol. 63, no. 4, pp. 841–855, 2008, doi: 10.1016/j.ces.2007.10.011.

[32] A. D. Dorado *et al.*, “Evaluation of mass transfer coefficients in biotrickling filters: Experimental determination and comparison to correlations,” *Chemical Engineering and Technology*, vol. 32, no. 12, pp. 1941–1950, 2009, doi: 10.1002/ceat.200900275.

[33] J. F. Rejl, V. Linek, T. Moucha, and L. Valenz, “Methods standardization in the measurement of mass-transfer characteristics in packed absorption columns,” *Chemical Engineering Research and Design*, vol. 87, no. 5, pp. 695–704, 2009, doi: 10.1016/j.cherd.2008.09.009.

[34] C. O. Vandu and R. Krishna, “Volumetric mass transfer coefficients in slurry bubble columns operating in the churn-turbulent flow regime,” *Chemical Engineering and Processing: Process Intensification*, vol. 43, no. 8, pp. 987–995, 2004, doi: 10.1016/j.cep.2003.09.007.

[35] J. M. Estrada, A. Dudek, R. Muñoz, and G. Quijano, “Fundamental study on gas-liquid mass transfer in a biotrickling filter packed with polyurethane foam,” *Journal of Chemical Technology and Biotechnology*, vol. 89, no. 9, pp. 1419–1424, 2014, doi: 10.1002/jctb.4226.

[36] E. Erhan, E. Yer, G. Akay, B. Keskinler, and D. Keskinler, “Phenol degradation in a fixed-bed bioreactor using micro-cellular polymer-immobilized Pseudomonas syringae,” *Journal of Chemical Technology and Biotechnology*, vol. 79, no. 2, pp. 195–206, 2004, doi: 10.1002/jctb.938.

[37] G. Rodriguez, A. D. Dorado, A. Bonsfills, R. Sanahuja, D. Gabriel, and X. Gamisans, “Optimization of oxygen transfer through venturi-based systems applied to the biological sweetening of biogas,” *Journal of Chemical Technology and Biotechnology*, vol. 87, no. 6, pp. 854–860, 2012, doi: 10.1002/jctb.3731.

[38] M. K. Stenstrom *et al.*, “Oxygen Transfer in a Full-Depth Biological Aerated Filter,” *Water Environment Research*, vol. 80, no. 7, pp. 663–671, 2008, doi: 10.2175/106143008x268452.

[39] M. Kordač, M. Opletal, and V. Linek, “Measurement of mass transfer characteristics of gas/liquid reactors by sulphite system using on-line monitoring UV absorption,” *Chemical Engineering Journal*, vol. 167, no. 1, pp. 314–321, 2011, doi: 10.1016/j.cej.2010.12.075.

[40] M. Sattari-Najafabadi, M. Nasr Esfahany, Z. Wu, and B. Sunden, “Mass transfer between phases in microchannels: A review,” *Chemical Engineering and Processing - Process Intensification*, vol. 127, no. February, pp. 213–237, 2018, doi: 10.1016/j.cep.2018.03.012.

[41] T. V. Kirk and N. Szita, “Oxygen transfer characteristics of miniaturized bioreactor systems,” *Biotechnology and Bioengineering*, vol. 110, no. 4, pp. 1005–1019, 2013, doi: 10.1002/bit.24824.

[42] C. O. Vandu, H. Liu, and R. Krishna, “Mass transfer from Taylor bubbles rising in single capillaries,” *Chemical Engineering Science*, vol. 60, no. 22, pp. 6430–6437, 2005, doi: 10.1016/j.ces.2005.01.037.

[43] J. Yue, G. Chen, Q. Yuan, L. Luo, and Y. Gonthier, “Hydrodynamics and mass transfer characteristics in gas-liquid flow through a rectangular microchannel,” *Chemical Engineering Science*, vol. 62, no. 7, pp. 2096–2108, 2007, doi: 10.1016/j.ces.2006.12.057.

[44] G. Mehta *et al.*, “Quantitative measurement and control of oxygen levels in microfluidic poly(dimethylsiloxane) bioreactors during cell culture,” *Biomedical Microdevices*, vol. 9, no. 2, pp. 123–134, 2007, doi: 10.1007/s10544-006-9005-7.

[45] S. D. Doig, K. Ortiz-Ochoa, J. M. Ward, and F. Baganz, “Characterization of oxygen transfer in miniature and lab-scale bubble column bioreactors and comparison of

microbial growth performance based on constant kLa," *Biotechnology Progress*, vol. 21, no. 4, pp. 1175–1182, 2005, doi: 10.1021/bp050064j.

[46] J. Tan, Y. C. Lu, J. H. Xu, and G. S. Luo, "Mass transfer performance of gas-liquid segmented flow in microchannels," *Chemical Engineering Journal*, vol. 181–182, pp. 229–235, 2012, doi: 10.1016/j.cej.2011.11.067.

[47] B. Xu, W. Cai, X. Liu, and X. Zhang, "Mass transfer behavior of liquid-liquid slug flow in circular cross-section microchannel," *Chemical Engineering Research and Design*, vol. 91, no. 7, pp. 1203–1211, 2013, doi: 10.1016/j.cherd.2013.01.014.

[48] J. Rocha-Rios, N. J. R. Kraakman, R. Kleerebezem, S. Revah, M. T. Kreutzer, and M. C. M. van Loosdrecht, "A capillary bioreactor to increase methane transfer and oxidation through Taylor flow formation and transfer vector addition," *Chemical Engineering Journal*, vol. 217, pp. 91–98, 2013, doi: 10.1016/j.cej.2012.11.065.

[49] E. Morral, C. Lao-Luque, D. Gabriel, X. Gamisans, and A. D. Dorado, "Capillary membrane bioreactor for abatement of low soluble compounds in waste gas," *Journal of Chemical Technology and Biotechnology*, vol. 93, no. 2, pp. 548–556, 2018, doi: 10.1002/jctb.5400.

[50] S. Achinas, J.-I. Heins, J. Krooneman, and G. J. W. Euverink, "Miniaturization and 3D Printing of Bioreactors: A Technological Mini Review," *Micromachines*, vol. 11, no. 9, p. 853, 2020, doi: 10.3390/mi11090853.

[51] S. A. and G. J. W. Euverink, "Development of an Anaerobic Digestion Screening System Using 3D-Printed Mini-Bioreactors," *New Advances on Fermentation Processes. IntechOpen*, 2019, doi: http://dx.doi.org/10.5772/57353.

[52] R. Hortsch and D. Weuster-Botz, *Milliliter-scale stirred tank reactors for the cultivation of microorganisms*, vol. 73, no. C. Elsevier Inc., 2010. doi: 10.1016/S0065-2164(10)73003-3.

[53] Z. Zhang, P. Boccazzi, H.-G. Choi, G. Perozziello, A. J. Sinskey, and K. F. Jensen, "Microchemostat-microbial continuous culture in a polymer-based, instrumented microbioreactor.," *Lab on a chip*, vol. 6, no. 7, pp. 906–913, 2006, doi: 10.1039/b518396k.

[54] T. L. Philichi and M. K. Stenstrom, "Effects of dissolved oxygen probe lag on oxygen transfer parameter estimation," *Journal of the Water Pollution Control Federation*, vol. 61, no. 1, pp. 83–86, 1989.

[55] M. A. Deshusses, G. Hamer, and I. J. Dunn, "Behavior of Biofilters for Waste Air Biotreatment. 1. Dynamic Model Development," *Environmental Science and Technology*, vol. 29, no. 4, pp. 1048–1058, 1995, doi: 10.1021/es00004a027.

[56] L. Arellano-García, A. D. Dorado, A. Morales-Guadarrama, E. Sacristan, X. Gamisans, and S. Revah, "Modeling the effects of biomass accumulation on the

performance of a biotrickling filter packed with PUF support for the alkaline biotreatment of dimethyl disulfide vapors in air," *Applied Microbiology and Biotechnology*, vol. 99, no. 1, pp. 97–107, 2014, doi: 10.1007/s00253-014-5929-7.

[57] M. N. Kashid, A. Renken, and L. Kiwi-Minsker, "Influence of Flow Regime on Mass Transfer in Different Types of Microchannels," *Industrial and Engineering Chemistry Research*, vol. 50, no. 11, pp. 6906–6914, 2011, doi: 10.1021/ie102200j.

[58] M. Roudet, K. Loubiere, C. Gourdon, and M. Cabassud, "Hydrodynamic and mass transfer in inertial gas-liquid flow regimes through straight and meandering millimetric square channels," *Chemical Engineering Science*, vol. 66, no. 13, pp. 2974–2990, 2011, doi: 10.1016/j.ces.2011.03.045.

[59] G. Li, M. Shang, Y. Song, and Y. Su, "Characterization of liquid–liquid mass transfer performance in a capillary microreactor system," *AIChE Journal*, vol. 64, no. 3, pp. 1106–1116, 2018, doi: 10.1002/aic.15973.

[60] N. J. R. Kraakman, J. Rocha-Rios, and M. C. M. Van Loosdrecht, "Review of mass transfer aspects for biological gas treatment," *Applied Microbiology and Biotechnology*, vol. 91, no. 4, pp. 873–886, 2011, doi: 10.1007/s00253-011-3365-5.

[61] "Standard Guidelines for In-Process Oxygen Transfer Testing (ASCE 18-96)," ASCE 18-96, 1997.

[62] K. E. Deaton, L. R. López de León, S. Pascual, and M. A. Deshusses, "Critical assessment of gassing-in methods to determine mass transfer coefficient in miniature and microbioreactors with gas-liquid flow," *Biochemical Engineering Journal*, vol. 187, p. 108655, Nov. 2022, doi: 10.1016/j.bej.2022.108655.

[63] D. M. Fries and P. R. von Rohr, "Liquid mixing in gas-liquid two-phase flow by meandering microchannels," *Chemical Engineering Science*, vol. 64, no. 6, pp. 1326–1335, 2009, doi: 10.1016/j.ces.2008.11.019.

[64] X. Wang *et al.*, "Scale-up of microreactor: Effects of hydrodynamic diameter on liquid–liquid flow and mass transfer," *Chemical Engineering Science*, vol. 226, p. 115838, Nov. 2020, doi: 10.1016/j.ces.2020.115838.

[65] R. Karande, B. Halan, A. Schmid, and K. Buehler, "Segmented flow is controlling growth of catalytic biofilms in continuous multiphase microreactors," *Biotechnology and Bioengineering*, vol. 111, no. 9, pp. 1831–1840, 2014, doi: 10.1002/bit.25256.

[66] L. R. López de León, K. E. Deaton, J. Junkin, and M. A. Deshusses, "Capillary microbioreactors for VOC vapor treatment: Impacts of operating conditions," *Chemosphere*, vol. 258, pp. 1–9, 2020, doi: 10.1016/j.chemosphere.2020.127286.

[67] C. Yang *et al.*, "Simultaneous Removal of Multicomponent VOCs in Biofilters," *Trends in Biotechnology*, vol. 36, no. 7, pp. 1–13, 2018, doi: 10.1016/j.tibtech.2018.02.004.

[68] M. M. Amin *et al.*, “Biodegradation of n-hexane as single pollutant and in a mixture with BTEX in a scoria/compost-based biofilter,” *Process Safety and Environmental Protection*, vol. 107, pp. 508–517, 2017, doi: 10.1016/j.psep.2017.03.019.

[69] D. Liao *et al.*, “Removal of benzene, toluene, xylene and styrene by biotrickling filters and identification of their interactions,” *PLOS ONE*, vol. 13, no. 1, p. e0189927, Jan. 2018, doi: 10.1371/journal.pone.0189927.

[70] J. Hu, L. Zhang, J. Chen, Y. Luo, B. Sun, and G. Chu, “Performance and microbial analysis of a biotrickling filter inoculated by a specific bacteria consortium for removal of a simulated mixture of pharmaceutical volatile organic compounds,” *Chemical Engineering Journal*, vol. 304, pp. 757–765, 2016, doi: 10.1016/j.cej.2016.06.078.

[71] R. Lebrero, D. Volckaert, R. Pérez, R. Muñoz, and H. Van Langenhove, “A membrane bioreactor for the simultaneous treatment of acetone, toluene, limonene and hexane at trace level concentrations,” *Water Research*, vol. 47, no. 7, pp. 2199–2212, 2013, doi: 10.1016/j.watres.2013.01.041.

[72] R. A. LaCroix, B. O. Palsson, and A. M. Feist, “A Model for Designing Adaptive Laboratory Evolution Experiments,” *Applied and Environmental Microbiology*, vol. 83, no. 8, pp. 1–14, 2017.

[73] S. Singh, B. B. Singh, R. Chandra, D. K. Patel, and V. Rai, “Synergistic biodegradation of pentachlorophenol by Bacillus cereus (DQ002384), Serratia marcescens (AY927692) and Serratia marcescens (DQ002385),” *World Journal of Microbiology and Biotechnology*, vol. 25, no. 10, pp. 1821–1828, 2009, doi: 10.1007/s11274-009-0083-6.

[74] A. Gaszczak, G. Bartelmus, and A. Rotkegel, “Modelling of the VOCs biodegradation process in the trickle-bed bioreactor - analysis of the model parametric sensitivity,” *AIChE Journal*, no. December 2020, pp. 1–13, 2021, doi: 10.1002/aic.17180.

[75] K. F. Reardon, D. C. Mosteller, J. B. Rogers, N. M. DuTeau, and K. H. Kim, “Biodegradation kinetics of aromatic hydrocarbon mixtures by pure and mixed bacterial cultures,” *Environmental Health Perspectives*, vol. 110, no. SUPPL. 6, pp. 1005–1011, 2002, doi: 10.1289/ehp.02110s61005.

[76] C. E. Lawson, W. R. Harcombe, and R. Hatzenpichler, “Common principles and best practices for engineering microbiomes,” *Nature Reviews Microbiology*, pp. 1–17, 2019, doi: 10.1038/s41579-019-0255-9.

[77] F. Arias-Sanchez, B. Vessman, and S. Mitri, “Artificially selecting microbial communities: If we can breed dogs, why not microbiomes?,” *plos Biology*, vol. 17, no. 8, pp. 1–8, 2019, doi: https://doi.org/10.1371/ journal.pbio.3000356 Published:

[78] J. Liu, B. Zhao, Y. Lan, and T. Ma, “Enhanced degradation of different crude oils by defined engineered consortia of Acinetobacter venetianus RAG-1 mutants based on

their alkane metabolism," *Bioresource Technology*, vol. 327, p. 124787, May 2021, doi: 10.1016/j.biortech.2021.124787.

[79] M. Macchi *et al.*, "Design and evaluation of synthetic bacterial consortia for optimized phenanthrene degradation through the integration of genomics and shotgun proteomics," *Biotechnology Reports*, vol. 29, p. e00588, Mar. 2021, doi: 10.1016/j.btre.2021.e00588.

[80] R. Muñoz, S. Villaverde, B. Guieysse, and S. Revah, "Two-phase partitioning bioreactors for treatment of volatile organic compounds," *Biotechnology Advances*, vol. 25, no. 4, pp. 410–422, 2007, doi: 10.1016/j.biotechadv.2007.03.005.

[81] P. E. Puentes-Téllez and J. Falcao Salles, "Construction of Effective Minimal Active Microbial Consortia for Lignocellulose Degradation," *Microbial Ecology*, vol. 76, no. 2, pp. 419–429, 2018, doi: 10.1007/s00248-017-1141-5.

[82] B. Burgunter-Delamare *et al.*, "Metabolic Complementarity Between a Brown Alga and Associated Cultivable Bacteria Provide Indications of Beneficial Interactions," *Frontiers in Marine Science*, vol. 7, no. February, pp. 1–11, 2020, doi: 10.3389/fmars.2020.00085.

[83] E. D. Lee, E. R. Aurand, and D. C. Friedman, "Engineering Microbiomes-Looking Ahead," *ACS synthetic biology*, vol. 9, no. 12, pp. 3181–3183, 2020, doi: 10.1021/acssynbio.0c00558.

[84] R. U. Sheth, "New Tools for Understanding and Engineering Complex Microbial Communities," Columbia University, 2019.

[85] C. M. Singleton *et al.*, "Connecting structure to function with the recovery of over 1000 high-quality metagenome-assembled genomes from activated sludge using long-read sequencing," *Nature Communications*, vol. 12, no. 1, pp. 1–13, 2021, doi: 10.1038/s41467-021-22203-2.

[86] M. Zilli, E. Palazzi, L. Sene, A. Converti, and M. D. Borghi, "Toluene and styrene removal from air in biofilters," *Process Biochemistry*, vol. 37, no. 4, pp. 423–429, 2001, doi: 10.1016/S0032-9592(01)00228-X.

[87] G. Alagappan and R. Cowan, "Substrate inhibition kinetics for toluene and benzene degrading pure cultures and a method for collection and analysis of respirometric data for strongly inhibited cultures," *Biotechnology and Bioengineering*, vol. 83, no. 7, pp. 798–809, 2003, doi: 10.1002/bit.10729.

[88] R. Feng *et al.*, "Structure and predictive functional profiling of microbial communities in two biotrickling filters treated with continuous/discontinuous waste gases," *AMB Express*, vol. 9, no. 1, p. 2, 2019, doi: 10.1186/s13568-018-0726-9.

[89] A. Wongbunmak, Y. Panthongkham, M. Suphantharika, and T. Pongtharangkul, "A fixed-film bioscrubber of Microbacterium esteraromaticum SBS1-7 for

toluene/styrene biodegradation," *Journal of Hazardous Materials*, vol. 418, no. April, p. 126287, 2021, doi: 10.1016/j.jhazmat.2021.126287.

[90] K. F. Reardon, D. C. Mosteller, and J. D. Bull Rogers, "Biodegradation kinetics of benzene, toluene, and phenol as single and mixed substrates for Pseudomonas putida F1.," *Biotechnology and bioengineering*, vol. 69, no. 4, pp. 385–400, 2000, doi: 10.1002/1097-0290(20000820)69:4<385::AID-BIT5>3.0.CO;2-Q.

[91] F. Beltrametti *et al.*, "Sequencing and functional analysis of styrene catabolism genes from Pseudomonas fluorescens ST," *Appl Environ Microbiol*, vol. 63, no. 6, pp. 2232–2239, Jun. 1997, doi: 10.1128/aem.63.6.2232-2239.1997.

[92] L. Malhautier, G. Quijano, M. Avezac, J. Rocher, and J. L. Fanlo, "Kinetic characterization of toluene biodegradation by Rhodococcus erythropolis: Towards a rationale for microflora enhancement in bioreactors devoted to air treatment," *Chemical Engineering Journal*, vol. 247, pp. 199–204, 2014, doi: 10.1016/j.cej.2014.02.099.

[93] E. H. Lee and K. S. Cho, "Effect of substrate interaction on the degradation of methyl tert-butyl ether, benzene, toluene, ethylbenzene, and xylene by Rhodococcus sp," *Journal of Hazardous Materials*, vol. 167, no. 1–3, pp. 669–674, 2009, doi: 10.1016/j.jhazmat.2009.01.035.

[94] A. Belcour, C. Frioux, M. Aite, F. Hildebrand, and A. Siegel, "Metage2Metabo, Microbiota-Scale Metabolic Complementarity for the Identification of Key Species," *eLife*, vol. 9, pp. 1–33, 2020.

[95] P. D. Karp *et al.*, "Pathway Tools version 24.0: Integrated Software for Pathway/Genome Informatics and Systems Biology." arXiv, Nov. 12, 2020. doi: 10.48550/arXiv.1510.03964.

[96] R. Caspi *et al.*, "The MetaCyc database of metabolic pathways and enzymes - a 2019 update," *Nucleic Acids Research*, vol. 48, no. D1, pp. D445–D453, Jan. 2020, doi: 10.1093/nar/gkz862.

[97] R. Sander, "Compilation of Henry's law constants (version 4.0) for water as solvent," *Atmospheric Chemistry and Physics*, vol. 15, no. 8, pp. 4399–4981, 2015, doi: 10.5194/acp-15-4399-2015.

[98] B. J. Callahan, P. J. McMurdie, M. J. Rosen, A. W. Han, A. J. A. Johnson, and S. P. Holmes, "DADA2: High resolution sample inference from Illumina amplicon data," *Nat Methods*, vol. 13, no. 7, pp. 581–583, Jul. 2016, doi: 10.1038/nmeth.3869.

[99] C. Quast *et al.*, "The SILVA ribosomal RNA gene database project: improved data processing and web-based tools," *Nucleic Acids Res*, vol. 41, no. Database issue, pp. D590–D596, Jan. 2013, doi: 10.1093/nar/gks1219.

[100] P. J. McMurdie and S. Holmes, “phyloseq: An R Package for Reproducible Interactive Analysis and Graphics of Microbiome Census Data,” *PLoS One*, vol. 8, no. 4, p. e61217, Apr. 2013, doi: 10.1371/journal.pone.0061217.

[101] H. Wickham *et al.*, “Welcome to the Tidyverse,” *Journal of Open Source Software*, vol. 4, no. 43, p. 1686, Nov. 2019, doi: 10.21105/joss.01686.

[102] P. M. Varner, M. N. Allemann, J. K. Michener, and C. K. Gunsch, “The effect of bacterial growth strategies on plasmid transfer and naphthalene degradation for bioremediation,” *Environmental Technology & Innovation*, vol. 28, p. 102910, Nov. 2022, doi: 10.1016/j.eti.2022.102910.

[103] M. R. Weigand *et al.*, “Conserved Patterns of Symmetric Inversion in the Genome Evolution of Bordetella Respiratory Pathogens,” *mSystems*, vol. 4, no. 6, pp. e00702-19, Nov. 2019, doi: 10.1128/mSystems.00702-19.

[104] F. Bianchi, M. Careri, L. Mustat, A. Malcevschi, and M. Musci, “Bioremediation of Toluene and Naphthalene: development and Validation of a GC-FID Method for Their Monitoring,” *Annali di Chimica*, vol. 95, no. 7–8, pp. 515–524, 2005, doi: 10.1002/adic.200590061.

[105] P. J. Planet *et al.*, “Bordetella holmesii : initial genomic analysis of an emerging opportunist,” *Pathogens and Disease*, vol. 67, no. 2, pp. 132–135, Mar. 2013, doi: 10.1111/2049-632X.12028.

[106] M. C. Cho, D.-O. Kang, B. D. Yoon, and K. Lee, “Toluene degradation pathway from Pseudomonas putida F1: substrate specificity and gene induction by 1-substituted benzenes,” *J Ind Microbiol Biotech*, vol. 25, no. 3, pp. 163–170, Sep. 2000, doi: 10.1038/sj.jim.7000048.

[107] W. A. Duetz, C. De Jong, P. A. Williams, and J. G. Van Andel1, “Competition in Chemostat Culture between Pseudomonas Strains That Use Different Pathways for the Degradation of Toluene,” 1994. [Online]. Available: https://journals.asm.org/journal/aem

[108] K. J. Portune, M. C. Pérez, F. J. Álvarez-Hornos, and C. Gabaldón, “Investigating bacterial populations in styrene-degrading biofilters by 16S rDNA tag pyrosequencing,” *Applied Microbiology and Biotechnology*, vol. 99, no. 1, pp. 3–18, 2015, doi: 10.1007/s00253-014-5868-3.

[109] L. C. Stillwell, S. J. Thurston, R. P. Schneider, M. F. Romine, J. K. Fredrickson, and J. D. Saffer, “Physical mapping and characterization of a catabolic plasmid from the deep-subsurface bacterium Sphingomonas sp. strain F199,” *Journal of Bacteriology*, vol. 177, no. 15, pp. 4537–4539, Aug. 1995, doi: 10.1128/jb.177.15.4537-4539.1995.

[110] R. Omrani, G. Spini, E. Puglisi, and D. Saidane, “Modulation of microbial consortia enriched from different polluted environments during petroleum biodegradation,” *Biodegradation*, vol. 29, no. 2, pp. 187–209, 2018, doi: 10.1007/s10532-018-9823-3.

[111] J. B. J. H. van Duuren *et al.*, “pH-stat fed-batch process to enhance the production of cis, cis-muconate from benzoate by Pseudomonas putida KT2440-JD1,” *Biotechnology Progress*, vol. 28, no. 1, pp. 85–92, 2012, doi: 10.1002/btpr.709.

[112] P. M. Varner and C. K. Gunsch, “Complete Genome Sequence of NAH7-Harboring Pseudomonas putida Strain G7,” *Microbiol Resour Announc*, vol. 11, no. 10, p. e0039422, Oct. 2022, doi: 10.1128/mra.00394-22.

[113] A. Sayqal *et al.*, “Metabolic analysis of the response of Pseudomonas putida DOT-T1E strains to toluene using Fourier transform infrared spectroscopy and gas chromatography mass spectrometry,” *Metabolomics*, vol. 12, no. 7, pp. 1–12, 2016, doi: 10.1007/s11306-016-1054-1.

[114] A. M. Warhurst, K. F. Clarke, R. A. Hill, R. A. Holt, and C. A. Fewson, “Metabolism of styrene by Rhodococcus rhodochrous NCIMB 13259.,” *Appl Environ Microbiol*, vol. 60, no. 4, pp. 1137–1145, Apr. 1994.

Biography

Kelsey Deaton received her BA in Environmental Studies and BS in Biological Sciences (with Distinction in the Major) from University of California Santa Barbara in 2011. Kelsey worked for three years with the environmental biotech startup Mango Materials in Berkeley, CA, in the bioproduction of biodegradable biopolymers from waste methane. Kelsey has been a doctoral student in the lab of Marc Deshusses since 2016.